UNIVERSITY OF OKLAHOMA
GRADUATE COLLEGE

# DEVELOPING A FRAMEWORK FOR EVALUATING SOURCES OF PREDICTABILITY FOR EXTREME EVENTS ON SUBSEASONAL TIMESCALES IN SOUTHEAST ASIA & SOUTH AMERICA

A THESIS
SUBMITTED TO THE GRADUATE FACULTY
in partial fulfillment of the requirements for the
Degree of
MASTER OF SCIENCE

By

GABRIELLE R. H. BROWN
Norman, Oklahoma
2025

DEVELOPING A FRAMEWORK FOR EVALUATING SOURCES OF PREDICTABILITY FOR EXTREME EVENTS ON SUBSEASONAL TIMESCALES IN SOUTHEAST ASIA & SOUTH AMERICA

A THESIS APPROVED FOR THE
SCHOOL OF METEOROLOGY

BY THE COMMITTEE CONSISTING OF

Dr. Kathleen Pegion (Chair)

Dr. Elinor Martin

Dr. Renee McPherson

# Acknowledgments

The saying ”it takes a village” is often used in the context of raising a child, but its true meaning extends far beyond that. It reminds us that success is rarely achieved alone, but through the combined efforts and support of a community. The same is true for my journey in completing this thesis, and I would like to take this opportunity to acknowledge those in my village.

First, I want to thank my advisor, Dr. Kathy Pegion, whose guidance, wisdom, and encouragement throughout this research have been invaluable. Her mentorship has helped me grow as both a researcher and a communicator beyond what I ever imagined for myself at the start of this journey.

I would also like to thank the members of my committee, Drs. Elinor Martin and Renee McPherson, for their time, valuable feedback, thoughtful insights, and support throughout my graduate studies. Collectively, my committee has fueled my excitement to continue as a woman and leader in this field.

I am sincerely grateful to my friends and colleagues in the School of Meteorology, the Earth System Prediction Lab, the Global Water Security Center, the South American Climate Security Team, The Climate Consensus, and my undergraduate institution, Vermont State University - Lyndon. Working alongside such talented, knowledgeable, and supportive individuals has made this experience both productive and rewarding. Many within these groups, including my undergraduate advisor, Dr. Janel Hanrahan, reminded me during moments of doubt that I was needed and that my contributions mattered. You will never know just how much that encouragement meant to me.

I am deeply grateful to my family, especially my mom, dad, brother, and dog, Brady, whose unwavering love and encouragement are the reason I am here today. They instilled in me a determination and resilience that have helped me face life’s challenges, and their steadfast support has allowed me to pursue my dreams, no matter how far they have taken me from home.

Finally, I owe my some of my deepest thanks to my boyfriend and partner, Bobby. I have been incredibly lucky to share both my undergraduate and graduate experiences with him. He has been one of my loudest cheerleaders, brightest lights, and has believed in me even when I did not believe in myself. I hope to one day reflect the same unwavering confidence in myself that he has consistently shown and carried for me.

Thank you to everyone who has been a part of this journey - my village. You helped make this thesis possible.

# Table of Contents

# List Of Tables

# List Of Figures

# Abstract

Rising temperatures due to climate change are leading to an increase in extreme weather events, posing significant risks to vulnerable regions worldwide. These areas are already experiencing extreme precipitation, droughts, and floods, which threaten climate security and endanger lives and property. Subseasonal prediction can provide more timely information for effective climate adaptation strategies than short-term forecast with lead times of 1 - 2 weeks.

This study aims to develop a framework, or generalizable methodology, for analyzing past extreme weather events and their predictability to improve subseasonal forecasts and make them more useful for organizations involved in disaster preparedness and climate security. These include international and national agencies such as the Global Water Security Center (GWSC), emergency management authorities, and local governments, organizations, and individuals in climate-sensitive regions.

In this work, recent extreme weather events are analyzed, including extreme precipitation events that caused extensive flooding in Pakistan during 2022 and Peru in 2017 and 2023. Using ECMWF Reanalysis v5 (ERA5) and observational datasets, such as Climate Hazards Group InfraRed Precipitation with Station (CHIRPS) data, potential drivers and mechanisms behind these events are examined. NCAR Community Earth System Model Version 2 (CESM2) skill is used to understand how far in advance potentially useful information could have been provided to organizations like the GWSC to be translated to impacted countries. Further, a unique set of initialized prediction experiments from NCAR CESM2 with climatological initial conditions for different combinations of earth system components (e.g., land, ocean, and atmosphere) are used to identify which components contribute most to the occurrence and prediction of these events. These experiments are used as a springboard to analyze the drivers and mechanisms of these events.

For the 2022 precipitation in Pakistan, atmospheric initial conditions contributed more to forecast skill in early July and August, while oceanic initial conditions had a greater influence in late July. These results provided a launching point for assessing potential drivers. Our findings indicate that anomalous easterly wind south of the Tibetan Plateau and an enhanced Somali Jet, both influenced by sea surface temperatures, were primary contributors to the 2022 Pakistan floods. Moisture flux analysis indicated that northward propagating monsoon surges were not primary drivers. In Peru, oceanic initial condition contribution to skill dominated supporting the role of Coastal El Niño as a potential driver of the precipitation for both 2017 and 2023. Predictive skill was limited for the 2017 Peru and 2022 Pakistan events, but skill improved significantly for the 2023 Peru event, with forecasts providing useful precipitation information up to 3 - 4 weeks in advance. These findings demonstrate the potential of targeted subseasonal forecasts to inform risk reduction efforts across diverse geographic regions.

# Chapter 1

# Introduction

Rising temperatures driven by climate change are intensifying extreme weather, posing serious threats to vulnerable regions around the world. These areas already are experiencing more frequent and severe occurrences of extreme precipitation, droughts, and floods. These conditions jeopardize climate security, endangering lives and property. To reduce these growing risks, immediate preparation and adaptive responses are essential. Subseasonal prediction offers a valuable tool by providing timely and actionable information to guide effective climate adaptation strategies (VanBuskirk et al. 2021, 2023a; Schroers et al. 2024). Building a robust framework to analyze extreme events and their predictability is key to enhancing subseasonal forecasting capabilities, ultimately helping to safeguard at-risk communities.

## 1.1 Climate Change Impacts on Extreme Weather

The rising frequency and intensity of extreme weather events, such as heatwaves, storms, droughts, and heavy precipitation, have become a growing concern globally. These changes are influenced in part by climate change, which has increased the likelihood and severity of many such events (Trenberth 2018; Seneviratne et al. 2021). While the scientific mechanisms linking global warming to extreme weather are well established (Trenberth 2018; Seneviratne et al. 2021), the significance of these events extends beyond their physical causes. Extreme weather can disrupt infrastructure, displace populations, and strain political systems, making them important to study. Heavy precipitation, for instance, has already become more common in many regions, contributing to more frequent and intense flooding (Blöschl et al. 2019; Berghuijs et al. 2017). Whether driven by climate trends or other factors, the consequences of extreme events demand attention, particularly for their impact on geopolitical dynamics.

## 1.2 Extreme Weather Impacts on the Geopolitical Landscape

The onset of an extreme weather event, or climate shock, can trigger a wide range of consequences, including significant geopolitical impacts. Immediate effects often include water and energy shortages, property loss, and infrastructure damage. In more developed countries, these direct impacts tend to be the most prominent (Beames et al. 2025). However, secondary effects such as disruptions to livelihoods, threats to food and water security, and increased public health risks are also critical (Hendrix and Glaser 2007; Burke et al. 2009; Hanjra and Qureshi 2010; Misra 2014; Norwegian Refugee Council 2024). Recognizing these risks, the 2015 U.S. White House National Security Strategy highlighted climate change as a pressing national security threat, citing its potential to exacerbate natural disasters, forced migration, and conflict driven by resource scarcity (The White House 2015). These challenges are particularly acute in vulnerable regions already burdened by fragile governance or a history of conflict.

Extreme weather events, and, more broadly, climate change, can lead to significant insecurity, often manifesting as migration or conflict in affected regions. Burke et al. (2009) found a correlation between rising average temperatures and increased conflict. In Africa, even a single degree of warming was associated with a 4.5% rise in civil wars and violence, with effects that persisted into the following year. Their projections indicated a potential 54% increase in armed conflict incidences by 2030 (Burke et al. 2009). On the issue of migration and displacement, the 2024 Global Report on Internal Displacement reported that by the end of 2023, 75.9 million people were living in internal displacement worldwide which was up from 71.1 million in 2022. Disasters alone triggered 26.4 million new displacements across 148 countries and territories in 2023, marking the third highest figure in the past decade. Additionally, violence and conflict accounted for 68.3 million people living in internal displacement by the end of 2023, a 49% increase over the past five years (Norwegian Refugee Council 2024).

## 1.3 Importance of Subseasonal-to-Seasonal Prediction

Traditional weather forecasts provide predictions up to two weeks in advance, offering only a limited window for disaster preparedness. On the other hand, climate projections look so far into the future, years or decades ahead, making them less relevant for real-time, operational decisions in the near future. Subseasonal-to-seasonal (S2S) prediction, forecasts spanning several weeks to a few months, can bridge this gap (Kirtman et al. 2014; Robertson et al. 2015). This intermediate timescale holds significant potential for improving climate adaptation and preparedness efforts. Accurate S2S forecasts can benefit a range of economic sectors and provide critical lead time for implementing protective measures ahead of extreme weather events (White et al. 2017). In doing so, they may help reduce the risks associated with climate shocks, including the potential for insecurity, violence, conflict, and displacement, especially in vulnerable regions.

The subseasonal timescale, covering prediction from three to eight weeks, remains a developing area of research, yet it is drawing increasing interest and demand. Compared to traditional weather forecasts, seasonal outlooks, and long-term climate projections, this timescale has received significantly less attention. However, notable advancements have emerged including the international S2S project and database (Vitart et al. 2017; Vitart and Robertson 2018), the Subseasonal Experiment (Pegion et al. 2019), and the application of climate models such as the National Center for Atmospheric Research (NCAR) Community Earth System Model (CESM) to S2S predictions (Richter et al. 2022). These efforts provide both real-time forecasts and historical reforecasts, which are vital for research and model improvement. Forecasting at this timescale is particularly challenging because it lies in a "prediction gap" where it is too far ahead for the current atmospheric state to reliably inform predictions, yet too near for slower components like oceanic or soil moisture changes to exert their full influence (Brunet et al. 2010; Vitart et al. 2012; Black et al. 2017; DelSole et al. 2017; Mariotti et al. 2018). Nevertheless, researchers have identified several sources of predictability that evolve more slowly than atmospheric variability. These include coupled ocean-atmosphere processes such as the Madden-Julian Oscillation (MJO), El Niño-Southern Oscillation (ENSO), stratosphere-troposphere interactions, tropical-extratropical teleconnections, ocean conditions, snow, soil moisture, and sea ice cover (Dirmeyer et al. 2009; Miralles et al. 2014; Mariotti et al. 2020).

As a relatively new area of research, most studies on subseasonal predictability have focused on surface variables related to temperature and precipitation (Ford et al. 2018; De Andrade et al. 2019; Xiang et al. 2020; Wu et al. 2023; Liu et al. 2024; Malik and Mishra 2025), as well as dominant modes of subseasonal variability like the North Atlantic Oscillation (NAO) and the MJO (Stan et al. 2017; Vitart et al. 2017; Kim et al. 2018b; Lim et al. 2018; Sun et al. 2020; Yamagami and Matsueda 2020). However, recent research has begun to expand beyond these areas, exploring the predictability of additional variables and processes, including land surface conditions (e.g., soil moisture and snowpack) (Zhu et al. 2019; Diro and Lin 2020; Benson and Dirmeyer 2021), sudden stratospheric warmings (Tripathi et al. 2015; Millin and Furtado 2022), the quasi-biennial oscillation (Kim et al. 2019; Lim et al. 2019; Huang et al. 2023), and sea ice (Zampieri et al. 2018; Wayand et al. 2019; Wang et al. 2023).

As with any emerging field, subseasonal predictability faces a range of scientific and technical challenges. These include issues related to forecast initialization, ensemble generation, bias correction and calibration, assessment of forecast quality and skill, model errors and resolution, and understanding key sources of predictability. Additionally, bridging the gap between research and operational forecasting, and ensuring forecasts meet user needs to support decision-making (VanBuskirk et al. 2021, 2023a; Schroers et al. 2024), remain ongoing hurdles (Merryfield et al. 2020; Meehl et al. 2021). While these challenges are complex and wide-ranging, they also represent valuable opportunities for continued progress and innovation in the field (Mariotti et al. 2020; Merryfield et al. 2020).

## 1.4 Developing a Framework for Evaluating the Subseasonal Predictability of Extreme Events

To improve subseasonal forecasts of future extreme weather events, it is essential to first evaluate how well past events were predicted. Merryfield et al. (2020) emphasized the importance of assessing the predictability of historical high-impact weather events to overcome existing challenges and highlight the potential benefits of S2S forecasting. In this study, we develop a framework to evaluate the sources of predictability for extreme events on subseasonal timescales in Southeast Asia and South America through examination of the subseasonal predictability of recent extreme precipitation events in Pakistan and Peru.

According to the World Bank Group, poverty in Pakistan has worsened due to recent shocks, including natural disasters and the COVID-19 pandemic. The lower-middle income poverty rate reached 42.3% in fiscal year 2024, with an additional 2.6 million people falling below the poverty line compared to the previous year (World Bank Group 2025a). In Peru, economic growth averaged 2.3% between 2014 and 2023, and one in three Peruvians now lives in poverty. In contrast, the economy grew at an average rate of 6.4% from 2004 to 2013, reducing poverty by 27%. This stark difference is largely attributed to the impacts of COVID-19, fragile governance, political instability, and extreme weather events (World Bank Group 2025b).

This study focuses on extreme precipitation events in Pakistan (2022) and Peru (2017 and 2023). The 2022 floods in Pakistan submerged one-third of the country (Government of Pakistan 2022), affecting approximately 50 million people and resulting in widespread homelessness, fatalities and property loss (Bhutto 2022; Fadil 2022). Damages were estimated at $30 billion, severely impacting agriculture, food production, livestock, fisheries, housing, transportation, and communication infrastructure (Bhutto 2022; Chughtai 2022; Government of Pakistan 2022; Otto et al. 2023). In the aftermath, famine and disease further exacerbated the humanitarian crisis (Bhutto 2022).

The 2017 and 2023 floods in Peru had similarly devastating effects. In 2017, extreme rainfall led to over 100 deaths and displaced nearly 200,000 people. The country's infrastructure suffered significant damage with 260 bridges collapsing, 3,000 km of roads rendered unusable, and over 200,000 homes affected. Economic losses exceeded $3 billion, and the collapse of water distribution systems led to severe drinking water shortages (Collyns 2017). In 2023, intense precipitation again triggered widespread flooding affecting over 100,000 people and destroyed around 42,000 homes, 70 schools, and 130 health centers (Assessment Capacity Project 2024). The worst dengue outbreak in Peru's history occurred following this event, which is a mosquito-borne disease that surged due to post-flooding conditions (Pan American Health Organization 2023).

These events were selected for this study due to their significant social and economic impacts and to enable the development of a robust evaluation framework across two geographically and climatically distinct regions.

Given the significant societal impacts of these events, this work aims not only to advance understanding of the mechanisms driving extreme precipitation, such as the 2022 Pakistan floods and the 2017 and 2023 events in Peru, but also to provide insights into the potential utility of subseasonal forecasts. The definition of "useful" in this context varies depending on the audiences. For instance, the information considered valuable by a decision-maker may differ from that prioritized by a forecaster (VanBuskirk et al. 2023b). Specifically, this study seeks to demonstrate to organizations like the Global Water Security Center (GWSC), which serves as a bridge between scientific research and potential users, whether subseasonal forecasts have skill in predicting past extreme events relevant to their mission. By focusing on the predictability of previous high-impact events, this work provides a foundation for improving the application of suseasonal forecasting for future events. It offers a starting point for using these forecasts which can be a valuable tool for policymakers, risk managers, and a range of other stakeholders (VanBuskirk et al. 2021, 2023a; Schroers et al. 2024).

## 1.5 2022 Pakistan Extreme Precipitation

Pakistan's diverse climates, ranging from high-elevation mountainous terrain in the north to arid conditions in the southern provinces, drive latitudinal variations in extreme precipitation trends. Across Asia, especially in South Asia, strong evidence indicates an increase in extreme precipitation since the 1950s, though patterns remain highly variable across regions (Pai et al. 2015; Siswanto et al. 2015; Hu et al. 2016; Malik et al. 2016; Priya et al. 2017; Roxy et al. 2017; Kim et al. 2019; Yao et al. 2021). In Pakistan, some studies report widespread increases in extreme precipitation (Zahid and Rasul 2012), while others highlight more pronounced increases in the north-northeastern provinces compared to the south-southwest (Hanif et al. 2013; Hussain and Lee 2013; Hartmann and Buchanan 2014; Bhatti et al. 2020). The summer monsoon season further complicates Pakistan's rainfall variability, as studies show an overall increase in monsoonal rainfall (Hanif et al. 2013; Iqbal and Athar 2017). These increases in extreme rainfall amplify concerns about flooding.

During July and August 2022, extreme precipitation triggered unprecedented flooding in Pakistan (Hsu et al. 2022; He et al. 2023; Ma et al. 2023; Nanditha et al. 2023). The flooding primarily devastated Pakistan's southern provinces (Otto et al. 2023; Singh et al. 2024). The summer of 2022 became the wettest since 1979, with total accumulated precipitation reaching four times the previously recorded levels (Ma et al. 2023).

Research widely agrees that Pakistan's extreme precipitation in summer 2022 was anomalous (Hsu et al. 2022; Chen et al. 2023; He et al. 2023; Ma et al. 2023; Nanditha et al. 2023; Otto et al. 2023; Qiao et al. 2023; Annamalai 2024; Singh et al. 2024). However, studies offer different explanations for its drivers and characteristics. A so-called "triple-dip" La Niña, which began in 2020 and persisted for multiple years, remained active during this event (Hsu et al. 2022; He et al. 2023; Ma et al. 2023; Otto et al. 2023; Qiao et al. 2023). Additionally, negative sea-surface temperature anomalies in the Indian Ocean, linked to a negative Indian Ocean Dipole, may have influenced the event (Ma et al. 2023; Otto et al. 2023). He et al. (2023) found that these negative sea surface temperature anomalies weakened the meridional temperature gradient, which in turn disrupted the typical westerly flow over the Tibetan Plateau and shifted it to easterly flow. This shift likely enhanced moisture transport from the Bay of Bengal into Pakistan (Ma et al. 2023). Furthermore, He et al. (2023) argued that this shift in zonal wind flow contributed to stronger ascent over West Asia, leading to extreme precipitation, while also driving descent over East Asia, where an extreme heatwave developed (He et al. 2023). Although this anomalous flow persisted into August, it began to weaken later in the month (Ma et al. 2023). Studies suggested that atmospheric circulation, including a strengthened Indian monsoon and a blocking pattern, played a key role in the anomalous easterly flow and extreme precipitation (Hsu et al. 2022; Chen et al. 2023; Ma et al. 2023; Qiao et al. 2023; Singh et al. 2024). Ma et al. (2023) described how the eastward extension of the middle Iranian high and the westward extension of the western Pacific subtropical high combined to generate an unusual zonal wind over the Tibetan Plateau.

In August, a blocking high over Europe and a trough with upper-level cyclonic circulation over northwest Pakistan influenced the extreme precipitation. As atmospheric blocking over Europe intensified, the trough over Pakistan deepened (Hsu et al. 2022; Ma et al. 2023; Otto et al. 2023). Previous research shows that blocking patterns can trigger downstream energy dispersion, which contributes to trough deepening (Rasmussen et al. 2015). This process also played a role in Pakistan's 2010 extreme precipitation event, which caused similar impacts to those seen in 2022 (Hong et al. 2011; Trenberth and Fasullo 2012; Lau and Kim 2012; Otto et al. 2023). Blocking patterns often occur during positive phases of the North Atlantic Oscillation (NAO) (Croci-Maspoli et al. 2007), which leads to increased precipitation in Pakistan (Syed et al. 2006; Yao et al. 2016). In August 2022, the NAO reached its third strongest level since 1979 (Ma et al. 2023).

Since this event occurred during the monsoon season, some researchers attribute the extreme precipitation to an anomalously strong monsoon, identifying periods of increased rainfall as Monsoon Intra-seasonal Oscillation (MISO) events (Ma et al. 2023; Singh et al. 2024). Outgoing longwave radiation anomalies were used to identify these events, as lower outgoing longwave radiation anomaly values indicate convection and increased precipitation (Ma et al. 2023; Singh et al. 2024). Singh et al. (2024) identified three distinct MISO events that coincided with the timing and duration of the extreme rainfall.

While previous studies have identified a wide range of potential synoptic and localized drivers associated with high-impact extreme events such as the 2022 Pakistan floods, uncertainty remains around which of these factors played a primary role. Existing methodologies have not yet provided sufficient clarity to isolate the dominant contributors, highlighting the need for a more targeted analysis to distinguish key mechanisms from background variability. Climate model experiments project an increase in the intensity and frequency heavy rainfall in Asia (Endo et al. 2017; Xu et al. 2017; Guo et al. 2018; Han et al. 2018; Kim et al. 2018a; Nayak et al. 2018; Sui et al. 2018; Lee et al. 2021). This increase in heavy rainfall highlights the urgent need to improve event prediction, allowing for longer lead times to support preparation and adaptation efforts. Subseasonal forecasts can play a crucial role in this process, making it essential to first examine the subseasonal predictability of this extreme event.

Singh et al. (2024) evaluated the performance of the European Centre for Medium-Range Weather Forecasts (ECMWF) from the World Climate Research Programme/ World Weather Research Program subseasonal-to-seasonal database (Vigaud et al. 2017) to determine how far in advance it could have provided useful information about Pakistan's extreme precipitation during the summer of 2022. They used tercile-category probabilistic subseasonal prediction for precipitation initialized at the beginning of each month between June and September. Their analysis found that forecasts remained informative up to four weeks in advance throughout the monsoon season (Singh et al. 2024). MISO is considered to be a significant source of subseasonal predictability for South Asia (Goswami et al. 2006). For this reason, they featured this result in their study attributing the precipitation skill to the model's ability to predict the MISOs. However, they do not explore the other suggested causes of the Pakistan floods as potential sources of skill and they use a limited set of initial conditions to assess skill (Singh et al. 2024).

## 1.6 2017 and 2023 Peru Extreme Precipitation

Peru's terrain is remarkably diverse, comprising a narrow coastal plain in the west, the Andes Mountains in the center, and the Amazon Basin to the east, each contributing to a wide range of climates. This country's typical wet season runs from December to March, but the coastal region receives only about 5 cm of precipitation annually, making it one of the driest areas on Earth (Rau et al. 2017). There is evidence of an increase in heavy precipitation in South America; however, this trend is not robust across the entire continent (Seneviratne et al. 2021). Specifically, large regions in north, northwest, and southeast South America show increasing trends (de los Milagros Skansi et al. 2013).

In northeast Peru, rainfall is influenced by the southward migration of the Intertropical Convergence Zone (ITCZ) and the westward shift of monsoonal convection crossing the western Andes (Lagos and Buizer 1992). Additionally, sea surface temperatures in the tropical Pacific significantly affect coastal rainfall. In particular, phases of the

ENSO play a major role in the precipitation variability (Coelho et al. 2002; Sulca et al. 2018). During El Niño events, warming of the central Pacific Ocean weakens the Walker circulation – a large-scale east-west atmospheric pattern driven by sea surface temperature and pressure differences. This positive phase of ENSO leads to warmer waters in the eastern Pacific, which promote deep convection and result in above average rainfall along the Peruvian coast. Strong El Niño events have previously been associated with historic floods in the region (Goldberg et al. 1987; Takahashi 2004).

In 2017 and 2023, Peru experienced devastating rainfall that triggered widespread flooding and landslides. Between January and March 2017, cumulative rainfall across the northern and central coasts, the Andes, and the Amazon Basin exceeded any recorded value for the same period since 1982 (Rodriguez-Morata et al. 2019). Similarly, in March and April 2023, heavy rainfall caused comparable impacts, intensified by Cyclone Yaku, the first tropical cyclone to make landfall in Peru in 40 years (Peng et al. 2024).

A common driver behind these events is the phenomenon known as Coastal El Niño. Coastal El Niño occurs when strong, localized positive sea surface temperature anomalies develop in the Niño 1+2 region or along the Peruvian coast. Coastal El Niño events are relatively rare, typically forming when the basin-wide tropical Pacific sea surface temperatures are neutral or outside of a basin-scale El Niño (Ormaza-González and Cedeño 2017; Echevin et al. 2018; Garreaud 2018; Hu et al. 2019; Lübbecke et al. 2019; Rodriguez-Morata et al. 2019; Takahashi and Martínez 2019; Son et al. 2020; Rollenbeck et al. 2022; Zhao and Karamperidou 2022; Yglesias-González et al. 2023; Mayta et al. 2024; Peng et al. 2024). In 2023, the Coastal El Niño developed despite the presence of a basin-scale La Niña, during which sea surface temperature anomalies in the central Pacific were below -0.5°C. Sea surface temperatures offshore of Peru shifted dramatically within a month, from below average due to La Niña to over 4°C above average as a result of the Coastal El Niño (Peng et al. 2024). Although this Coastal El Niño event signaled the onset of a developing basin-scale El Niño, the broader evolution resembled a Rasmusson and Carpenter El Niño composite, a pattern more characteristic of events observed during the 1950s to 1970s (Rasmusson and Carpenter 1982; Peng et al. 2024). In 2017, the Coastal El Niño event both followed and preceded basin-scale La Niña conditions (Peng et al. 2019). Takahashi and Martínez (2019) suggested that La Niña conditions in the central Pacific can favor coastal warming by reducing atmospheric stability and destabilizing the ITCZ.

Several studies indicate that the initial coastal warming of 2017 was primarily associated with a regional weakening of winds in the eastern Pacific, as coastal winds were weak and decreasing from late 2016 through January 2017, leading to a cessation of upwelling along the Peruvian coast. In February, nearshore winds strengthened, including the northerly components, while offshore winds remained weak. This pattern reduced evaporation and enhanced a strong wind stress curl, which deepened the thermocline and intensified the warming through Ekman pumping. The anomalous wind stress curl further suppressed offshore winds and strengthened nearshore winds, amplifying sea-surface temperature anomalies (Echevin et al. 2018; Garreaud 2018; Peng et al. 2019; Son et al. 2020; Zhao and Karamperidou 2022).

Garreaud (2018) proposed that the local wind field changes, along with the presence of a persistent anticyclonic anomaly over the southern Pacific, reflected by values of the Southern Oscillation Index, may have played a key role in coastal warming. The persistent anticyclone likely generated Rossby wave trains, characteristic of the Pacific South American mode, influencing pressure anomalies (Garreaud 2018). Peng et al. (2019) similarly emphasized the importance of local winds but also argued that downwelling oceanic equatorial Kelvin waves contributed by pushing sea surface temperatures beyond the convective threshold, enhancing northerly alongshore wind anomalies and intensifying coastal warming. This process highlights the role of the Bjerknes feedback, a positive feedback loop between the tropical Pacific surface winds and sea surface temperatures, in the development of the 2017 Coastal El Niño.

However, other studies found little evidence that oceanic Kelvin waves were a significant driver of this event, noting the absence of a clear oceanic Kelvin wave propagation signal (Garreaud 2018; Hu et al. 2019; Lübbecke et al. 2019; Rodriguez-Morata et al. 2019). Further complicating the heavy precipitation observed in 2017 was a southward shift of the ITCZ (Son et al. 2020), a feature that can be reinforced by warm sea surface temperatures in the eastern Pacific (Takahashi and Martínez 2019).

Peng et al. (2024) is one of the first studies to characterize the features of the 2023 Coastal El Niño event. They found that a record-strong MJO phase drove westerly wind anomalies over the eastern equatorial Pacific. Cyclone Yaku further contributed to the anomalous wind patterns by enhancing northerly winds along the northwestern coast of Latin America. These anomalous winds were crucial for initiating the coastal El Niño event by weakening coastal upwelling and deepening the thermocline, with additional support from downwelling equatorial Kelvin waves. Similar to 2017, these findings indicated that the Bjerknes feedback played a key role in amplifying, sustaining, and predicting the event. Moreover, Peng et al. (2024) identified positive feedback between internal atmospheric variability, such as Cyclone Yaku, and sea surface temperatures. Their analysis suggested that Yaku formed as a part of the strong Phase 8 MJO (Peng et al. 2024), an eastward-moving region of suppressed cloudiness, rainfall, winds, and pressure disturbances currently situated over the tropical eastern Indian and western Pacific Oceans. Furthermore, they argue that the cyclone's development was influenced by the orographic effects of the Andes and further supported and amplified by anomalously warm sea surface temperatures (Peng et al. 2024).

Peng et al. (2024) found that the Bjerknes feedback is a key source of predictability for coastal El Niño events and that this phenomenon could be predicted up to a month in advance. During the 2017 event, the North American Multi-Model Ensemble (NMME) successfully predicted anomalously wet conditions, with February-initialized forecasts anticipating extreme precipitation by mid-March. Because the Bjerknes feedback helps maintain and amplify coastal sea surface temperature warming, forecasts initialized in February and March showed improved rainfall prediction skill (Peng et al. 2019). Similarly, in 2023, the NMME captured this feedback, enabling accurate forecasts of heavy rainfall along coastal South America for initialization dates between 1 March and 1 April (Peng et al. 2024).

Although there has been research on the characteristics and predictability of the 2017 and 2023 Coastal El Niño events and their associated extreme precipitation individually, no study to date has directly compared the two to assess their similarities and differences. This gap partly reflects the recency of the 2023 event but also highlights the broader underrepresentation of South America in climate research. Moreover, anthropogenic warming is expected to influence the characteristics of Coastal El Niño events (Cai et al. 2023). Notably, the two most extreme Coastal El Niño events since 1925 have occurred after 2017, and projections of an El Niño-like warming pattern suggest that the frequency and intensity of extreme Coastal El Niño events, and their associated impacts, are likely to increase (Peng et al. 2019, 2024). These trends underscore the urgent need for a deeper understanding of Coastal El Niño dynamics.

## 1.7 Research Questions

This study will investigate the potential sources of predictability for the 2022 Pakistan and 2017 and 2023 Peruvian heavy precipitation events by answering three questions:

(1) What are the key characteristics of the extreme event? (2) How far in advance could subseasonal forecasts have provided useful predictive information? (3) Which earth system components contributed most to the predictability and occurrence of the event?

To address these questions, we first characterize the extreme precipitation for Pakistan (Section 3.1.1) and Peru (Section 3.2.1). We then evaluate subseasonal forecasts from the National Science Foundation (NSF) National Center for Atmospheric Research (NCAR) Community Earth System Model Version 2 (CESM2) subseasonal forecasts (Richter et al. 2022) to determine how early these forecasts could have provided actionable information about the extreme precipitation. We also leverage a unique set of initialized CESM2 subseasonal prediction experiments with climatological initial conditions for different earth system components (e.g., land, ocean and atmosphere) (Richter et al. 2024). By isolating the components, we assess their individual contributions to the occurrence and predictability of extreme precipitation which is done in Section 3.1.2 for Pakistan and Section 3.2.2 for Peru.

We use these experiments as a launching point to clarify the specific drivers shaping these events. We do this by analyzing key atmospheric and oceanic drivers identified in previous literature. For Pakistan this includes zonal wind (Hsu et al. 2022; He et al. 2023; Ma et al. 2023), sea surface temperatures (Hsu et al. 2022; He et al. 2023), and a heightened monsoon season recognized by outgoing longwave radiation (Ma et al. 2023; Singh et al. 2024) (Section 3.1.3). For Peru this includes Coastal El Niño, anomalous wind (Echevin et al. 2018; Garreaud 2018; Peng et al. 2019; Son et al. 2020; Zhao and Karamperidou 2022), the ITCZ (Son et al. 2020), and internal atmospheric variability (Garreaud 2018; Peng et al. 2024) (Section 3.2.3). Lastly, for each case study, we add supporting analysis further examining what we identify as the primary drivers for both Pakistan (Section 3.1.4) and Peru (Chapter 4).

# Chapter 2

# Data & Methods

## 2.1 Subseasonal Reforecasts and Reforecast Experiments

Subseasonal daily precipitation from retrospective forecasts (reforecasts) are from the National Science Foundation (NSF) National Center for Atmospheric Research (NCAR) Community Earth System Model Version 2 (CESM2) (Richter et al. 2022). Reforecasts are generated with 21 ensemble members and initialized once a week with a 45-day forecast period following the initialization date. A unique set of initialized subseasonal reforecast experiments by CESM2 are used (Richter et al. 2024). Similarly, the experiments are initialized once a week with a 45-day forecast period following the initialization date but are generated with 11 ensemble members. Both the subseasonal reforecasts and reforecast experiments have a 1° horizontal resolution. The reforecasts and experiments are converted to anomalies using a 1999 – 2020 climatology.

Subseasonal reforecast experiments are a unique set of initialized prediction experiments that use climatological initial conditions to isolate and emphasize or eliminate different individual or combinations of earth system components (e.g., land, ocean, and atmosphere). These experiments are outlined in Table 2.1. Each experiment is defined by the earth system component set to climatological initial conditions. Climatological initial conditions are lead-dependent, meaning they are derived from the climatology of the initialization date, based on the 1999 – 2020 period corresponding to the forecast dataset.

The control experiment represents the unaltered subseasonal forecast, the ATM experiment sets the atmosphere's initial conditions to climatology, the OCN experiment sets the ocean's initial conditions to climatology, and the LND experiment sets the land's initial conditions to climatology. Further, combinations of earth system components can be set to climatology to isolate the roles of individual components. For example, the ATMOCN experiment sets the atmosphere and ocean to climatology isolating the role of the land observations at the time of forecast initialization, the ATMLND experiment sets the atmosphere and land to climatology isolating the role of the ocean observations at the time of initialization, and the OCNLND experiment sets the ocean and land to climatology isolating the role of the atmosphere observations at the time the forecast is initialized. The ALL experiment sets all components to climatological initial conditions.

| **Experiment** | **Atmosphere (ATM)** | **Ocean (OCN)** | **Land (LND)** |
|---|---|---|---|
| Control (CNTRL) | X | X | X |
| ATM | CLIMO | X | X |
| OCN | X | CLIMO | X |
| LND | X | X | CLIMO |
| ATMOCN | CLIMO | CLIMO | X |
| ATMLND | CLIMO | X | CLIMO |
| OCNLND | X | CLIMO | CLIMO |
| ALL | CLIMO | CLIMO | CLIMO |

Table 2.1: CESM2 subseasonal reforecast experiments. "CLIMO" represents experiments which component is set to lead-dependent climatological initial conditions and "X" indicates which is based off observations.

For interpretation, it is important to recognize that the initial conditions of all components of the earth system contribute to predictability. However, this study specifically aims to identify which component's initial conditions the model attributes as significant contributors to the forecast skill for the 2022 Pakistan and 2017 and 2023 Peru extreme precipitation events. Additionally, these experiments account for coupled processes. For instance, if ocean conditions influence atmospheric variables or processes that enhance precipitation skill, that influence will be captured through atmospheric initial conditions.

## 2.2 Reanalysis and Precipitation Datasets

The European Centre for Medium-Range Weather Forecasts (ECMWF) Reanalysis Version 5 (ERA5) dataset (Hersbach et al. 2020) is utilized to analyze daily sea surface temperature, 850 hPa geopotential height, 850 hPa zonal and meridional wind components, zonal and meridional vertically integrated moisture flux components, and outgoing longwave radiation. Covering the period from 1940 to 2023, ERA5 offers a spatial resolution of approximately 0.25°. The Climate Hazards Infrared Precipitation with Station dataset (CHIRPS) is employed (Funk et al. 2015) to assess the daily precipitation in South Asia and South America. CHIRPS provides high-resolution (0.05°), gridded, observational precipitation data spanning 1981 to 2023. Regridding was applied to the CHIRPS data and 850 hPa zonal wind from ERA5 only when necessary for comparison with the reforecasts and reforecast experiments. Specifically, for evaluating model skill in predicting the precipitation and zonal wind. Regridding was performed using a linear interpolation to match the resolution of the model data. The observational and reanalysis datasets are converted to anomalies using a 1999 – 2020 climatology for all variables as this base period aligns with the length of the reforecast dataset.

## 2.3 Skill Metrics

Anomaly correlation coefficient (ACC) is a metric used to evaluate quantitatively how well the model performed with forecasting the spatial patterns of the observed above-average, normal, and below-average anomalies:

$$\mathrm{ACC} = \frac{\sum(f-c)(a-c)}{\sqrt{\sum(f-c)^2 \cdot \sum(a-c)^2}} \tag{2.1}$$

In Equation 2.1, "f" represents the forecast, "a" represents the actual values or observations, and "c" represents the climatology. ACC values fall between negative and positive one. A value of negative one represents an incorrect forecast, or the opposite of the observed anomalies. An ACC of zero shows that the model has no skill as there is no correlation between the prediction and observed anomalies. Lastly, a value of positive one represents a perfect forecast. Generally, positive values show that the model has some skill in predicting the observed anomalies.

To evaluate this metric, weekly averages in alignment with forecast initialization dates were calculated for both observations, reforecasts, and reforecast experiments. We specifically evaluated the ensemble mean of the reforecasts and reforecast experiments. Given that subseasonal predictability starts at three weeks lead time, our analysis of ACC isolates the week three forecasts (days 15-21). We also isolate the week one (days 0-6) forecast to compare subseasonal predictability to short term predictability.

## 2.4 Pakistan Methods

### 2.4.1 Extreme Precipitation Event Definition

Definitions of the extreme precipitation over summer 2022 for Pakistan varied across existing literature. Otto et al. (2023) characterized the precipitation over summer 2022 in two events separating July and August using two objective definitions that consider the physical and dynamical mechanisms behind the precipitation. Ma et al. (2023) similarly evaluated the summer 2022 as two events separating July and August. However, others have characterized the precipitation in July and August 2022 as three events. For example, Hsu et al. (2022) subjectively defined three events by peaks and duration of daily precipitation making note of the accumulated rainfall each event contributed. We define the extreme precipitation that occurred during July and August 2022 as three separate events with the dates the same as that defined by Hsu et al. (2022) (Fig. 2.1). Event One is from 1 to 18 July 2022, Event Two is from 23 to 30 July 2022, and Event Three is from 4 to 30 August 2022.

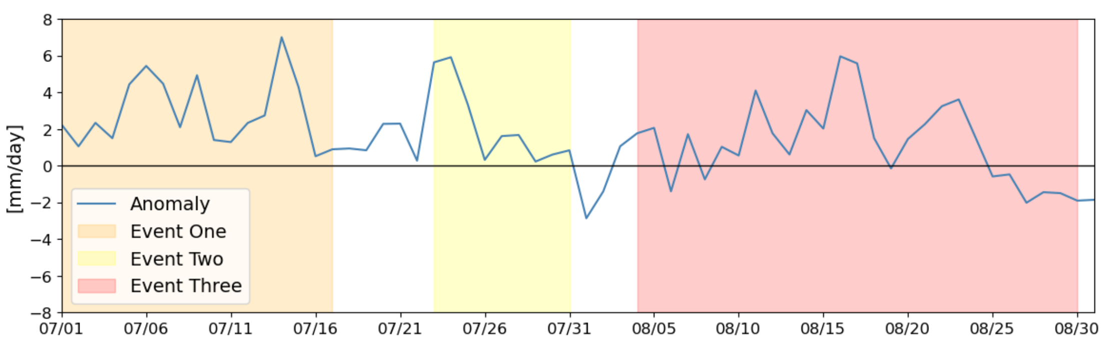


Figure 2.1: Daily average precipitation anomaly for July and August 2022 (blue, solid; mm/day) with Event One (orange shading), Event Two (yellow shading), and Event Three (red shading) dates. Adapted from Hsu et al. (2022).

## 2.5 Peru Methods

### 2.5.1 ENSO Classification and Event Identification

This study employs two climate indices to characterize ENSO variability: the Niño 1+2 (0°-10°S, 90°W-80°W) and the Niño 3.4 (5°N-5°S, 170°W-120°W) regions (Fig. 2.2). The Comité encargado del Estudio Nacional del Fenómeno El Niño (ENFEN) in Peru defines a Coastal El Niño event as occurring when the three-month running mean of the Niño 1+2 average sea surface temperature anomalies exceed 0.4°C for at least three consecutive months (L'Heureux et al. 2017; Hu et al. 2019). In this study, we specifically analyze Coastal El Niño events that occur independently of basin-scale El Niño events. That is, events that meet established criteria for Coastal El Niño but do not simultaneously satisfy the definition for basin-scale El Niño. A basin-scale El Niño (La Niña) event is identified when the three-month running mean of average sea surface temperature anomalies in the Niño 3.4 region remains above (below) 0.5°C (-0.5°C) for a minimum of five consecutive months (National Centers for Environmental Information 2025).

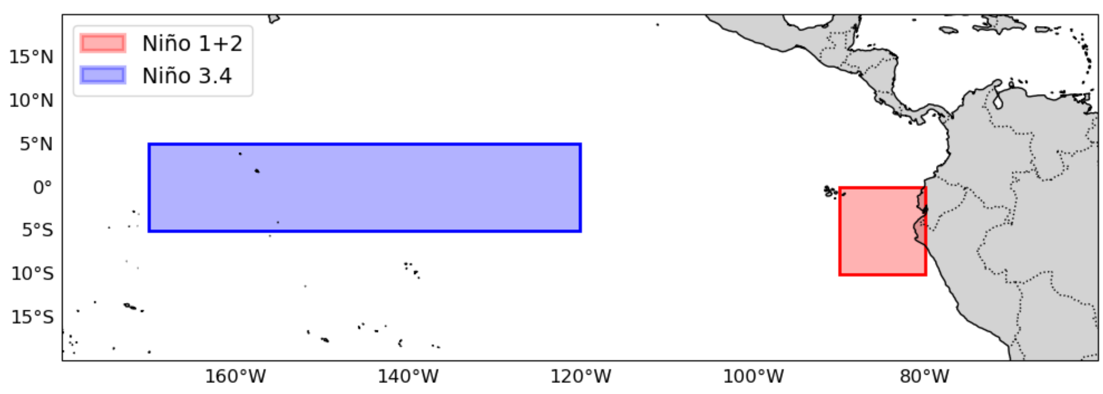


Figure 2.2: Map displaying the Niño 1+2 (0°-10°S, 90°W-80°W) and Niño 3.4 (5°N-5°S, 170°W-120°W) regions.

### 2.5.2 Long-Term Analysis of Coastal El Niño and Related Precipitation Methodology

For broader analyses of Coastal El Niño conditions, monthly averages and anomalies are calculated based on the 1999-2020 climatological baseline. Additionally, all variables are linearly detrended, and a 3-month running mean is applied to smooth short-term variability. The long-term analysis of Coastal El Niño applies compositing, empirical orthogonal function (EOF) analysis, and linear regression to examine Coastal El Niño events over many years. To isolate coastal warming events from concurrent basin-scale warming, variability associated with Niño 3.4 is removed from the Niño 1+2 index. This adjustment is achieved by subtracting the component of the Niño 3.4 index, resulting in a residual time series representing the Niño 1+2 that is linearly regressed onto the Niño 3.4 index, resulting in a residual time series representing the Niño 1+2 region with an ENSO adjustment. To assess the relationship between Coastal El Niño events and precipitation extremes in Peru, nine precipitation indices are employed to evaluate events after 1981 (Table 2.2). These indices are categorized into three groups: (1) general precipitation indices (Rx1day, Rx5day, Wet Days); (2) extreme precipitation indices (R95p, R99p, R10mm, R20mm); and (3) other indices (CWD and CDD). The selection of indices is based on the framework outlined by An et al. (2023).

| **Category** | **Index** | **Definitions** | **Units** |
|---|---|---|---|
| 1 | Wet Days | Number of days with daily total precipitation $\geq 1$ mm | days |
| 1 | Rx1day | Maximum daily total precipitation over a 1-day period | mm |
| 1 | Rx5day | Maximum daily total precipitation over a 5-day period | mm |
| 2 | R95p | Total precipitation from days when daily precipitation exceeds the 95th percentile | mm |
| 2 | R99p | Total precipitation from days when daily precipitation exceeds the 99th percentile | mm |
| 3 | CWD | Maximum number of consecutive wet days (daily total precipitation $\geq 1$ mm) | days |
| 3 | CDD | Maximum number of consecutive dry days (daily total precipitation $< 1$ mm) | days |

Table 2.2: Extreme precipitation indices used in this study. Adapted from An et al. (2023)

# Chapter 3

# Case Study Analysis

## 3.1 Pakistan

### 3.1.1 Precipitation Overview

Precipitation in Pakistan during July and August 2022 was unprecedented. Figure 3.1 illustrates the July – August average precipitation anomalies from 1981 to 2023, using the 1999 – 2020 period as the climatological baseline. The anomaly for 2022 stands out as being substantially more positive than in any other year within the time series. Additionally, the linear trend line indicates an overall positive trend, suggesting a potential increase in years with above average precipitation during July and August, and a decline in years with below average precipitation.

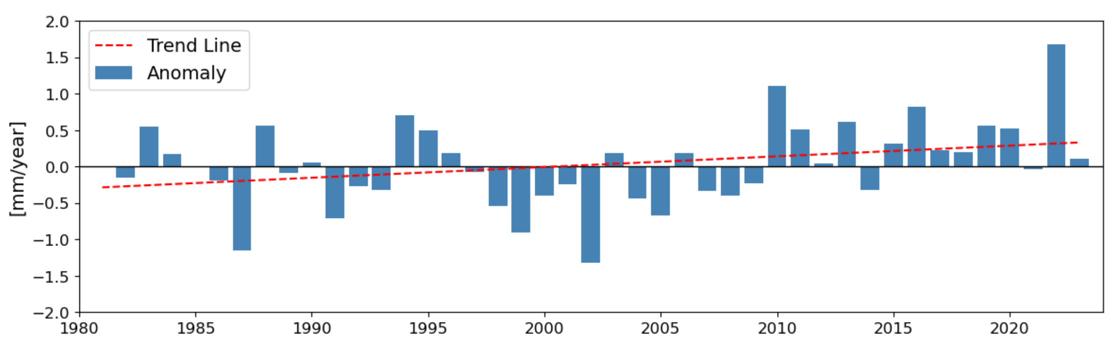


Figure 3.1: July and August annual average precipitation anomaly for 1981 – 2023 using a 1999 – 2020 climatology (blue bars; mm/year) and linear trend line (red, dashed).

Above average precipitation during July and August 2022 was widespread across Pakistan. Figure 3.2 presents the spatial distribution of weekly average precipitation anomalies for selected weeks during Events One, Two, and Three. These weeks predominantly exhibit above average anomalies, with only limited areas showing below average precipitation. While much of the country experienced above normal rainfall, regions of especially concentrated large positive anomalies, at times exceeding an average of 10 mm per week, were observed in Pakistan's southern provinces. These southern areas, typically characterized by hot, arid, desert-like climates, rarely receive such high levels of precipitation, unlike the more mountainous northern regions, where wetter conditions are more common. The magnitude and spatial pattern of above average precipitation remained generally consistent throughout most weeks in July and August 2022 during these events (not shown).

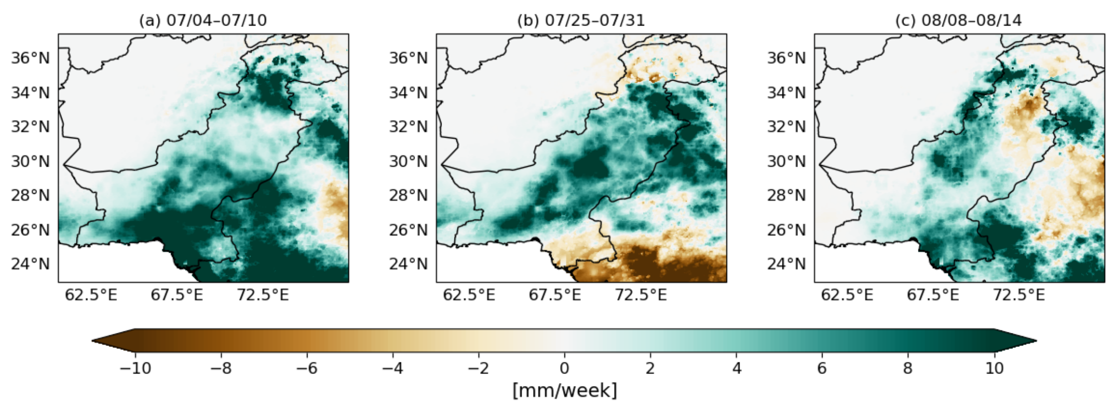


Figure 3.2: Weekly average precipitation anomaly (shading; mm/week) for week in (a) Event One (4 – 10 July 2022), (b) Event Two (25 – 31 July), and (c) Event Three (8 – 14 August).

### 3.1.2 Precipitation Predictability

Model skill was evaluated using the ACC between weekly average precipitation observations and ensemble mean reforecasts, including reforecast experiments that isolate specific Earth system components over Pakistan (Fig. 3.3). The figure highlights the skill of each extreme precipitation event by showing both subseasonal (left column) and short-term (right column) reforecast skill. Useful skill is subjectively defined by consistent positive ACCs amongst each event. Each date shown in the plots represents a reforecast initialization date used to predict any portion of the highlighted event, either at a week-3 (subseasonal) or week-1 (short-term) lead time. Reforecasts were initialized weekly from 13 June to 22 August 2022. Since the duration of each event varies, the number of initialization dates differs accordingly.

We compare ACC values for the unaltered forecast with those from experiments isolating the roles of the ocean and land, atmosphere and land, atmosphere only, and ocean only. The unaltered reforecasts show limited consistency in capturing the spatial patterns of precipitation anomalies, as reflected by variability in ACC across weeks and lead times. This inconsistency within each of the three extreme events, with little performance difference between short-term and subseasonal predictions.

Despite inconsistencies within the events, the reforecast experiments provide insight into sources of predictability. For Event One, the atmosphere appears to be a key contributor, with reforecast experiments isolating atmospheric initial conditions influence showing consistently higher ACCs than those isolating oceanic initial conditions influence, particularly at the subseasonal scale (Fig. 3.3a). Skill generally improves at the one-week lead time for all experiments except those initialized on 27 June, though the atmosphere still contributes more than the ocean (Fig. 3.3b).

In Event Two, this pattern reverses. The atmospheric initial conditions contribution to skill decreases, while the oceanic initial conditions contribution increases, especially during the first week of the event (Fig. 3.3c and Fig. 3.3d). This trend persists at other lead times, including weeks two and four (not shown). For Event Three, the sources of model skill resemble those of Event One, with atmospheric initial conditions influence again dominating, particularly at the subseasonal scale (Fig. 3.3e). Oceanic initial conditions contributions are notably lower for Event Three, with more frequent negative

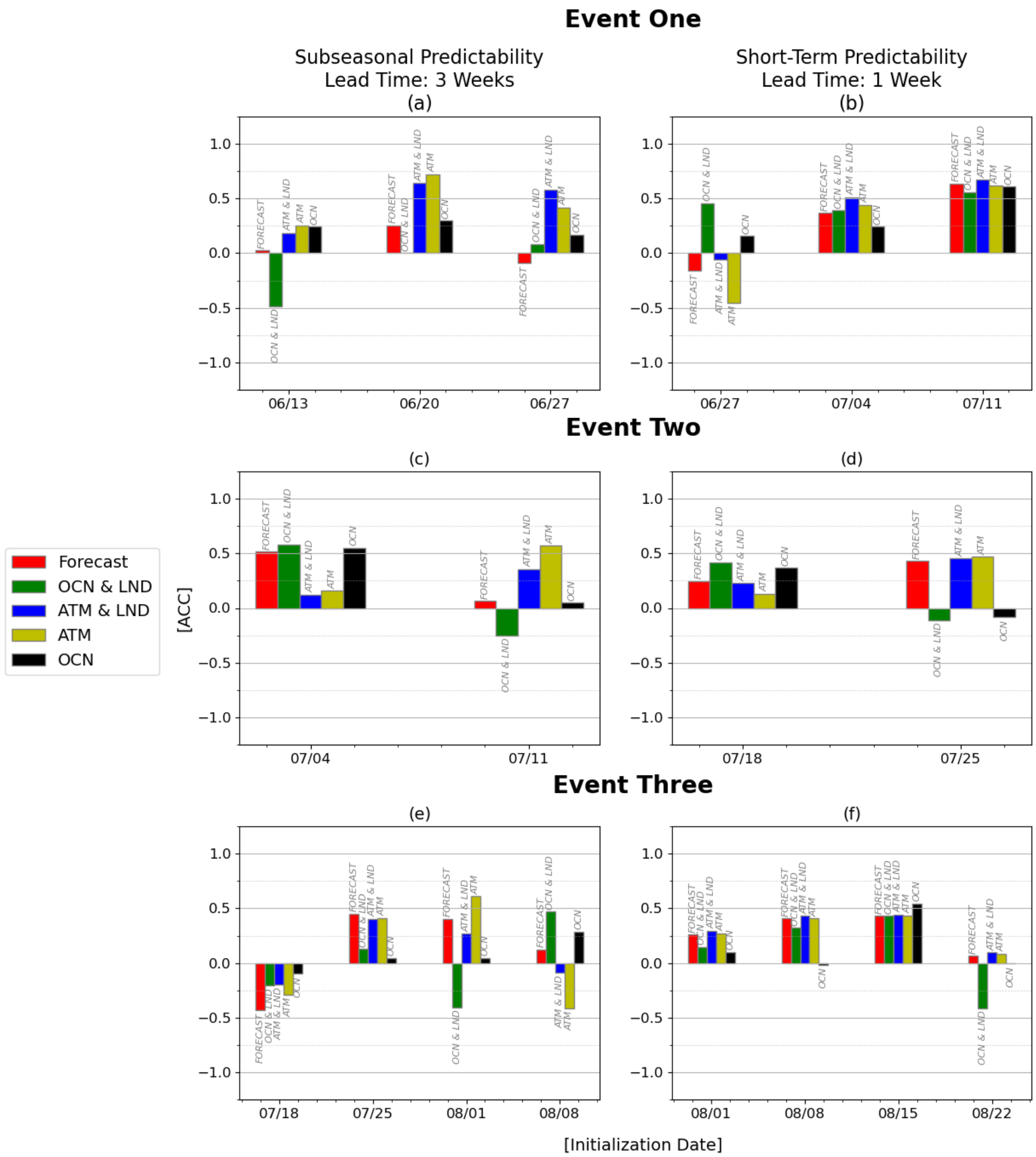


Figure 3.3: ACC of weekly average precipitation observations and ensemble mean of reforecasts and reforecast experiments labeled by the earth system component being isolated over Pakistan (23°- 37.5°N, 60.5° - 77.5°E). Forecast initialization dates with prediction skill for each extreme precipitation event (Event One: top row [a - b], Event Two: middle row [c - d], Event Three: bottom row [e - f]), highlighting subseasonal (week 3: second column) and short-term (week 1: first column) prediction skill.

ACCs. As with Event One, skill improves across most reforecast experiments for short-term lead times (Fig. 3.3f), except during the final week of the event when precipitation returns to normal or below average levels (Fig. 2.1). Experiments isolating the role of land show minimal contribution to skill across all events and initialization dates (not shown).

### 3.1.3 Precipitation Drivers and Mechanisms

To further understand these patterns of skill and their underlying drivers, we start by analyzing vertically integrated moisture flux. Vertically integrated moisture flux is used to assess where moisture is transported into and out of Pakistan. Figure 3.4a shows the net moisture convergence ($F_{\text{NET}}$) and its decomposition along four boundaries surround the country (Fig. 3.4b). Zonal moisture flux is calculated by latitudinally averaging the vertically integrated flux over the western (AB, denoted as $F_W$) and eastern (CD, $F_E$) boundaries. Meridional flux is similarly calculated by longitudinally averaging over the southern (BC, $F_S$) and northern (DA, $F_N$) boundaries. Net moisture convergence is computed as shown in Equation 3.1 following similar methodology of (Chakraborty and Singhai 2021):

$$F_{\text{NET}} = F_W - F_E + F_S - F_N \tag{3.1}$$

Equation 3.1 shows the net moisture convergence ($F_{\text{NET}}$) formula where the "$F_E$," "$F_W$," "$F_N$," and "$F_S$" are vertically integrated moisture flux anomalies latitudinally and longitudinally averaged over four boundaries. Positive $F_{\text{NET}}$ values indicate moisture convergence, proportional to precipitation, while negative values indicate divergence. Figure 3.4a shows positive net moisture convergence across all three events, consistent with the observed precipitation. The component-wise decomposition provides insight into the direction of moisture transport. Event One exhibits strong zonal inflow from the east and outflow to the west. Meridional components are minor, with limited inflow from the south and outflow from the north. Event Two shows weakened

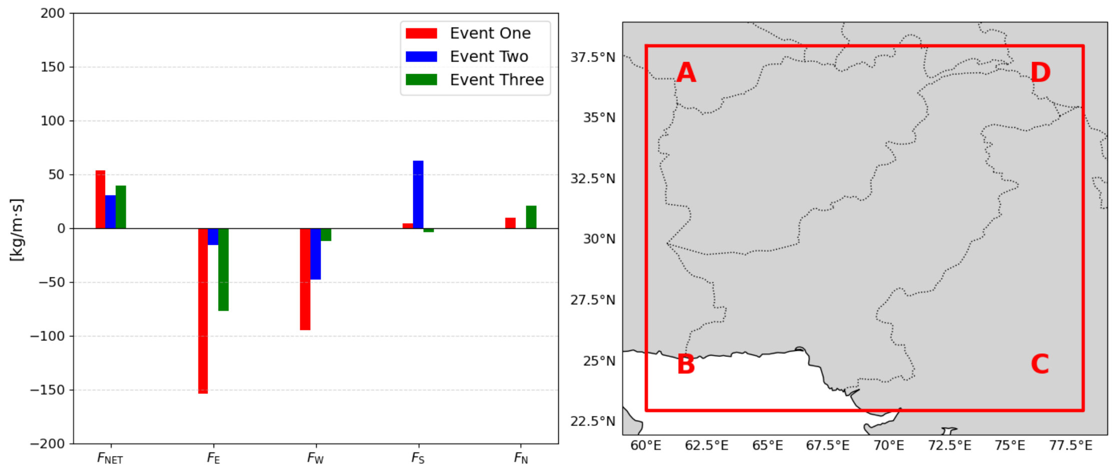


Figure 3.4: (a) Vertically integrated moisture flux anomalies latitudinally and longitudinally averaged over four boundaries (east [$F_E$], west [$F_W$], south [$F_S$], and north [$F_N$]) and net moisture convergence ($F_{\text{NET}}$) averaged over Event One (red bars), Event Two (blue bars), and Event Three (green bars) over (b) region marked ABCD (red box and labels; [23°- 37.5°N, 60.5° - 77.5°E]).

zonal components compared to Event One, but a substantial increase in southerly inflow, suggesting that the primary moisture source shifts from the east to the south. Event Three has similar east-to-west structure to Event One, with minor meridional flux. Like Event One, the zonal components dominate the moisture budget.

These results are further supported by the spatial distribution of weekly average zonal (top row) and meridional (bottom row) vertically integrated moisture flux anomalies (Fig. 3.5). In Event One, strong east-to-west moisture transport is clearly visible (Fig. 3.5a), along with moderate southward inflow that is largely cut off due to strong zonal dominance (Fig. 3.5d). In Event Two, this pattern reverses. Moisture now flows west to east across northern India from Pakistan (Fig. 3.5b), and the previously blocked southern inflow is now open (Fig. 3.5e). Event Three resembles Event One in structure, with easterly inflow and westerly outflow (Fig. 3.5c), while meridional flux (Fig. 3.5f) shows moisture exiting to the south.

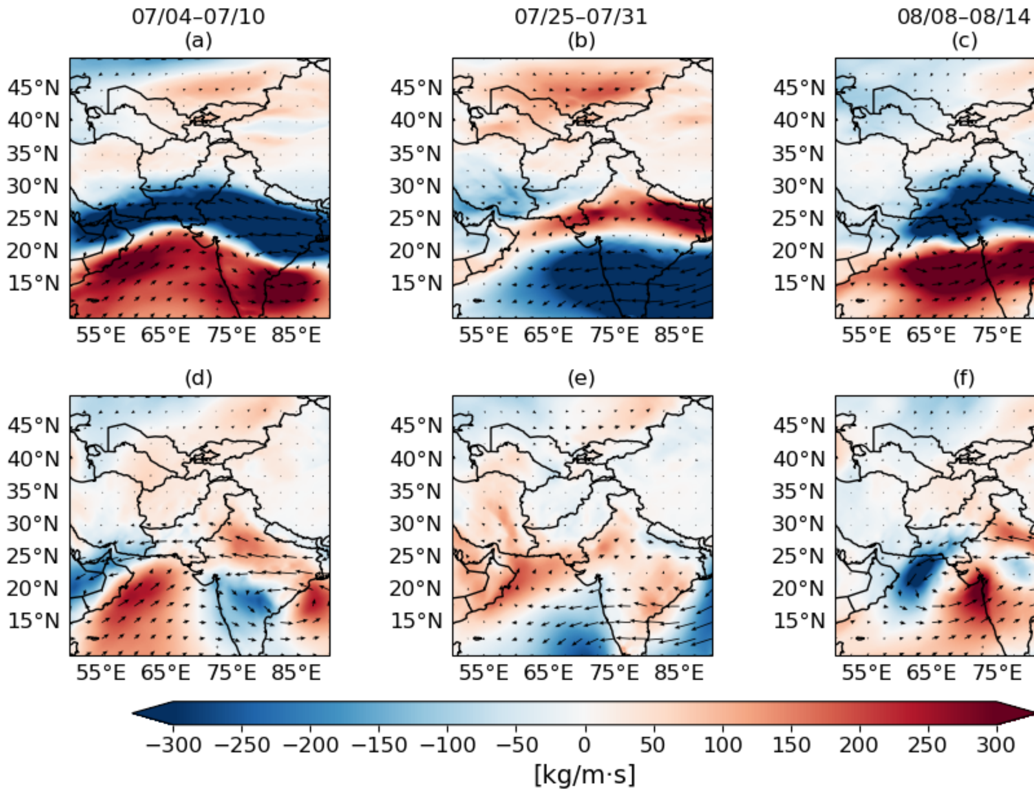


Figure 3.5: Weekly average zonal (top row) and meridional (bottom row) vertically integrated moisture flux anomalies (shading and vectors; kg/m·s) for week in (a and d) Event One (4 – 10 July 2022), (b and e) Event Two (25 – 31 July), and (c and f) Event Three (8 – 14 August).

To begin diagnosing the drivers of the vertically integrated moisture flux, we start by analyzing the role of the South Asian Monsoon. If monsoon surges were the primary contributors, we would expect substantial south-to-north moisture transport into Pakistan during the events. The moisture flux analysis shows that this pattern appears only during Event Two, initially suggesting a potential monsoon influence, in contrast to Events One and Three, where mositure predominantly enters from the east (Fig. 3.4 and Fig. 3.5).

To further evaluate the role of the monsoon in these events, we analyze Hovmöller diagrams of longitudinally averaged outgoing longwave radiation anomalies (60° – 100°E) from 30 May to 17 September 2022 (Fig. 3.6). Negative outgoing longwave radiation anomalies indicate enhanced convection and precipitation, with propagating anomalies signaling monsoon pulses. Two clear monsoon surges are visible during July and August 2022 (Fig. 3.6a). The first begins in early June and reaches Pakistan in early July, aligning with the onset of Event One. The second surge starts in late July and extends into Pakistan by mid-August, overlapping with Event Three. However, no monsoon surge activity is observed during the timing of Event Two. No monsoon surge activity suggests that while the moisture flux direction during Event Two may superficially resemble a monsoon-related pattern, it likely arose from other non-monsoonal mechanisms.

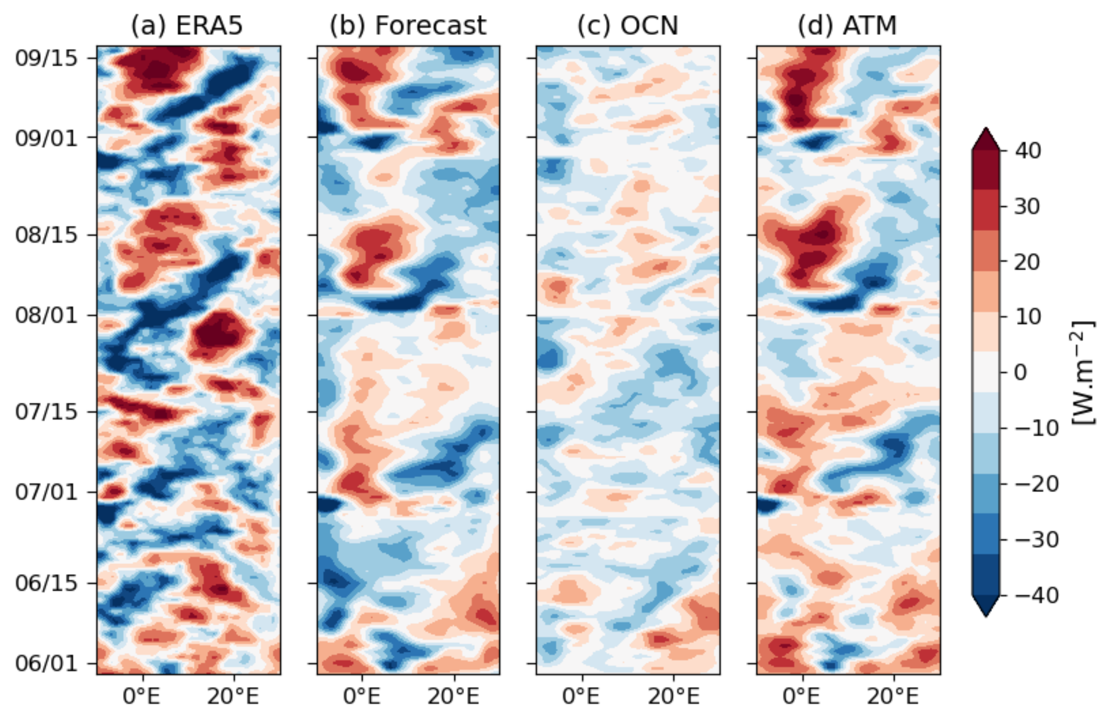


Figure 3.6: Hovmöller diagram of longitudinally averaged outgoing longwave radiation anomalies (shading; $W \cdot m^{-2}$) between $60° - 100°$E for 30 May – 17 September 2022 for (a) reanalysis, (b) ensemble mean reforecasts, and the reforecast experiments isolating the (c) oceanic initial conditions and (d) atmospheric initial conditions contributions initialized on 30 May, 27 June, 1 August, and 29 August.

To ensure that monsoon surges were not the primary drivers even for Events One and Three, despite their timing overlap, we examined the reforecasts and sensitivity experiments. While the reforecast ensemble mean captures the broad features of the monsoon surges (Fig. 3.6b), isolating the atmospheric initial conditions contribution in the reforecast experiments shows that the propagation of negative outgoing longwave radiation anomalies partially re-emerges, particularly for the second surge overlapping with Event Three (Fig. 3.6d). In contrast, the first surge is weakened and initiates north of the equator, lacking the equator-to-land propagation that would characterize a robust monsoon event. Because the atmospheric initial conditions-only contribution most clearly captures the monsoon surges, we would expect that if these surges were major drivers of precipitation, there would be a corresponding increase in atmospheric initial conditions contribution to precipitation predictability during their occurrence.

However, comparing this timing with the actual precipitation skill results reveals a mixed picture. In Event One, for instance, the atmospheric initial conditions contribution to predictive skill is inconsistent within the event and at times even negative surrounding early July initialization dates (Fig. 3.3a and Fig. 3.3b), suggesting that the first surge did not have a substantial impact on rainfall predictability. In Event Three, the second monsoon surge coincides with some increased atmospheric initial conditions contribution in the precipitation reforecasts surrounding late July – early August initialization dates (Fig. 3.3e and Fig. 3.3f), but the moisture flux patterns show east-to-west transport, and even northerly transport out of Pakistan's southern boundary, rather than the expected south-to-north influx typical of monsoon activity. This divergence in moisture pathways indicate that other processes, rather than monsoon surges, likely dominated the extreme rainfall in these events.

Overall, while the moisture flux patterns suggest that the monsoon may have played a role in Event Two, and while the outgoing longwave radiation analysis initially hints at monsoon surges for Events One and Three, multiple lines of evidence, including reforecast experiments and detailed moisture transport pathways, consistently show that the monsoon was not a primary driver for any of the events.

The east-west moisture transport, particularly in Events One and Three, appears to be driven by zonal wind anomalies. During Event One, anomalous easterly winds south of the Tibetan Plateau dominate (Fig. 3.7a), acting as the primary transport mechanism. In Event Two, this pattern reverses. Anomalous westerlies appear over northern India (Fig. 3.7b), disrupting the prior flow. Event Three reverts to the Event One pattern, with easterly winds reestablishing the transport from east to west (Fig. 3.7c). The Somali Jet also plays a role. It is strongest during Event One (Fig. 3.7d), providing some southerly moisture transport. It becomes increasingly localized along the coast during Event Two (Fig. 3.7e), aligning with the reversal of large-scale zonal winds and contributing to the moisture flux from the south. The jet is at its weakest in Event Three, consistent with limited moisture transport from the south and the presence of northerly outflow.

### 3.1.4 Primary Driver Predictability and Mechanisms

In addition to evaluating precipitation predictability, we assess the predictability of 850 hPa zonal wind anomalies over South Asia and the Indian Ocean Basin using ACC, since this feature is considered a primary driver of precipitation in these events (Fig. 3.8). Across all three events, the unaltered forecast at a one-week lead time consistently outperforms the subseasonal forecasts. This result is expected due to the shorter lead time however, this contrast with precipitation skill (Fig. 3.3), where even short-lead forecasts often lacked consistency. Importantly, subseasonal skill for 850 hPa zonal wind improves progressively from Event One to Event Three. For Event One, unaltered forecasts show low skill, with ACC decreasing across successive initialization

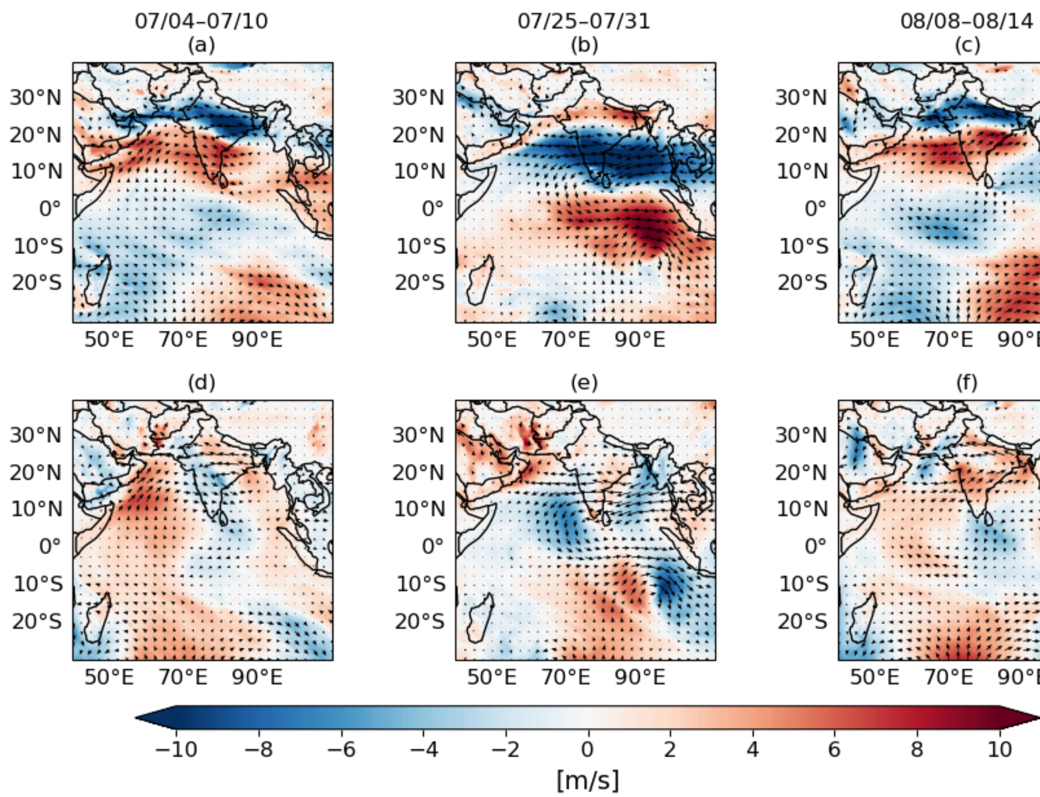


Figure 3.7: Weekly average zonal (top row) and meridional (bottom row) 850 hPa wind anomalies (shading and vectors; m/s) for week in (a and d) Event One (4 – 10 July 2022), (b and e) Event Two (25 – 31 July), and (c and f) Event Three (8 – 14 August).

dates (Fig. 3.8a). Event Two demonstrates moderate improvement (Fig. 3.8c), despite having only two initialization dates. Event Three shows the highest and most consistent skill among the events (Fig. 3.8e).

The reforecast experiments provide additional insight into the sources of predictability for the zonal wind anomalies. For Event One, while subseasonal predictions are generally inconsistent within the event, the atmospheric initial conditions-only experiment for the 20 June initialization stands out (Fig. 3.8a). It yields nearly double the ACC compared to the unaltered and oceanic initial conditions-only experiments, suggesting a strong atmospheric initial conditions contribution, especially at shorter lead times. For Event Two, consistent with the precipitation predition skill results, oceanic initial

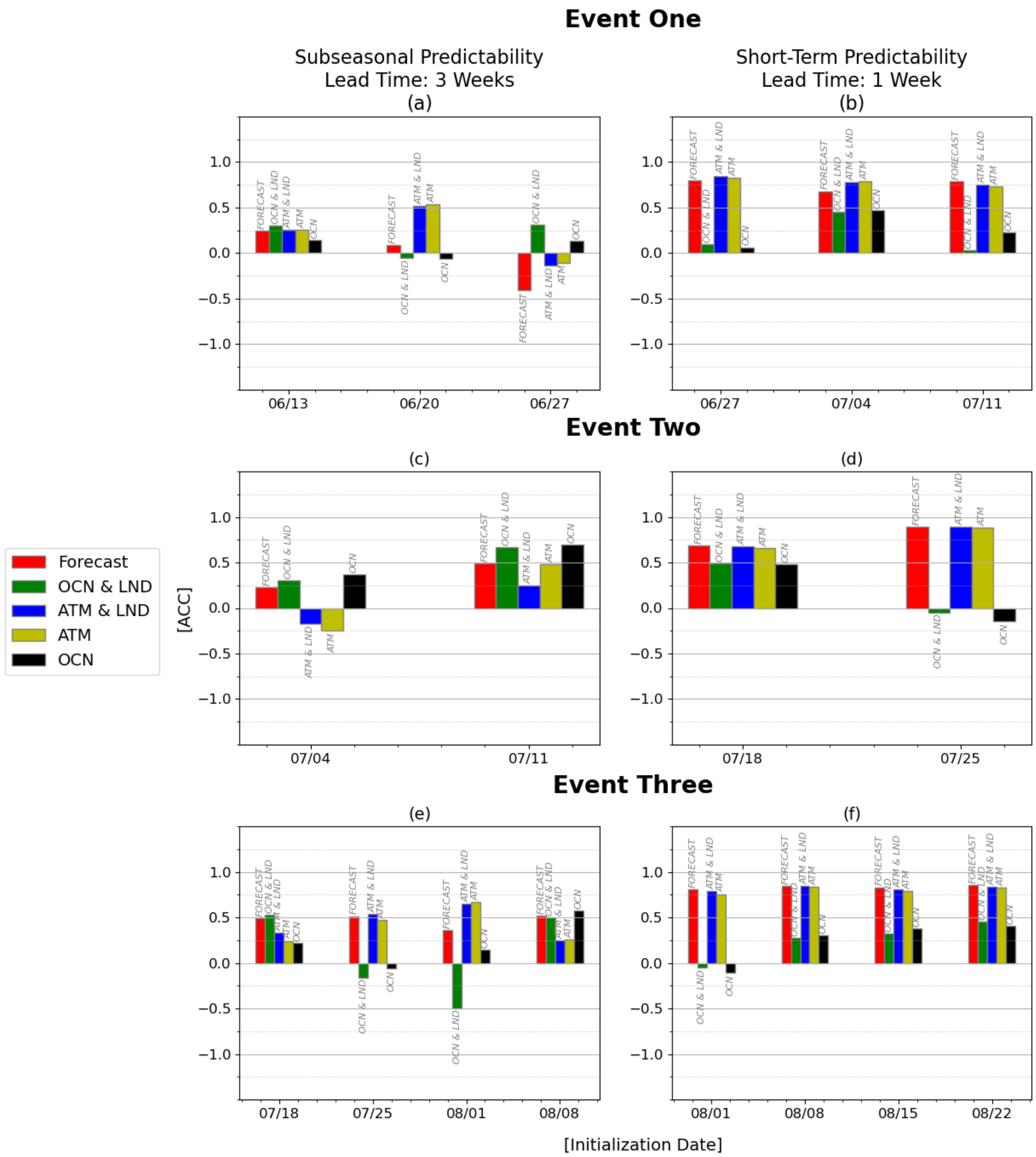


Figure 3.8: ACC of weekly average 850 hPa zonal wind reanalysis and ensemble mean reforecasts and reforecast experiments labeled by the earth system component being isolated over the Indian Ocean Basin (30°S - 40°N, 40° - 110°E). Forecast initialization dates with prediction skill for each extreme precipitation event (Event One: top row [a - b], Event Two: middle row [c - d], Event Three: bottom row [e - f]), highlighting subseasonal (week 3: second column) and short-term (week 1: first column) prediction skill.

conditions contribution to skill increase, while the role of the atmospheric initial conditions diminish (Fig. 3.8c). This trend is visible across all initialization dates except

25 July, where atmospheric initial conditions contribution to skill is relatively higher (Fig. 3.8d). Event Three resembles Event One in structure, showing a resurgence in atmospheric initial conditions contribution to prediction skill. The atmospheric initial conditions-only experiments yield strong positive ACCs, while the oceanic initial conditions-only experiments perform poorly, with some initialization dates showing negative ACCs (Fig. 3.8e). The short-term forecasts further support this pattern, with the unaltered and atmospheric initial conditions-only reforecasts consistently achieving high positive ACCs (Fig. 3.8f).

Overall, 850 hPa zonal wind anomalies were more skillfully predicted than precipitation across all reforecasts and experiments. However, the relative contributions, assessed subjectively, of atmospheric and oceanic initial conditions processes to forecast skill followed a consistent pattern across both variables with the atmospheric initial conditions dominating skill during Events One and Three and the oceanic initial conditions playing a larger role during Event Two. To better understand this reversal in sources of skill during Event Two, especially given the improved performance of the oceanic initial conditions-only experiments, we analyze weekly average sea surface temperature anomalies for key weeks during each event (Fig. 3.9).

During Event One, widespread negative sea surface temperature anomalies were observed in the Arabian Sea (Fig. 3.9a), particularly along the coasts of Somalia and Oman. These colder-than-average waters likely resulted from enhanced upwelling driven by a stronger Somali Jet (Fig. 3.7d). We hypothesize that these cooler sea surface temperatures weakened the meridional temperature gradient over South Asia, which in turn may have contributed to the development of anomalous easterly winds south of the Tibetan Plateau. The presence of this strong anomalous easterly wind redirected the Somali Jet to take a more westerly path over southern India, feeding into the anomalous easterly flow over the Bay of Bengal (Fig. 3.7a).

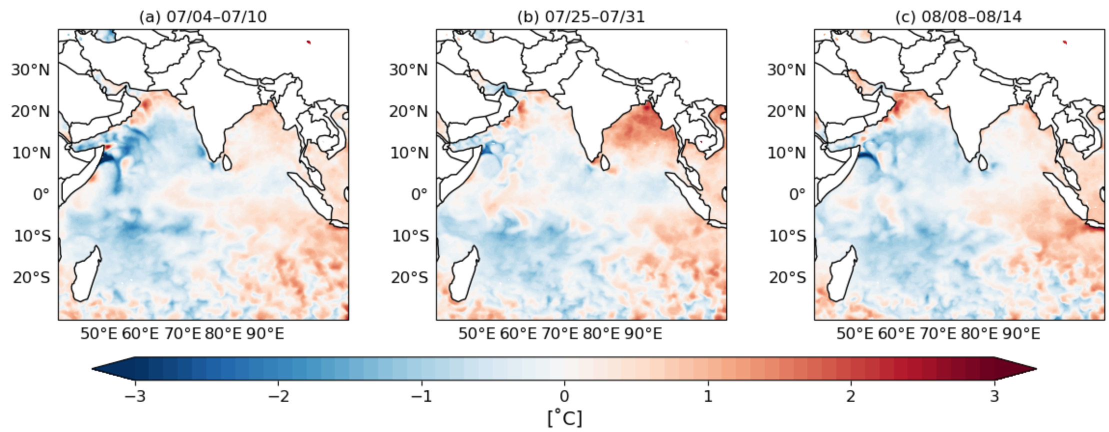


Figure 3.9: Weekly average sea-surface temperature anomalies (shading; °C) for week in (a) Event One (4 – 10 July 2022), (b ) Event Two (25 – 31 July), and (c) Event Three (8 – 14 August).

In contrast, during Event Two, the Somali Jet became more localized along the coastline (Fig. 3.7e), potentially reducing upwelling and contributing to warmer sea surface temperatures in the Arabian Sea (Fig. 3.9b). This warming may have helped restore the typical westerly flow south of the Tibetan Plateau, allowing moisture from the Somali Jet to be transported northward into Pakistan. Additionally, a substantial increase in positive sea surface temperature anomalies in the Bay of Bengal may have further influenced this shift in wind patterns. Supporting this interpretation, Figure 3.10b shows positive outgoing longwave radiation anomalies over both the Arabian Sea and Bay of Bengal, indicating increased solar insolation and subsequent sea surface temperature warming. In contrast, negative outgoing longwave radiation anomalies dominate the Bay of Bengal and Arabian Sea during Events One and Three, consistent with cooler sea surface temperatures and cloudier, convective conditions (Fig. 3.10a and Fig. 3.10c).

During Event Three, although the Somali Jet was at its weakest (Fig. 3.7f), it became more spatially widespread, resembling the pattern in Event One. This Somali Jet pattern, combined with negative outgoing longwave radiation anomalies (Fig. 3.10c),

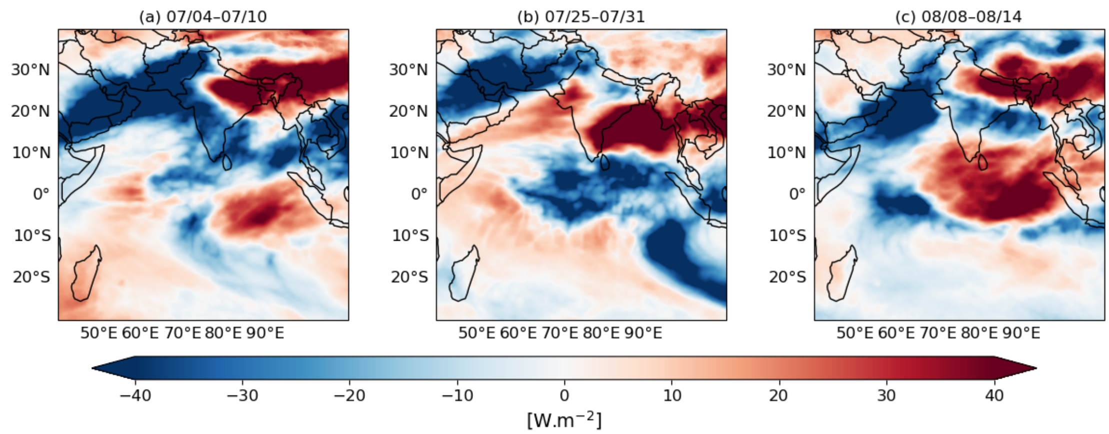


Figure 3.10: Weekly average outgoing longwave radiation anomalies (shading; $W \cdot m^{-2}$) for week in (a) Event One (4 – 10 July 2022), (b) Event Two (25 – 31 July), and (c) Event Three (8 – 14 August).

likely contributed to the resurgence of cooler sea surface temperatures in the Arabian Sea (Fig. 3.9c). these conditions would again weaken the meridional temperature gradient, allowing for a return of anomalous easterly flow south of the Tibetan Plateau. Additionally, the Bay of Bengal Sea surface temperatures returned to near-neutral or weakly positive anomalies, further supporting a shift back to the wind pattern observed in Event One.

### 3.1.5 Key Takeaways of Pakistan Study

In our analysis of the 2022 Pakistan floods, we found that the precipitation predictive skill varied by week, with limited consistency overall. The reforecast experiments revealed that the atmospheric initial conditions primarily governed skill for Events One and Three, while oceanic initial conditions influences played a heightened role in Event Two. By leveraging these reforecast experiments, we identified the anomalous easterly wind south of the Tibetan Plateau as a key driver of Events One and Three. In contrast, for Event Two, changes in sea surface temperature disrupted this easterly wind pattern, enabling the Somali Jet to transport moisture into Pakistan from the south.

## 3.2 Peru

### 3.2.1 Precipitation Overview

In January through May 2017, as well as in February, March, and April of 2023, Peru experienced anomalous precipitation that impacted the country's infrastructure, affecting hundreds of thousands of people, and led to long-term consequences, including public health risks. Figure 3.11a presents the annual average precipitation anomaly for January to May, spanning the period from 1981 to 2023. The years 2017 and 2023 stand out with higher positive anomalies compared to other years, particularly in contrast to the earlier part of the time series. The linear trend line highlights this positive trend.

Figure 3.11b and 3.11c display the daily average precipitation anomalies for 2017 and 2023, respectively. In both years, precipitation in this region exhibited high day-to-day variability. Although periods of below average precipitation did not have strongly negative values, periods of above average precipitation were substantial but short-lived. On days with above average precipitation, daily averages reached 10 to 15 mm. In early March 2023, Cyclone Yaku occurred (Fig. 3.11c, orange shading), contributing to nearly 15 mm above normal rainfall. Other days in the same period also reached similar daily average rainfall anomalies as high as 10mm, even in the absence of a tropical cyclone (Fig. 3.11c).

The spatial distribution of above-average precipitation was widespread during both events (Fig. 3.12), but week-to-week variability was also evident. In 2017, above average precipitation progressed from the northern provinces and southern coastal

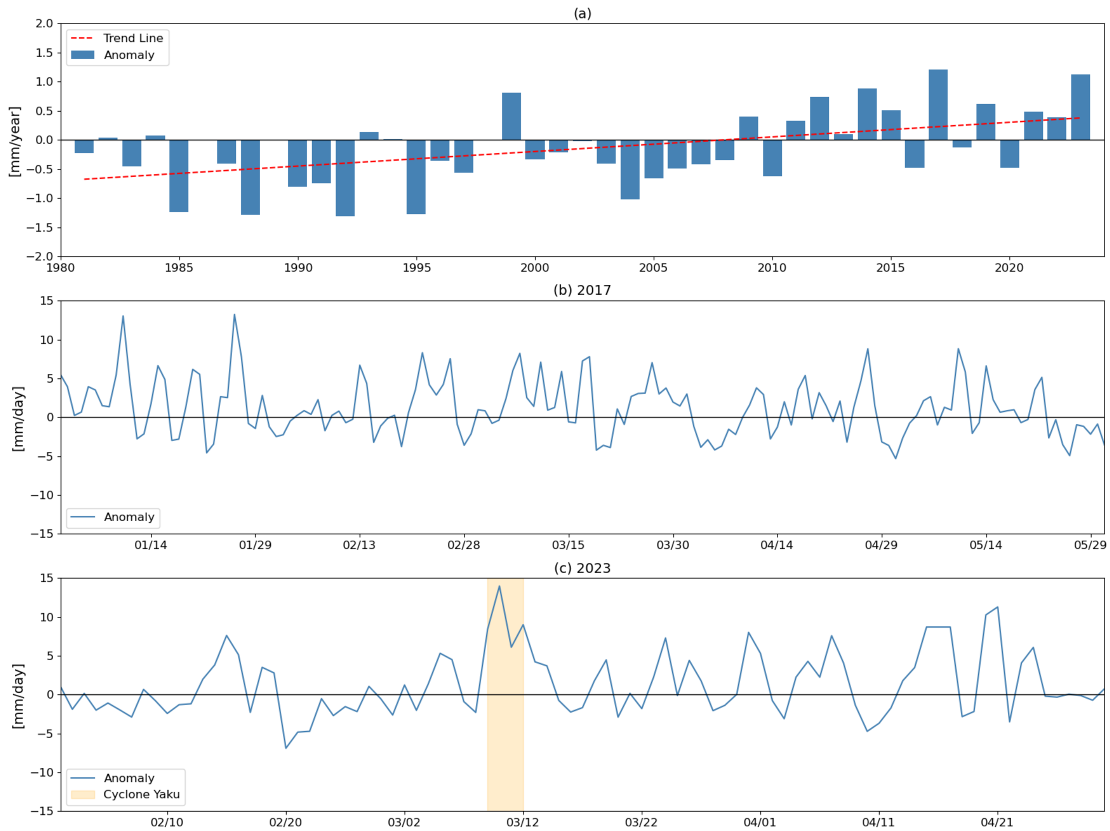


Figure 3.11: (a) January – May annual average precipitation anomaly for 1981 – 2023 (blue bars; mm/year) and linear trend line (red, dashed). Daily average precipitation anomaly (blue, solid; mm/day) for (b) January – May 2017 and (c) February – April 2023 with Cyclone Yaku contribution (orange shading).

regions in early January (Fig. 3.12a), to central inland Peru in early February (Fig. 3.12b), to widespread areas including the northern coast in early March (Fig. 3.12c). It then shifted to the Ecuadorian coast in early April (Fig. 3.12d) and finally became widespread again across the Ecuadorian coast and inland Peru in early May (Fig. 3.12e).

Above average precipitation in 2023 also showed high spatial variability. In late January to early February, it mainly impacted southern provinces (Fig. 3.12f). In late February to early March, it shifted to the north (Fig. 3.12g). In late March to early April, it became widespread with higher amplitude along the northern coast (Fig.

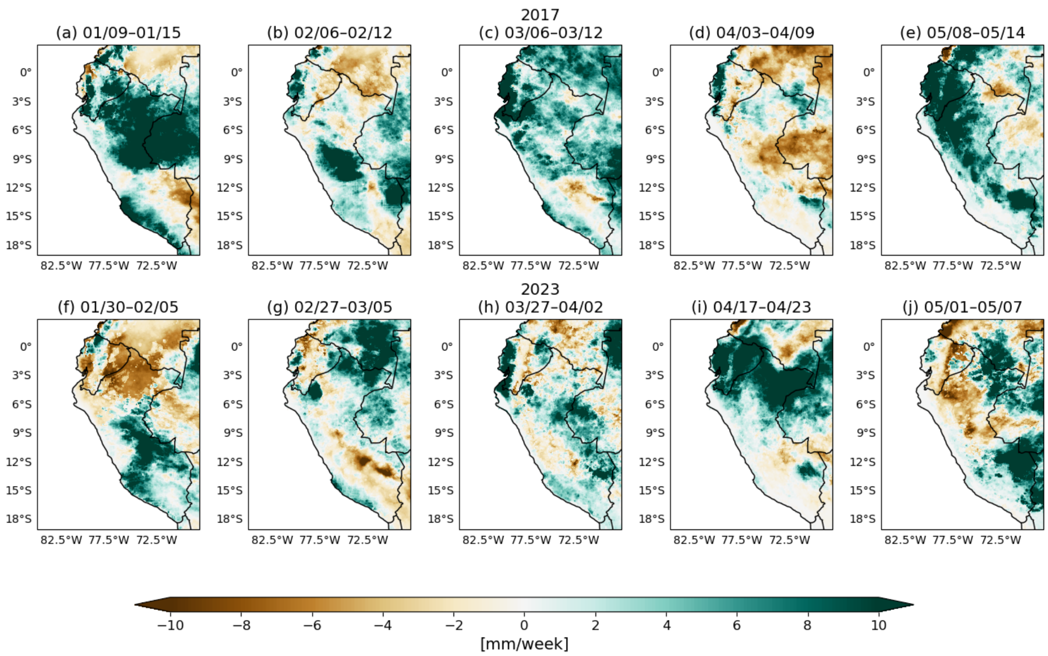


Figure 3.12: Weekly average precipitation anomaly (shading; mm/week) for weeks in 2017 (top row; (a) 1 – 15 January, (b) 6 – 12 February, (c) 6 – 12 March, (d) 3 – 9 April, and (e) 8 – 14 May) and 2023 (bottom row; (f) 30 January – 5 February, (g) 27 February – 5 March, (h) 27 March – 2 April, (i) 17 – 23 April, and (j) 1 – 7 May) Coastal El Niño events.

3.12h). In mid-April, it was concentrated in the north (Fig. 3.12i), and in early May, both the south and the north experienced above average precipitation (Fig. 3.12j). Another notable feature during these periods was the presence of areas with strong below average precipitation, particularly evident in early April 2017 (Fig. 3.12d), late January to early February 2023 (Fig. 3.12f), and early May 2023 (Fig. 3.12j).

### 3.2.2 Precipitation Predictability

Both the subseasonal and short-term prediction skill of the spatial pattern of the precipitation anomalies for 2017 are shown in Figure 3.13. Due to data availability, we focused specifically on January, February, and March, the first three months of the precipitation, to investigate the predictability and the main sources driving it. Reforecasts used were initialized weekly between 19 December and 27 March. Given previous studies suggesting that oceanic conditions could be key drivers of these events (Echevin et al. 2018; Garreaud 2018; Peng et al. 2019; Son et al. 2020; Peng et al. 2024), we aimed to isolate the roles of the atmospheric initial conditions-only and oceanic initial conditions-only contributions for both the 2017 and 2023 events. As a result, our analysis centered on these two types of experiments.

For 2017, we found that the model performed poorly on both the subseasonal and short-term timescales. High variability in reforecast skill from week to week within each month indicated inconsistency, and in general, the model showed little skill in forecasting the spatial pattern of the precipitation anomalies. This model performance was reflected in negative or near-zero ACC values overall. There are instances of short-term skill with positive ACCs that exceeded those of the subseasonal forecasts, particularly for the initialization dates of 30 January, 13 February, and 20 February (Fig. 3.13b and Fig. 3.13d).

As expected, the atmospheric initial conditions-only and oceanic initial conditions-only reforecast experiments generally mirrored the performance of the unaltered reforecast. When the unaltered reforecast performed poorly, the experiments did too. However, for the cases where the unaltered reforecasts performed well, the experiments provided insights on sources of predictability. During January and February, when the unaltered reforecast showed positive ACCs (indicating some skill), the oceanic initial conditions-only experiments also performed well, exceeding the ACCs of the atmospheric initial conditions-only experiments. This oceanic initial condition-only contribution to skill was evident for the 19 December, 2 January, 16 January, and 6 February initialization dates for the subseasonal lead-times (Fig. 3.13a and Fig. 3.13c), and for

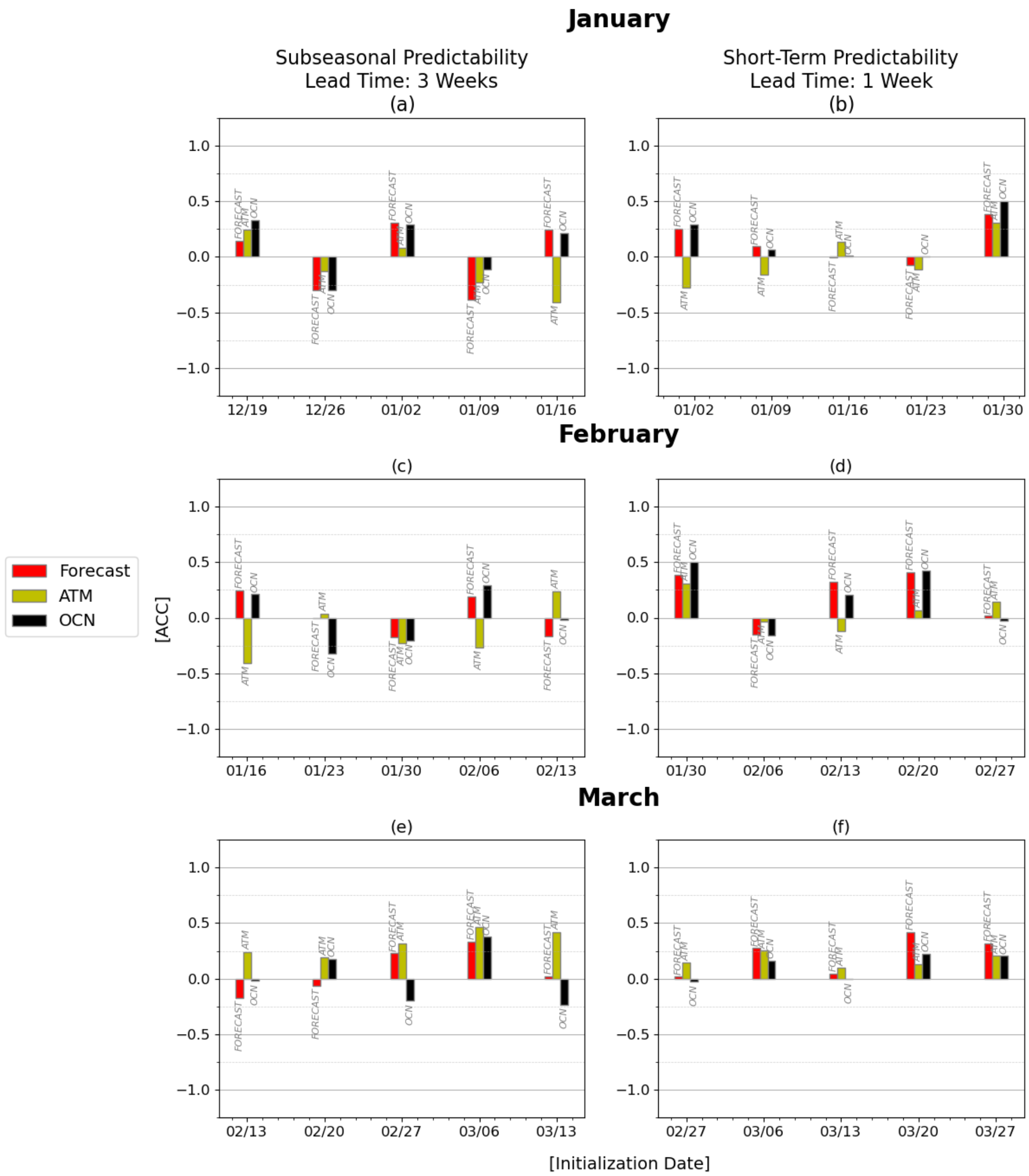


Figure 3.13: ACC of weekly average 2017 precipitation observations and ensemble mean of reforecasts and reforecast experiments labeled by the earth system component being isolated over Pakistan (23°- 37.5°N, 60.5° - 77.5°E). Forecast initialization dates with prediction skill for first three months of the 2017 Coastal El Niño event (January: top row [a - b], February: middle row [c - d], March: bottom row [e - f]), highlighting subseasonal (week 3: second column) and short-term (week 1: first column) prediction skill.

the 2 January, 9 January, 30 January, 13 February, and 20 February initialization dates in the short-term lead-times (Fig. 3.13b and Fig. 3.13d).

However, this pattern shifted for March. The atmospheric initial conditions-only experiments often outperformed the oceanic initial conditions-only experiments when the unaltered reforecast also performed well. This atmosphere initial condition-only contribution to skill was seen in the 27 February, 6 March, and 13 March initialization dates for both the subseasonal skill (Fig. 3.13e) and the short-term skill (Fig. 3.13f).

For 2023, we assessed ACCs for the entire precipitation period, again analyzing the atmospheric initial conditions-only and oceanic initial conditions-only contributions (Fig. 3.14). Reforecasts used for 2023 were initialized between 16 January and 24 April. The model performed markedly better in 2023 that in 2017 across both timescales. The forecasts showed increased consistency (except for subseasonal lead-times in February) and higher, positive ACCs, some exceeding 0.5. Notable examples include the 27 March initialization for subseasonal lead-times (Fig. 3.14e) and the 30 January and 20 February initializations for short-term lead-times (Fig. 3.14b), with other dates also approaching these high ACC values.

Similar to 2017, the oceanic initial conditions-only contributions typically outperformed the atmospheric initial conditions-only contributions across most weeks in 2023. This oceanic initial conditions-only contribution to skill was especially apparent in the short lead-times for February and March (Fig. 3.14b and Fig. 3.14d). This result is particularly striking because it runs counter to the typical expectation. The ocean, with its slower variability, usually contributes more to the skill at longer (subseasonal) lead times, while the atmosphere, with its faster-changing state, is generally more important for shorter lead times. The fact that the oceanic initial conditions-only contributions dominated even in the short-term forecasts suggests that oceanic conditions

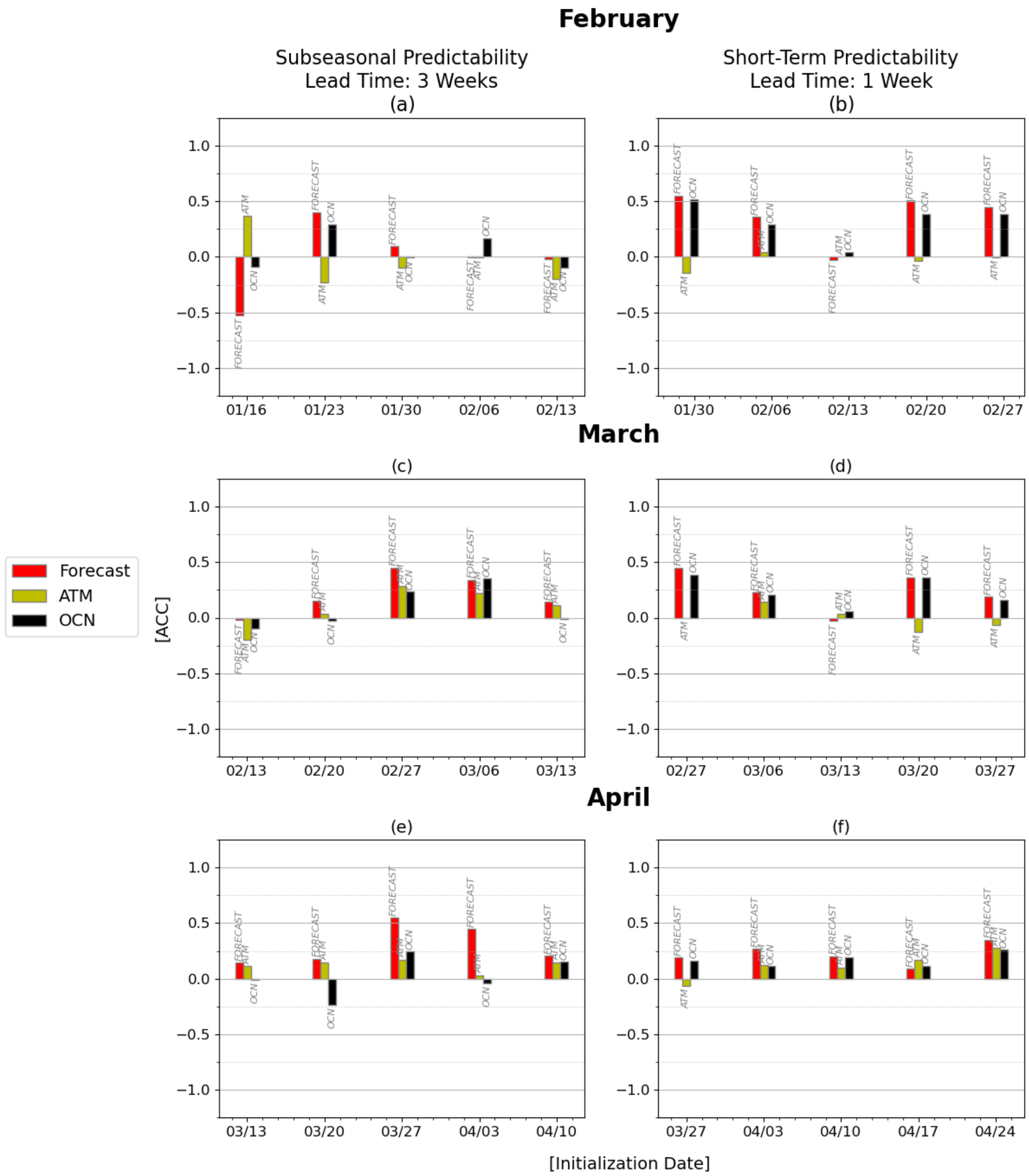


Figure 3.14: ACC of weekly average 2023 precipitation observations and ensemble mean of reforecasts and reforecast experiments labeled by the earth system component being isolated over Pakistan (23°- 37.5°N, 60.5° - 77.5°E). Forecast initialization dates with prediction skill for the three months of the 2023 Coastal El Niño event (February: top row [a - b], March: middle row [c - d], April: bottom row [e - f]), highlighting subseasonal (week 3: second column) and short-term (week 1: first column) prediction skill.

played a larger role than the atmosphere in driving the anomalous precipitation during both 2017 and 2023.

### 3.2.3 Drivers and Mechanisms of the 2017 and 2023 Precipitation Events

Between January and May 2017 and February and April 2023, sea surface temperature anomalies in the Niño 1+2 region were substantially above average. Figure 3.15 shows the January – May annual average sea surface temperature anomaly from 1940 to 2023. The years 1983 and 1998, related to well-documented strong basin-scale El Niño events, recorded the highest sea surface temperature anomalies for the entire period by a significant margin. Although these two years stand out, the annual average sea surface temperature anomalies for 2017 and 2023 remain notably positive compared to most other years. These more recent years even surpass the anomalies following 1998, an anomaly that is often used as a benchmark for understanding extreme Niño 1+2 sea surface temperatures. Despite the shorter period of warming in 2023 (February – April), the average sea surface temperature anomaly for January through May still exceeds that of 2017.

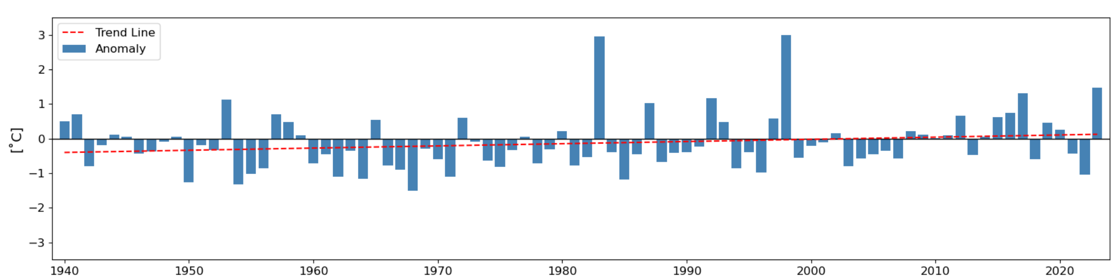


Figure 3.15: January - May annual average Niño 1+2 (0° - 10°S, 90°W - 80°W) sea surface temperature anomaly for 1940 – 2023 (blue bars; °C) and linear trend line (red, dashed).

Given the reforecast experiment outcomes, we hypothesize that the above average sea surface temperatures along the Peruvian and Ecuadorian coasts in the Niño 1+2 region is a driver of both the 2017 and 2023 events. The spatial distribution of sea surface temperature anomalies during these events also differs markedly (Fig. 3.16). In 2017, sea surface temperatures surrounding the Niño 1+2 region were above average and stronger positive anomalies were largely confined to the Ecuadorian coast and northern Peru. These localized anomalies developed and dissipated between early January and early May.

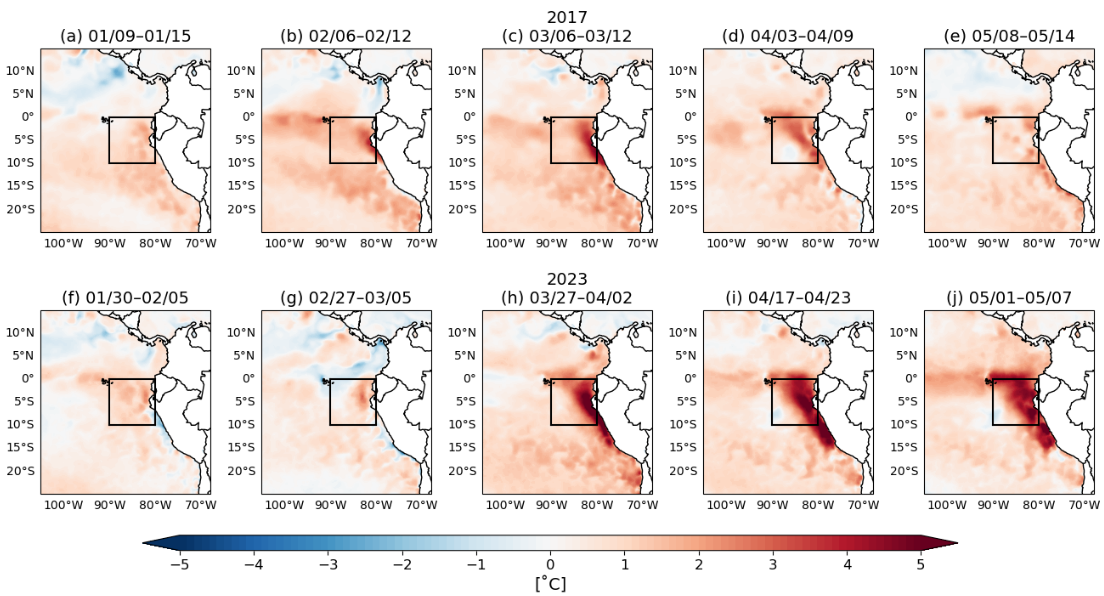


Figure 3.16: Weekly average sea surface temperature anomaly (shading; °C) for weeks in 2017 (top row; (a) 1 – 15 January, (b) 6 – 12 February, (c) 6 – 12 March, (d) 3 – 9 April, and (e) 8 – 14 May) and 2023 (bottom row; (f) 30 January – 5 February, (g) 27 February – 5 March, (h) 27 March – 2 April, (i) 17 – 23 April, and (j) 1 – 7 May) Coastal El Niño events. Black box displays the Niño 1+2 region (0°-10°S, 90°W-80°W).

In contrast, during the 2023 event, positive sea surface temperature anomalies emerged in January in the Niño 1+2 region, while below average sea surface temperatures persisted along the southern Peruvian coast south of the Niño 1+2, a residual from a basin-scale La Niña (Fig. 3.16f). This pattern persisted through much of February, with above average sea surface temperatures in the Niño 1+2 region intensifying and becoming more concentrated along the northern Peruvian and Ecuadorian coasts (Fig. 3.16g). In March, these above average sea surface temperature anomalies rapidly expanded along the coast, extending south of the Niño 1+2 region (Fig. 3.16h). In April, the anomalies continued expanding westward with consistent or even increased positive sea surface temperature anomalies (Fig. 3.16i). By May, the onset of a basin-scale El Niño led to the positive sea surface temperature anomalies along the coast becoming less localized and extending father westward into the Pacific Ocean basin (Fig. 3.16j).

Further, complicating the 2017 event's precipitation was the presence of the ITCZ, which we hypothesize was supported by the warming sea surface temperatures. Figure 3.17 shows the development of the ITCZ using weekly average outgoing longwave radiation anomalies. It began to develop in late January to early February, as indicated by a steady stream of negative outgoing longwave radiation anomalies, signifying increased convection, into the Niño 1+2 region. The ITCZ actively fed moisture and convection, ultimately enhancing precipitation in Peru and Ecuador (Fig. 3.17b).

In early March, enhanced convergence of anomalous northerly and southerly winds into the Niño 1+2 region (Fig. 3.18c) further intensified the ITCZ and supported coastal sea surface temperature warming. The strengthened ITCZ is shown by increasingly negative outgoing longwave radiation anomalies in Figure 3.17c. We hypothesize that this strengthening of convection contributed to a greater atmospheric initial conditions-only contribution to precipitation skill for March (Fig. 3.14e and Fig. 3.14f). By April the ITCZ begins to weaken and break down (Fig. 3.17d) as the anomalous winds (Fig. 3.18d) and sea surface temperature anomalies (Fig. 3.16d) start to diminish. Given that Figures 3.17f – j showed limited negative outgoing longwave radiation

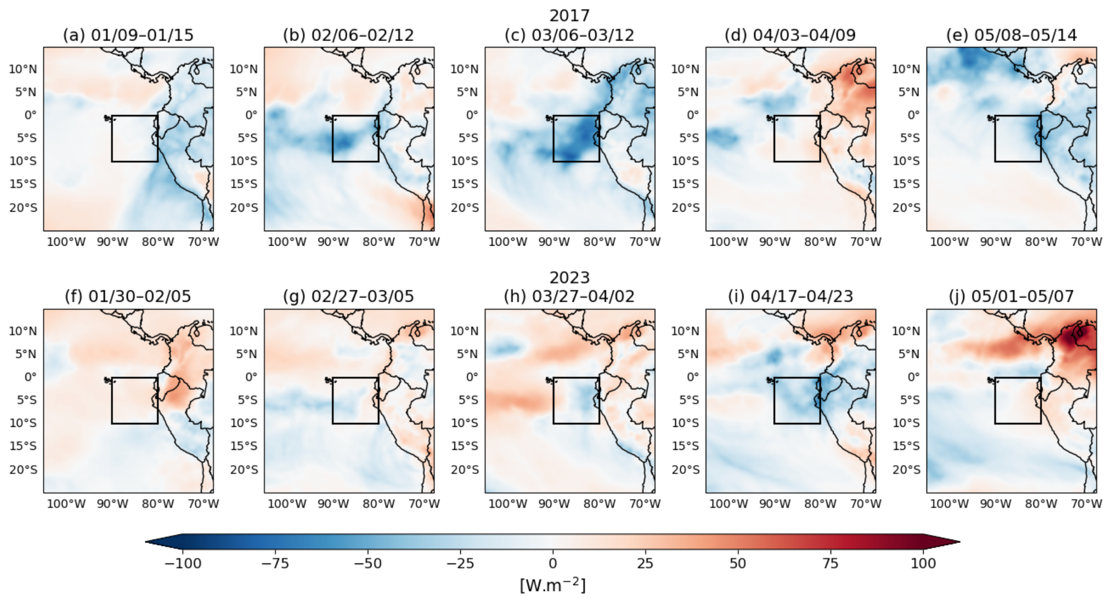


Figure 3.17: Weekly average outgoing longwave radiation anomaly (shading; $W \cdot m^{-2}$) for weeks in 2017 (top row; (a) 1 – 15 January, (b) 6 – 12 February, (c) 6 – 12 March, (d) 3 – 9 April, and (e) 8 – 14 May) and 2023 (bottom row; (f) 30 January – 5 February, (g) 27 February – 5 March, (h) 27 March – 2 April, (i) 17 – 23 April, and (j) 1 – 7 May) Coastal El Niño events. Black box displays the Niño 1+2 region (0°-10°S, 90°W-80°W).

anomalies, and therefore convection, being fed into the Niño 1+2 region, Ecuador, and northern Peru, it was determined that the ITCZ was not a primary contributor of the 2023 precipitation.

The anomalous low level meridional winds were a consistent feature in both the 2017 and 2023 events. In both cases, the onset of coastal warming was typically associated with anomalous northerly winds flowing into the Niño 1+2 region. This wind pattern can be seen in early January 2017 (Fig. 3.18a). In March 2017, this feature strengthened (Fig. 3.18c) as previously discussed with the intensification of the ITCZ (Fig. 3.17c). By early April, the anomalous northerly winds began to weaken, while anomalous southerly winds south of the Niño 1+2 region began to shift and feed into the area of interest (Fig. 3.18d). This transition coincided with the decrease in sea surface temperature anomalies along the coast (Fig. 3.18d). North of the Niño

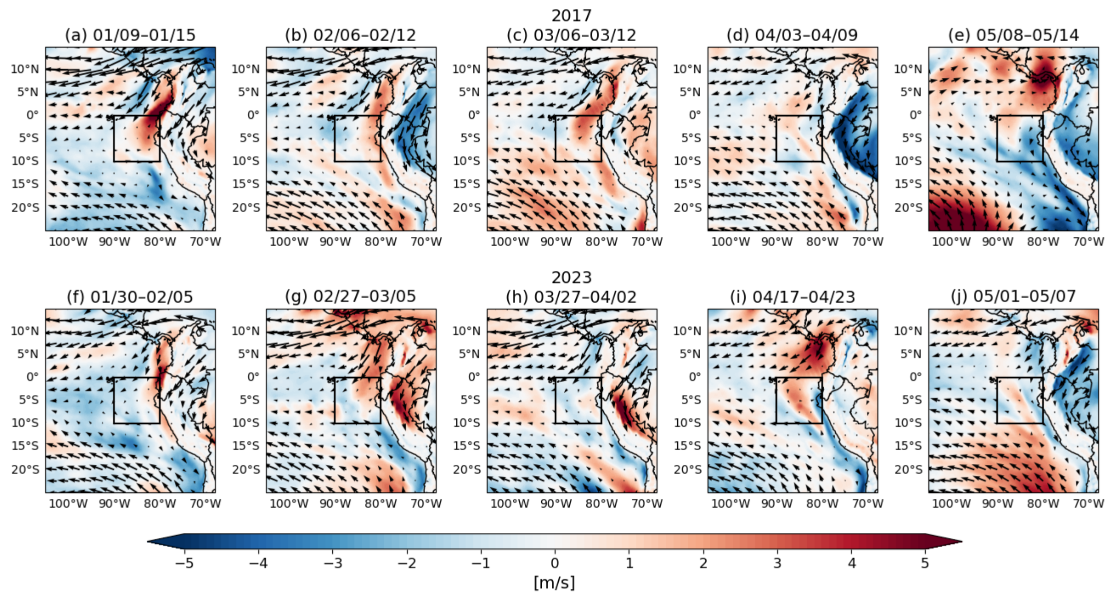


Figure 3.18: Weekly average 850 hPa meridional wind anomaly (shading; m/s) and raw wind (vectors; m/s) for weeks in 2017 (top row; (a) 1 – 15 January, (b) 6 – 12 February, (c) 6 – 12 March, (d) 3 – 9 April, and (e) 8 – 14 May) and 2023 (bottom row; (f) 30 January – 5 February, (g) 27 February – 5 March, (h) 27 March – 2 April, (i) 17 – 23 April, and (j) 1 – 7 May) Coastal El Niño events. Black box displays the Niño 1+2 region (0°-10°S, 90°W-80°W).

1+2 region, the anomalous northerly winds disappear in May, replaced by anomalous southerly winds. Enhanced southerlies also develop southwest of the Niño 1+2 region, marking the end of the 2017 coastal sea surface temperature warming event.

In 2023, the onset of the anomalous northerly winds and coastal sea surface temperature warming occurred in late January to early February (Fig. 3.18f). The link between northerly flow and sea surface temperatures was notable, particularly during the selected week in late February to early March, when a decrease in northerly winds into the Niño 1+2 region (Fig. 3.18g) corresponded with cooler sea surface temperatures north of the Niño 1+2 region (Fig. 3.16g). The northerly winds persisted through March and early April (Fig. 3.18h). In mid-April, the anomalous northerly flow weakened (Fig. 3.18i). In early May, although there was a slight return of northerly winds during this selected week, there was also an increase in anomalous southerly flow into the Niño 1+2 region (Fig. 3.18j), leading to a slight reduction in sea surface temperatures as they expanded westward, marking the first month of a basin-scale El Niño event (Fig. 3.18j).

### 3.2.4 Key Takeaways of Peru Study

For Peru, we found that the extreme precipitation events in 2017 and 2023 were predicted with varying degrees of skill. Predictive skill improved substantially in 2023 compared to 2017, with precipitation forecasts extending up to three weeks in advance. Our reforecast experiments indicate that the primary sources of the model skill in both events were linked to the ocean, except for March 2017, when enhanced atmospheric initial conditions contribution, likely related to the strengthening of the ITCZ, played a significant role. Overall, the heightened role of the oceanic initial conditions in driving skill led us to identify the Coastal El Niño as the main driver of the extreme precipitation in both 2017 and 2023, although the ITCZ also contributed in 2017 and Cyclone Yaku played a role in 2023.

# Chapter 4

# Coastal El Niño

## 4.1 Coastal El Niño as a Driver of Precipitation Extremes

The coastal sea surface temperature warming experienced in 2017 and 2023 is known as a phenomenon called Coastal El Niño where the sea surface temperatures warm substantially along the coast of northern Peru and Ecuador, specifically in the Niño 1+2 region. Using the criteria previously outlined, all Coastal El Niño events from 1940 to 2023 are summarized in Table 4.1. This table lists the event year and start month, duration, peak linearly detrended three-month running mean sea surface temperature anomaly, and the linkages to basin-scale ENSO phases, defined by the Niño 3.4 region. As discussed previously, the Coastal El Niño events included in this analysis are those that occurred outside of a concurrent basin-scale El Niño event.

Given that the 2023 Coastal El Niño event followed a basin-scale La Niña, we aimed to understand whether this sequence is typical of other Coastal El Niño events. Specifically, we wanted to explore whether Coastal El Niño events more broadly tend to be linked to basin-scale El Niño or La Niña conditions. To examine linkages between basin-scale El Niño events, we identified events that were directly preceded by a basin-scale El Niño. To qualify, there had to be consecutive months in which one month was classified as a basin-scale El Niño and the next as a Coastal El Niño, with no overlap.

| Event | Year | Start Month | Length | Max SST Anom | Preceded by | Followed by | Coincided with |
|---|---|---|---|---|---|---|---|
| 1 | 1943 | May | 4 | 0.82 | La Niña | | |
| 2 | 1944 | Mar | 3 | 0.69 | | | |
| 3 | 1944 | Jul | 4 | 0.84 | | | |
| 4 | 1945 | Mar | 11 | 1.57 | | | La Niña |
| 5 | 1949 | Mar | 3 | 0.69 | | | |
| 6 | 1963 | Jun | 4 | 0.93 | | | |
| 7 | 1969 | Oct | 3 | 0.63 | | | |
| 8 | 1972 | Feb | 3 | 1.05 | La Niña | El Niño | |
| 9 | 1976 | May | 10 | 1.19 | La Niña | | |
| 10 | 1979 | May | 8 | 0.63 | | | |
| 11 | 1980 | Mar | 3 | 0.52 | | | |
| 12 | 1983 | Jun | 7 | 4.26 | El Niño | | La Niña |
| 13 | 1993 | Mar | 8 | 0.85 | | | |
| 14 | 1998 | May | 5 | 2.77 | El Niño | | La Niña |
| 15 | 2008 | Mar | 7 | 1.08 | | | La Niña |
| 16 | 2011 | May | 3 | 0.53 | La Niña | | |
| 17 | 2012 | Mar | 5 | 1.14 | | | La Niña |
| 18 | 2014 | May | 5 | 1.09 | | El Niño | |
| 19 | 2017 | Jan | 5 | 1.52 | | | |
| 20 | 2023 | Feb | 3 | 2.02 | La Niña | El Niño | |

Table 4.1: Summary of Coastal El Niño events including their year, initialization month, length (months), maximum linearly detrended three month running mean sea surface temperature (SST) anomaly (°C), and linkages to basin-scale ENSO phases.

Events where this pattern occurred include 1983 and 1998. The same approach was used to identify cases where a basin-scale El Niño event directly followed a Coastal El

Niño event, marked in the "Followed by" column. This pattern was observed in 1972, 2014, and 2023.

We also documented basin-scale La Niña events that were linked to Coastal El Niño events. Coastal El Niño events that were preceded by a basin-scale La Niña occurred in 1943, 1972, 1976, 2011, and 2023, more frequently than events preceded by a basin-scale El Niño. There were no cases of a basin-scale La Niña event following a Coastal El Niño. Another noteworthy finding was that some Coastal El Niño events overlapped with a basin-scale La Niña event. This overlap occurred in the 1945, 1983, and 1998 events, where a basin-scale La Niña began during the Coastal El Niño. Additionally, the 2008 and 2012 Coastal El Niño events started during an ongoing basin-scale La Niña. Overall, nearly half of the Coastal El Niño events occurred independently of any basin-scale ENSO phase.

Understanding the seasonality of Coastal El Niño is crucial because it can help communities prepare for its impact. By knowing when, and for how long, these disruptive events are most likely to occur, this information allows for timely alerts and better planning, reducing the damage. Coastal El Niño events typically begin during the Southern Hemisphere fall. March saw the highest number of events (seven), followed by May (six). Fewer events occurred in February and June (two each), and there was one event each in January, July, and October. The duration of these events tended to be short with seven events lasting three months, three lasting four months, and four lasting five months. A few events had longer durations, with two events each lasting seven and eight months, and one event each lasting 10 and 11 months. We observe a slight decrease in event duration over time, especially in the second half of events where event duration is more frequently over four months.

Finally, the peak sea surface temperature anomalies varied widely. The highest anomaly was observed in the 1983 event (4.26°C), while the lowest was in 1980 (0.52°C).

The 2017 and 2023 events both exceeded the average anomaly of 1.24°C, with values of 1.52°C and 2.02°C, respectively.

To better understand the modes of variability in the Niño 1+2 sea surface temperature region and the spatial patters of variables most strongly correlated with this variability, we conducted an EOF analysis on monthly mean sea surface temperature anomalies over the region (Fig. 4.1; 0°-10°S, 90°W-80°W).

Specifically, this analysis focuses on sea surface temperature anomalies within the Niño 1+2 region to examine the nature of variability within this area, whether surrounding areas exhibit coherent behavior, and how these patterns influence or are influenced by adjacent variables. EOF analysis enables us to isolate dominant patterns of sea surface temperature variability and quantify the proportion of total variance each mode explains.

Figures 4.1a and 4.1b display regressions of SST anomalies and 850 hPa wind anomalies (Fig. 4.1a), and precipitation anomalies (Fig. 4.1b), onto the standardized first principle component (PC1), which represent the leading mode of variability. This first mode explains 90.7% of the total variance, indicating that it captures the most significant and coherent signal in the SST anomalies.

The leading mode reveals that when sea surface temperature anomalies in the Niño 1+2 region are positive, surrounding sea surface temperatures in the eastern Pacific are also generally positive, though this pattern does not extend beyond 120°W. West of this longitude, sea surface temperature anomalies tend to be opposite that in the eastern Pacific. This sea surface temperature pattern is accompanied by eastward low-level wind anomalies in the central-eastern Pacific (Fig. 4.1a) and increased precipitation along the coasts of Ecuador and northern Peru (Fig. 4.1b).

Figure 4.1c shows the standardized Niño 1+2 sea surface temperature index along with its nine-month running mean. Red markers on the PC1 time series indicate the

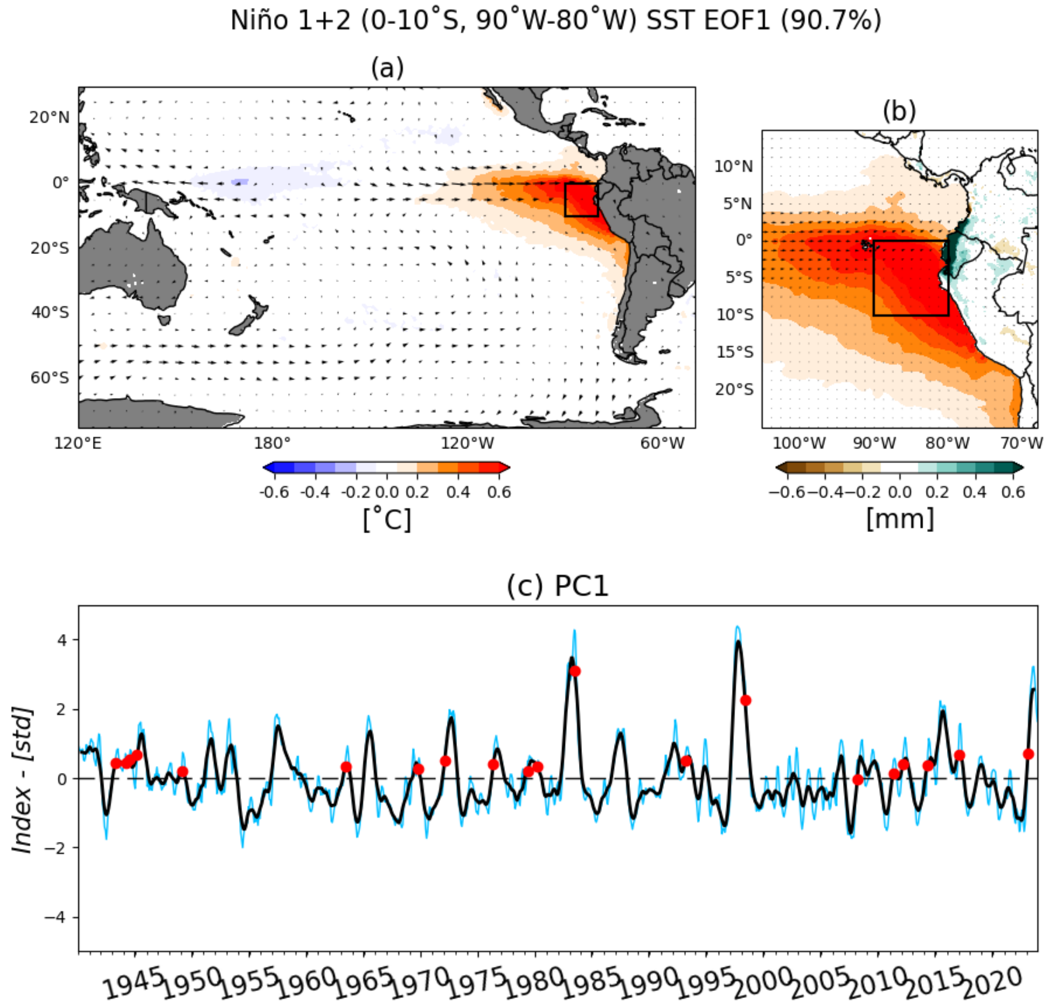


Figure 4.1: (a) Regression of 1981 – 2023 SST anomalies (shading, °C), and 850 hPa wind anomalies (vectors, m s-1) onto the leading EOF mode (1981 – 2023). Domain for EOF analysis shown (black box: 0°-10°S, 90°W-80°W). (b) Same as (a), with precipitation anomalies (green/brown shading, mm). (c) Standardized Niño 1+2 SST index (blue) with nine-month running mean (black); red points mark Coastal El Niño onset months (1940 – 2023).

onset months of each Coastal El Niño event, as summarized in Table 4.1 and defined in the methodology. Because PC1 represents the dominant mode of variability, the time series primarily captures low frequency changes. The Niño 1+2 index varies on multiple timescales, with certain periods dominating. As shown in Figure 4.1c, Coastal

El Niño events tend to occur in episodic bursts, separated by multi-year lulls or periods of relative inactivity, suggesting a non-uniform temporal distribution.

To investigate the localized sea surface temperature and precipitation relationships more closely, correlation analysis between precipitation anomalies over Peru and Ecuador and Niño 1+2 sea surface temperatures was performed (Fig. 4.2). Positive correlations indicate increased precipitation with warmer SSTs, while negative correlations reflect decreased precipitation. Stippling marks statistically significant correlations ($p < 0.1$), determined using bootstrapping with 5,000 samples and replacement. Inland areas are dominated by moderate negative correlations ranging between, with some non-significant positive patches near the Colombia and Brazil borders approximately between 0.1 and 0.2 in terms of correlation coefficient. Significant positive correlations appear along the coast in a similar pattern as the precipitation anomaly regression in Figure 4.1b with correlation coefficients over 0.3. Inland, additional significant regions of moderate negative correlation are located in southern Peru, Brazil, and Colombia with correlation coefficients around -0.3. Although the above average precipitation over the course of the 2017 and 2023 events was variable and widespread (Fig. 3.12), the above average precipitation along the northern Peruvian and Ecuadorian coasts was consistent with the statistically significant positive correlation in Figure 4.2. This above average precipitation along the northern Peruvian and Ecuadorian coasts is linked to the warmer sea surface temperatures in the Niño 1+2 region with the significance supporting that this relationship is robust.

To get a sense of how the magnitude and variability of Coastal Niño events has shifted over the decades we assess how average sea surface temperature anomalies have changed over time during each Coastal El Niño event. Figure 4.3a shows detrended three-month running mean SST anomalies over the Niño 1+2 region during each Coastal El Niño event from 1940 – 2023 (20 events total). Before 1980, average

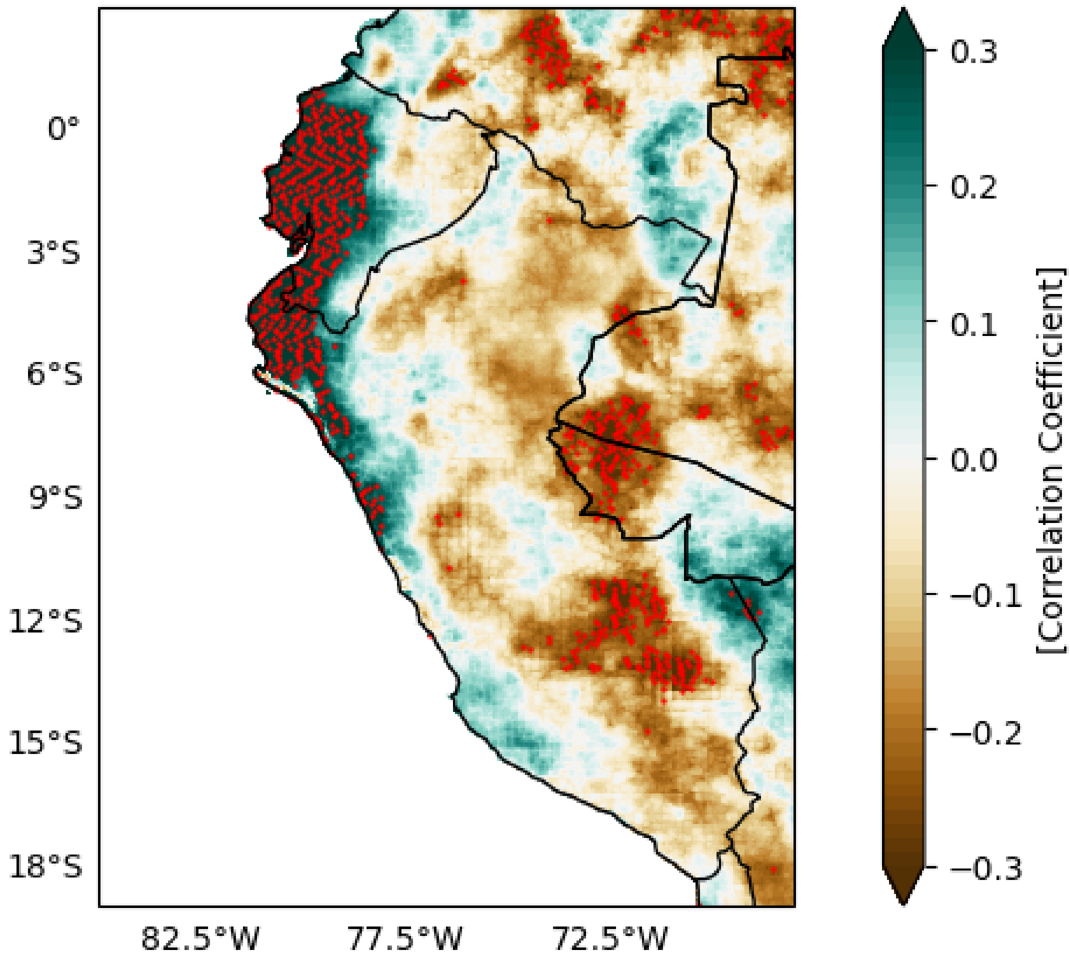


Figure 4.2: Correlation (shading) between precipitation anomalies in Peru and Ecuador (19°S – 3°S, 85°W – 68°W) and Niño 1+2 SST (0°-10°S, 90°W-80°W). Red stippling indicates significance at $p < 0.1$ based on bootstrapping.

SST anomalies remained below 2°C with low variability between events. After 1980, both the average sea surface temperature anomalies and their variability increased, highlighted by the 1983 event with the highest anomalies and largest range. From 2011 to 2023, a slight upward trend in average, maximum, and range of sea surface temperature anomalies is evident indicating overall warmer Coastal El Niño events in the later period (1981 – 2023) compared to earlier decades. Of the 20 Coastal El Niño events, precipitation data are available for the last nine (1981 – 2023). Figure 4.3b shows that early events (1983, 1993, 1998, and 2008) had near-zero or below – average precipitation anomalies. Since 2011, precipitation anomalies have been consistently positive and show an increasing trend, along with a growing range between maximum and minimum anomalies.

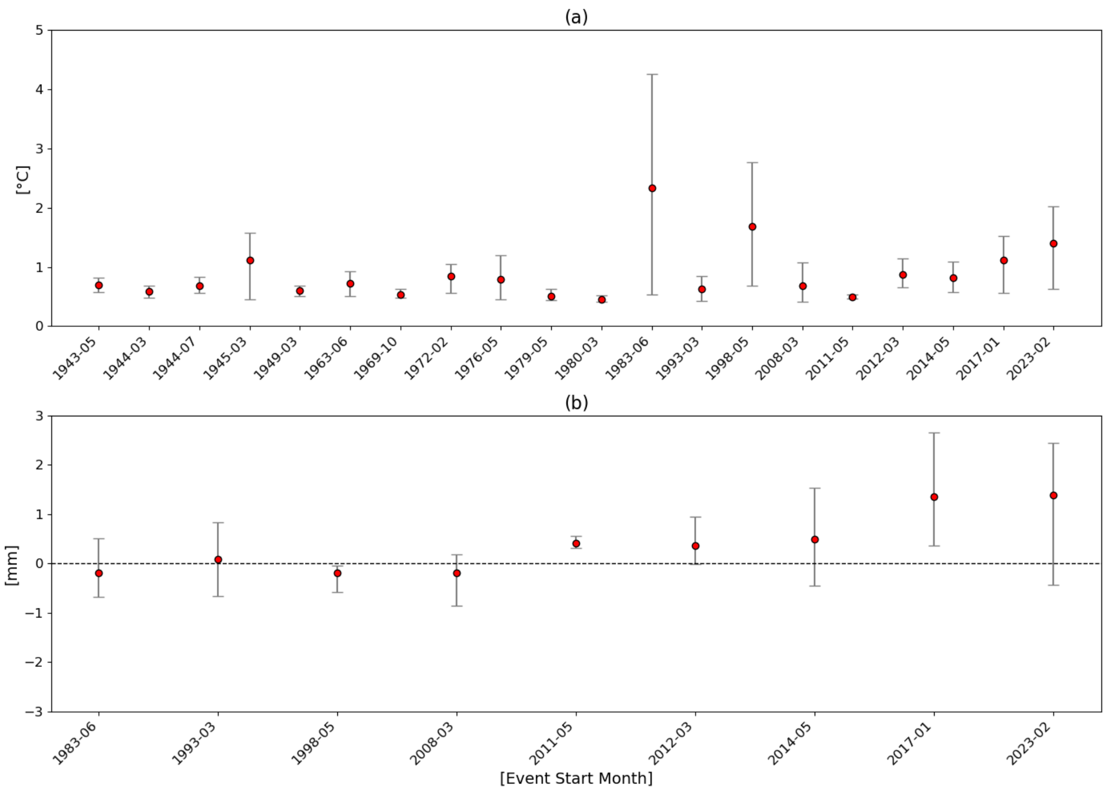


Figure 4.3: (a) Detrended three-month running mean Niño 1+2 SST anomalies (red dots, °C) during Coastal El Niño events (0°-10°S, 90°W-80°W; 1940 – 2023) with error bars showing event-specific minima and maxima. (b) Average precipitation anomalies (red dots, mm) over Peru and Ecuador (19°S – 3°S, 85°W – 68°W; 1981 – 2023) for each event, with error bars indicating range.

Composite averages of precipitation anomalies over Peru and Ecuador (19°S – 3°S, 85°W – 68°W) are shown to understand how precipitation anomalies vary and compare amongst various ENSO phases. Figure 4.4 shows composite averages during Coastal El Niño (Fig. 4.4a), basin-scale El Niño (Fig. 4.4b), and basin-scale La Niña events (Fig. 4.4c). Figure 4.4a shows that during Coastal El Niño events, widespread positive precipitation anomalies dominate northern Peru, Ecuador, and Colombia with small negative anomalies in southern Peru and near the Peru-Colombia border. Basin-scale El Niño (Fig. 4.4b) features more localized coastal positive anomalies, while negative anomalies prevail inland, particularly in eastern Ecuador. Basin-scale La Niña (Fig. 4.4c) shows a reversed pattern, with coastal negative anomalies and inland positive anomalies across Peru, Ecuador, and Colombia.

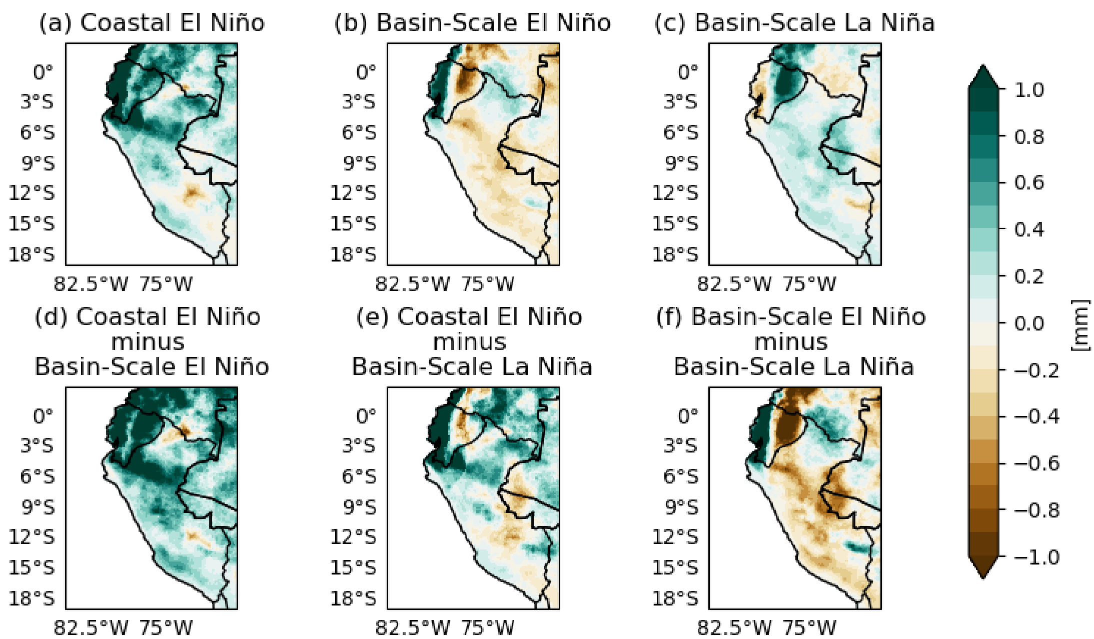


Figure 4.4: Composite precipitation anomalies over Peru and Ecuador (19°S – 3°S, 85°W – 68°W) during (a) Coastal El Niño, (b) basin-scale El Niño, and (c) basin-scale La Niña periods. Composite differences shown between (d) Coastal El Niño and basin-scale El Niño, (e) Coastal El Niño and basin-scale La Niña, and (f) basin-scale El Niño and La Niña.

Composite differences between event types are shown in Figures 4.4d-f to compare precipitation patterns across ENSO phases. The composite difference plots highlight contrasts between event types. Figure 4.4d shows predominantly positive precipitation differences, indicating wetter conditions during Coastal El Niño compared to basin-scale El Niño, with negative differences in southern Peru and along the Colombia border. In Figure 4.4e, Coastal El Niño also appears wetter than basin-scale La Niña, especially along the Ecuadorian and northern Peruvian coasts and parts of Colombia and Brazil, though the pattern is less widespread. Figure 4.4f shows basin-scale El Niño is wetter along the northern Peru-Ecuador coast and the Peru- Colombia border, while La Niña brings wetter conditions to southern Peru, eastern Ecuador, and western Colombia.

To better understand precipitation during Coastal El Niño events after 1980, precipitation indices (Table 2.2) were analyzed using precipitation observations. Figure 4.5a shows the approximate length of the Coastal El Niño events and reinforces there being a slight decrease in event duration over time. Although the absolute number of wet days (Fig. 4.5b) declines, the proportion of wet days relative to the event length increases. Similarly, both the maximum 1-day and 5-day precipitation totals (Fig. 4.5c and Fig. 4.5d) show upward trends in magnitude and contribution to total event rainfall. Climatology lines indicate that these maximum precipitation values increasingly exceed average conditions during Coastal El Niño events.

Extreme precipitation indices (R95p, R99p, R10mm, and R20mm) confirm that Coastal El Niño events are associated with heavy rainfall in the region. While total precipitation from days exceeding the 95th and 99th percentiles show no clear trend, these days contribute substantially to event totals (Fig. 4.5e and Fig. 4.5f), with climatology indicating above-average values during events. The number of days exceeding 10 mm and 20 mm (Fig. 4.5g and Fig. 4.5h) shows slight increases, especially for R10mm, which also accounts for a growing share of total precipitation. Climatological baselines for R10mm and R20mm are zero, emphasizing the impact of Coastal El Niño. Finally, CWD show a slight increase (Fig. 4.5i), with 2017 and 2023 events featuring continuous rainfall, while CDD show no clear trend but reflect prolonged wet periods during these events.

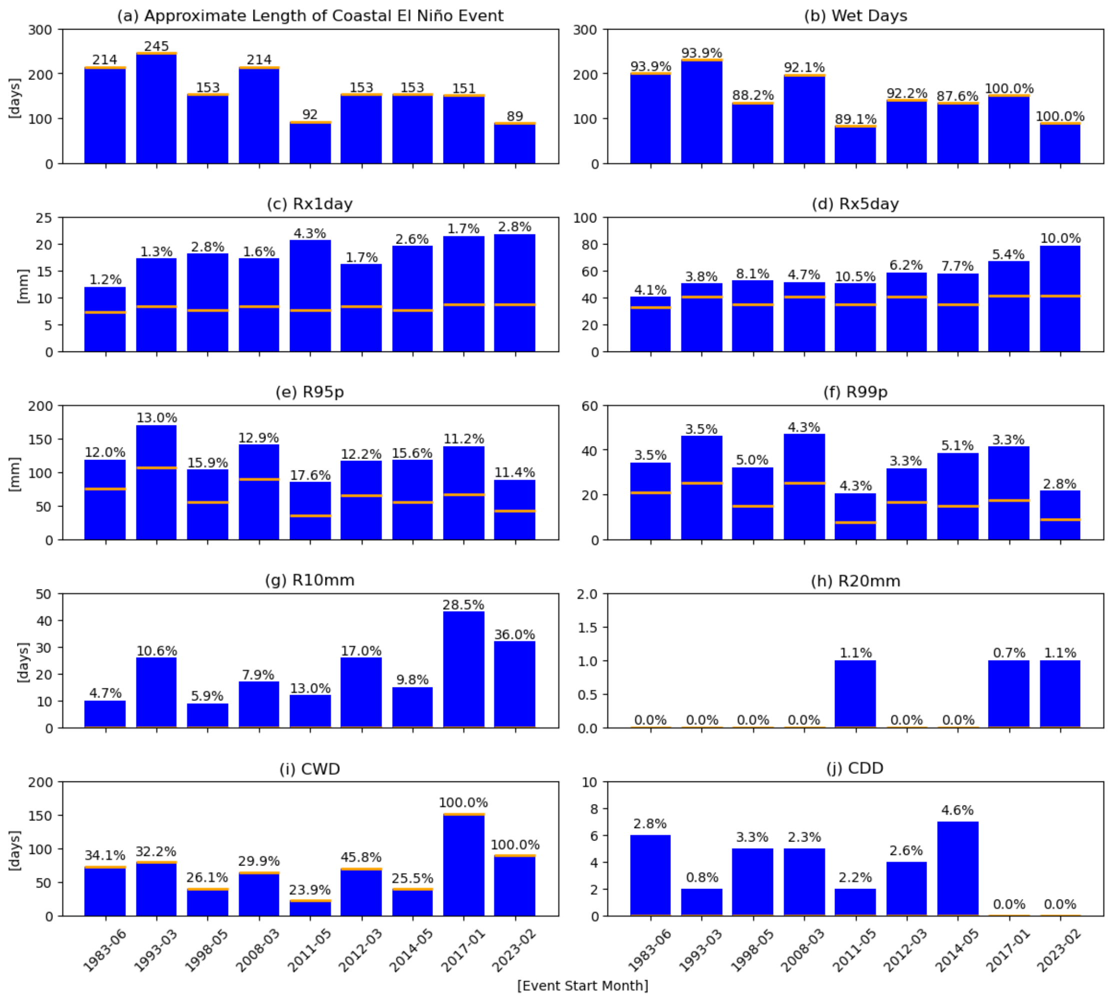


Figure 4.5: Bar plot of precipitation observations for each precipitation index during Coastal El Niño event (1981 – 2023) averaged over Peru and Ecuador (19°S – 3°S, 85°W – 68°W). (a) Event duration (number of days in months meeting Coastal El Niño criteria. Panels (b-j) show: (b) Wet Days, (c) Rx1day, (d) Rx5day, (e) R95p, (f) R99p, (g) R10mm, (h) R20mm, (i) CWD, and (j) CDD. Percentages reflect each index's contribution to event totals. Orange lines show 1991 – 2020 climatology based on event timing and length.

In reviewing the 2017 and 2023 events, their associated precipitation compared to previous Coastal El Niño events are particularly noteworthy. Both events, when averaged spatially, recorded wet days throughout their entire duration (100% wet days) shown by Figure 4.5b. Additionally, they had the highest maximum daily total precipitation over one- (Fig. 4.5c) and five-day (Fig. 4.5d) periods compared to any previous

Coastal El Niño events evaluated, with 2023 slightly exceeding 2017. However, when examining the contribution of extreme rainfall days (daily precipitation exceeding the 95th [Fig. 4.5e] and 99th [Fig. 4.5f]), 2017 and 2023 did not have the highest absolute rainfall. Instead, extreme rainfall accounted for the lowest percentage of total precipitation during these events, suggesting that the overall high rainfall was driven more by moderate events than by rare extremes. Even when daily precipitation reached the 95th or 99th percentile, its relative impact on total rainfall was minor if the rest of the days were also wet. This result highlights the importance of considering both frequency and intensity of rainfall and underscores that extremes alone do not always dominate the water budget for a given period.

Furthermore, these events had the highest number of days with daily total precipitation equal to or exceeding 10 mm (Fig. 4.5g). Notably, they were two of only three events that had at least one day with daily precipitation equal to or greater than 20 mm (Fig. 4.5h), with the third occurrence being in 2011. This finding is particularly interesting considering that the 2011 event had the lowest linearly detrended three-month running mean peak sea surface temperature anomaly (Table 4.1) and the lowest linearly detrended three-month running mean average sea surface temperature anomaly (Fig. 4.3a).

Lastly, the 2017 and 2023 events stand out for having the highest number of consecutive wet days (Fig. 4.5i), spanning the entire Coastal El Niño event, and the fewest consecutive dry days (Fig. 4.5j), with a value of zero.

An additionally notable feature of Figure 4.5 is that, despite the 1983 and 1998 events having the highest linearly detrended three-month running mean average sea surface temperature anomaly and peak sea surface temperature anomaly, they underperformed in terms of associated extreme precipitation. They had the fewest days meeting the R10mm threshold (Fig. 4.5g) compared to the other Coastal El Niño events and no days meeting the 20 mm threshold (R20mm) on average (Fig. 4.5h). Similarly, they had the lowest maximum daily precipitation (Rx1day; Fig. 4.5c) and five-day precipitation (Rx5day; Fig. 4.5d) in comparison to other events.

To evaluate some of these metrics further, we examined precipitation observations for select precipitation indices spatially (Fig. 4.6). We selected four of the Coastal El Niño events. The first is the 1983 event as this event had the highest peak and average linearly detrended three-month running mean sea surface temperature anomalies. The second is the 2011 event as this event had the lowest peak and average linearly detrended three-month running mean sea surface temperature anomalies. Lastly, we evaluate the spatial features of 2017 and 2023 as these are the main events being evaluated in this work. Further, each of the selected events had notable takeaways from Figure 4.5. We also examine two indices each from the general and extreme precipitation indices including wet days, Rx1day, R99p, and R10mm.

Spatially, the number of wet days generally aligns with expectation for 1983 (Fig. 4.6a) and 2011 (Fig. 4.6b), with more grid points experiencing higher numbers of wet days in 1983 compared to 2011. This difference aligns with the sea surface temperature differences in the Niño 1+2 region between these two events. When comparing 2017 (Fig. 4.6c) and 2023 (Fig. 4.6d), we observe a widespread increase in wet days for 2017 relative to 2023. However, this can largely be attributed to the longer duration of the 2017 event (five months) compared to 2023 (three months).

The spatial patterns of maximum daily total precipitation over a one-day period are relatively consistent across all events, showing concentrations of higher values in the northern provinces. Specifically, in 1983 (Fig. 4.6e) and 2011 (Fig. 4.6f), these higher maximum daily precipitation totals are most prominent in eastern Ecuador and southern Colombia extending into northern Peru. In contrast, 2017 (Fig. 4.6g) and 2023 (Fig. 4.6h) show increased concentrations of larger maximum daily totals along

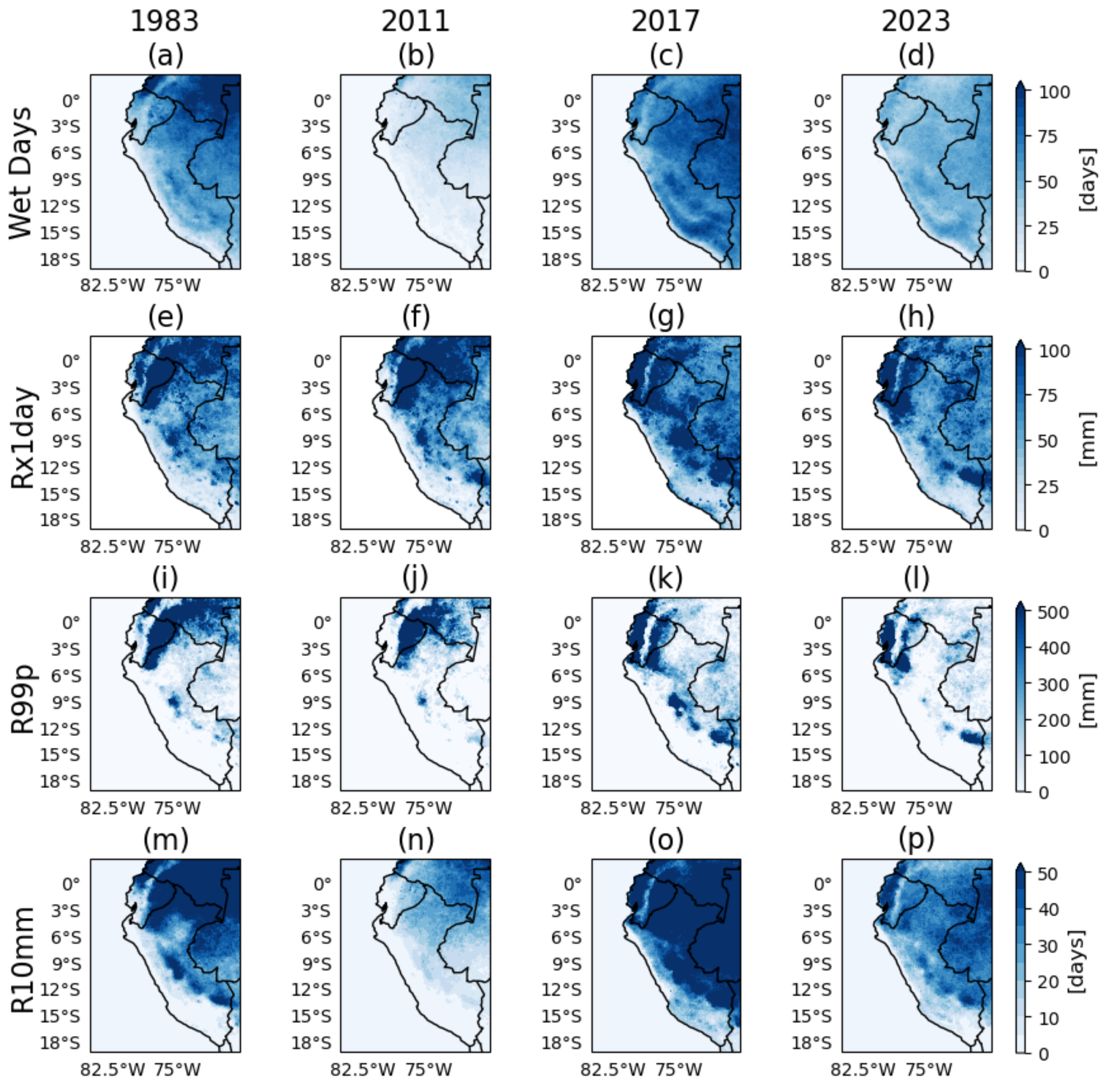


Figure 4.6: Spatial pattern of general and extreme precipitation observations for precipitation indices including Wet Days (first row), Rx1day (second row), R99p (third row), and R10mm (fourth row) for the 1983 (first column), 2011 (second column), 2017 (third column), and 2023 (fourth column) Coastal El Niño events over Peru and Ecuador (19°S – 3°S, 85°W – 68°W).

the coast, consistent with the above-average precipitation anomalies associated with the Niño 1+2 region shown in Figure 4.2. Additionally, there is a noticeable increase in larger maximum daily totals in the inland southern regions, which is minimal in 1983 but progressively more concentrated in 2011, 2017, and 2023.

Supporting these patterns are the precipitation totals from days exceeding the 99th percentile. In 1983 (Fig. 4.6i) and 2011 (Fig. 4.6j), these regions are most pronounced in eastern Ecuador and southern Colombia. While still present there in 2017 (Fig. 4.6k) and 2023 (Fig. 4.6l), these extremes also shift closer to the coastal regions of Ecuador and northern Peru, as well as more concentrated inland areas in the southern provinces of Peru.

Finally, examining the number of days each grid point experiences daily precipitation equal to or greater than 10 mm reveals similar spatial patterns. Across all events, higher numbers of such days are located in Colombia, Ecuador, and northern Peru. For 1983 (Fig. 4.6m), 2017 (Fig. 4.6o), and 2023 (Fig. 4.6p), these numbers are more widespread, with 2017 in particular showing many grid points exceeding 50 days. Surprisingly, 2023 shows fewer high-count grid points, likely due to its shorter duration compared to 1983 and 2017.

## 4.2 Meridional Wind as a Driver of Coastal El Niño

Anomalous northerly wind north of the Niño 1+2 region was a feature of the 2017 and 2023 Coastal El Niño events. Given that this was one of the few similarities between the events, we were interested in evaluating whether northerly winds into the Niño 1+2 region are typically associated with sea surface temperatures. Figure 4.7a shows the correlation between 850 hPa meridional winds and Niño 1+2 sea surface temperatures. Positive correlations indicate that warmer sea surface temperatures in the Niño 1+2 region coincide with stronger northward winds (or weaker southward winds). Negative correlations indicate that warmer sea surface temperatures coincide with enhanced southward winds (or weaker northward winds). Significant positive correlations, strong northward winds associated with warmer sea surface temperatures, are evident along the coast, extending from the Niño 1+2 region. This feature was present in our analysis of the 850 hPa meridional winds during 2017 and 2023 Coastal El Niño events, particularly in early January (Fig. 3.18c) of 2017, and in late January to early February of 2023 (Fig. 3.18f). Significant negative correlations, strong southward winds associated with warmer sea surface temperatures, are located northwest of the Niño 1+2 region. Although the placement of these northerly winds does not exactly match the patterns observed in 2017 and 2023, it does show that meridional winds north of the Niño 1+2 region are moderately correlated with warmer sea surface temperatures.

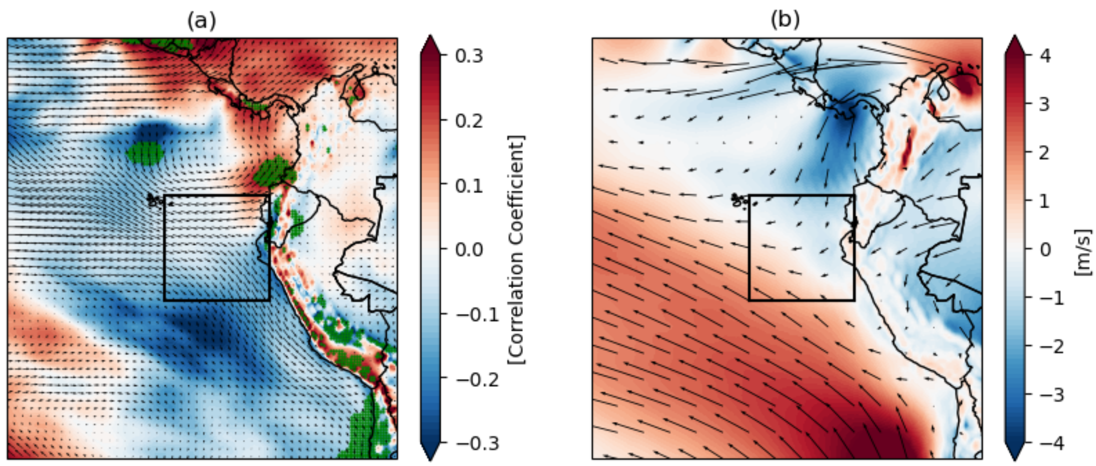


Figure 4.7: (a) Correlation (shading and vectors) between 1981 – 2023 850 hPa meridional wind anomalies and Niño 1+2 sea surface temperatures (0°-10°S, 90°W-80°W). Green stippling indicates significance at $p < 0.1$ based on bootstrapping. (b) Composite 850 hPa meridional wind anomalies during all 20 Coastal El Niño events.

To further evaluate the typical 850 hPa meridional wind patterns during Coastal El Niño events, we created a composite of the 850 hPa meridional winds for all events from 1940 to 2023. This composite analysis showed that anomalous northerly winds north of the Niño 1+2 region are common during these events. Additionally, anomalous southerly winds south of the Niño 1+2 region are also commonly observed, consistent with what was seen during the 2017 and 2023 events.

# Chapter 5

# Discussion

## 5.1 Pakistan

The precipitation over July and August 2022 was unprecedented. Our findings show that the annual average July – August precipitation anomaly for 2022 was substantially higher than any other year between 1981 and 2023, using a 1999 – 2020 climatology. Additionally, over this 42-year period, we identified a slight increasing trend in July – August annual average precipitation. This potential increase in above average precipitation, and decrease in below average precipitation, has major implications for flood risk and preparedness in Pakistan. This risk is particularly concerning if similar events become more likely under a changing climate. These findings highlight the urgent need to improve the accuracy and lead time of subseasonal forecasts and identify key drivers and mechanisms contributing to predictability in the region.

Although the precipitation anomalies in July and August 2022 were widespread, much of the above average rainfall was concentrated in the southern provinces of Pakistan for all three extreme precipitation events over the course of the summer. Climatologically, the northern provinces are typically wetter due to the temperate climate and orographic lift provided by the Himalayas, while the southern provinces are generally hot, arid, and desert-like. The concentration of anomalies in the south presents a climatological mismatch. Regions not adapted to heavy rainfall may face disproportionate damage, underscoring the need for improved forecasts and preparedness.

When comparing the CESM2 short-term and subseasonal reforecasts, we found that the precipitation anomaly spatial patterns over Pakistan for each event in July – August 2022 were not well predicted at either timescale. However, considering the wind patterns over South Asia and the Indian Ocean Basin as a primary driver, we found that the short-term predictions of the 850 hPa zonal wind anomalies were much improved compared to the subseasonal forecasts for all events. In subseasonal predication, the skill in predicting wind anomaly patterns improved across the events where the patterns were not well predicted for Event One but best predicted for Event Three. Unfortunately, these improvements in wind prediction did not translate to improved precipitation forecasts.

Singh et al. (2024) assess the predictability of this event using the ECMWF model and found that above average precipitation from June to September 2022 was predicted up to four weeks in advance. Their methodology focused on initialization dates close to the start of each month (2 June, 30 June, 38 July, and 1 September). In contrast, we analyzed all initialization dates encompassing forecasts for any dates in July – August 2022 and found increased inconsistency in the model's predictions, suggesting that precipitation forecasts are highly sensitive to initialization timing. It is important to note that Singh et al. (2024) also used forecast downscaling, calibration, and tercile categories, which we did not.

Using the reforecast experiments, we isolated the roles of the atmosphere and ocean. Although some experiments also assess the contribution of land initial conditions, we found that land played a minimal role in prediction skill for summer precipitation and therefore excluded this from our analysis. The reduced contribution to skill from the land initial conditions does not imply that land initial conditions are unimportant as a source of predictability in general, but rather that, for these specific events and in this model, it does not contribute significantly for the forecast skill. The atmospheric initial conditions dominated prediction skill for Events One and Three, while contributions of oceanic initial conditions to skill increased during Event Two. Given this variability in sources of skill, this further supports our decision to split the extreme precipitation of July - August 2022 into three distinct events. The number of evens assessed aligns with Hsu et al. (2022). This number of events differs from other research that grouped the summer precipitation into two events or considered the entire summer as one large event.

By analyzing the vertically integrated moisture flux pathways, we determined that for Events One and Three, moisture was transported from the east, whereas for Event Two, it was transported from the south. Initially, we considered monsoon surges to be a contributor only to Event Two. However, given the absence of negative outgoing longwave radiation anomaly propagation in Event Two (unlike Events One and Three), we ultimately ruled out monsoon pulses as a primary contributor to any of the events. This conclusion differs from Singh et al. (2024), who attributed the extreme precipitation to three northward propagating distinct MISO events, a significant source of subseasonal predictability for South Asia. Our moisture flux findings and reforecast experiments further support our conclusion that northward propagating monsoon surges from the Indian Ocean are not a key factor of the extreme precipitation in Pakistan. For example, the contribution of atmospheric initial conditions to outgoing longwave radiation anomaly analysis for Event One showed a weakened delayed surge, and inconsistencies in the contribution of atmospheric initial conditions to precipitation skill, eliminating monsoon surges as a primary driver. For Event Three, while a second surge re-emerges, moisture flux analyses showed moisture exiting Pakistan through the southern boundary, opposite to what would be expected from northward propagating monsoon pulses.

Instead, we attribute the direct influx of moisture from the east in Events One and Three to anomalous low-level easterly winds in northern India and south of the Tibetan Plateau transporting moisture into Pakistan from the Bay of Bengal. This easterly flow is possibly associated with the South Asian monsoon trough (Annamalai 2010; Choudhury and Krishnan 2011). Supporting this interpretation, Takahashi (2024) attributed the 2022 precipitation to westward-propagating tropical disturbances along the South Asian monsoon trough, consistent with the observed easterly moisture transport. He et al. (2023) similarly attributed anomalous precipitation in Southwest Asia and the Southeast Asian heatwave to reversed flow suggesting this flow caused ascent in the southwest and decent in the southeast. They suggested that this reversal was caused by anomalous sea surface temperatures in the Indian Ocean Basin. Below average sea surface temperatures weakened the meridional temperature gradient, ultimately reversing westerly flow south of the Tibetan Plateau. We align with this hypothesis, noting that during this period there was a “triple-dip” La Niña and a negative phase of the Indian Ocean Dipole.

For Event Two, the moisture influx from the south is linked to the Somali Jet. Sea surface temperatures shifted to be near-normal in the Arabian Sea and increased in the Bay of Bengal. We suggest that this shift weakened the anomalous low-level easterly winds and localized the Somali Jet along the coast, altering wind patterns over the Indian Ocean Basin. Previous research shows that Somali Jet intensity is inversely proportional to sea surface temperature anomalies meaning that a more enhanced Somali Jet is associated with cooler sea surface temperatures (Pushpanjali et al. 2014). Pushpanjali et al. (2014) supported this by comparing jet intensity with ENSO phases concluding that during La Niña years the Somali Jet was strengthened. This result form Pushpanjali et al. (2014) aligns with our findings of an enhanced Somali Jet during Event One, driven by below-average sea surface temperatures in the Arabian

Sea. As sea surface temperature anomalies increased in both the Arabian Sea and Bay of Bengal, the Somali Jet weakened and became more localized, redirecting moisture transport into Pakistan from the south. After Event Two, sea surface temperature anomalies returned to below average, and although the Somali Jet near the coast remained weak, the widespread wind patterns over the Arabian Sea returned to above average. During Events One and Three, the Somali Jet directly fed into the anomalous easterly winds in the Bay of Bengal.

For these reasons, there was enhanced contributions from atmospheric initial conditions to precipitation prediction skill for Events One and Three that is likely linked to anomalous zonal wind patterns. In contrast, the increased contribution from oceanic initial conditions during Event Two is likely driven by shifts in sea surface temperature anomalies and associated changes in the wind pattern. It is important to emphasize that increased contribution of one earth system component's initial conditions does not imply there are not coupled processes at play. As discussed, many of the wind patterns analyzed in this study are likely influenced by sea surface temperature anomalies. As a result, it is possible that oceanic variability has shaped the atmospheric initial conditions, meaning the atmosphere's response to ocean variability is already embedded within those initial conditions.

## 5.2 Peru

Peru experienced widespread anomalous precipitation during the Southern Hemisphere fall in both 2017 and 2023. Our analysis shows that average precipitation from January through May in those years exceeded all other years from 1981 to 2023, based on a 1999 – 2020 climatology. These extreme rainfall totals coincided with highly localized and positive sea surface temperature anomalies off the coasts of Ecuador and northern Peru, specifically within the Niño 1+2 region, characteristic of Coastal El Niño events. While precipitation anomalies in both years were widespread, the week-to-week precipitation patterns in 2017 and 2023 differed. However, the most extreme precipitation indices were concentrated along the coast, closely mirroring the spatial extent of above average precipitation anomalies typically associated with Niño 1+2 warming. For this reason, we suggest that a Coastal El Niño may have been a potential driver of these events.

Although some Coastal El Niño events are linked to basin-scale ENSO phases, the Coastal El Niño phenomenon is distinct. Of the 20 identified events, almost half occurred independently of basin-scale ENSO phases, while the rest often followed or coincided with La Niña conditions or followed or preceded El Niño conditions. Composite analyses reveal differing precipitation patterns associated with basin-scale ENSO phases, reinforcing the independence of Coastal El Niño. Coastal El Niño events typically produce more widespread rainfall anomalies compared to basin-scale El Niño events, which tend to have more localized coastal effects. Notably, the extreme nature of the 2017 and 2023 events may have amplified precipitation patterns, making them resemble basin-scale El Niño regression analyses. Conversely, basin-scale La Niña events consistently correlate with widespread drier conditions along the coast, as expected due to their opposite phase relationship.

Despite these general patterns, our analysis of Coastal El Niño-related precipitation from 1983 to 2023 reveals complexity and variability in the event impacts. For example, although 1983 and 1998 featured the highest sea surface temperature anomalies in the Niño 1+2 region, they underperformed in several precipitation indices relative to less intense warming events. This finding suggests that sea surface temperature magnitude alone does not determine rainfall impact. While interactions with basin-scale El Niño may have influenced these outcomes, we also observed an upward trend in many precipitation indices over time. Although our sample includes only nine precipitation events, the trend suggests a potential climate change-related shift toward more frequent or intense precipitation during Coastal El Niño events. However, unlike the detailed analysis for 2017 and 2023, we did not examine contributing atmospheric or oceanic features for earlier events, which limits the robustness of this conclusion.

The 2017 precipitation event was shaped not only by sea surface temperature anomalies but also by the behavior of the ITCZ. In late January to early February, the ITCZ extended southward into the Niño 1+2 region, enhancing convection and precipitation over northern Peru. This shift was likely supported by coastal warming (Takahashi and Martínez 2019). The ITCZ strengthened through early March, supported by converging northerly and southerly winds, before weakening and dissipating by April. (Son et al. 2020) noted that the ITCZ during this period formed earlier and farther south than typical seasonal climatology would suggest. This behavior may represent an instance of a double ITCZ, a feature that commonly appears over the eastern Pacific in March and April (Yan and Li 2018). The presence and structure of the double ITCZ are influenced by the shape of sea surface temperature anomalies during different types of El Niño events (Yan and Li 2018), further supporting the possibility that this pattern was present in 2017.

In contrast, a distinguishing feature of the 2023 event was the presence of Cyclone Yaku, the first cyclone to make landfall in Peru in over 40 years. Like the ITCZ in 2017, Cyclone Yaku was likely reinforced by warm coastal sea surface temperatures (Peng et al. 2024). We hypothesize that the ITCZ was not a prominent feature during 2023 because this Coastal El Niño event coincided with the formation and landfall of the cyclone. Takahashi and Martínez (2019) propose that basin-scale La Niña conditions can destabilize the ITCZ, which may have contributed to its absence in 2023. Moreover, these destabilizing conditions can reduce atmospheric stability, favoring coastal warming.

Despite both events being driven primarily by Coastal El Niño conditions, differences in their accompanying features, such as the ITCZ in 2017 and Cyclone Yaku in 2023, likely contributed to disparities in precipitation varied markedly between the two events. Forecast skill during the first three months of the 2017 event was low across both subseasonal and short-term timescales, whereas forecast skill during 2023 improved significantly. We hypothesize that the ITCZ's dynamic behavior in 2017 contributed to low ACCs across all months. However, we also acknowledge gaps in available reforecast data for the full 2017 event, highlighting an area for future investigation.

Although the unaltered reforecast performed poorly, we found that the oceanic initial conditions were the primary source of prediction skill for both events. This finding is notable given that oceanic initial conditions contribute to predictability typically at longer lead times due to slower variability, whereas atmospheric contribution to skill increased in March 2017, possibly linked to the intensification of the ITCZ.

A consistent feature across both events was the presence of anomalous northerly winds north of the Niño 1+2 region from the onset through peak warming. These winds, varying in intensity, are known to enhance wind stress curl and reduce evaporation, deepening the thermocline through Ekman pumping and intensifying warming (Echevin et al. 2018; Garreaud 2018; Peng et al. 2019; Son et al. 2020; Zhao and Karamperidou 2022). Our correlation and composite analyses suggest that this northerly wind anomaly is a general feature of Coastal El Niño development. The dissipation of coastal warming in both 2017 and 2023 was associated with the southward intrusion and strengthening of southerly winds into the Niño 1+2 region, promoting upwelling and cooling sea surface temperatures. In this case study, since the ocean is the primary driver and the atmosphere is also suggested to influence sea surface temperature variability, any atmospheric impacts on the ocean would be captured in the oceanic initial conditions.

Finally, our results reveal a positive linear trend in January - May annual average precipitation anomalies from 1981 to 2023, with a noticeable shift toward above average rainfall beginning in the early 2000s. We also observe an increased frequency of Coastal El Niño events since 2008, with 2017 and 2023 being the most extreme. These findings underscore the urgent need to improve subseasonal predictions of precipitation and sea surface temperatures in the eastern Pacific to support adaptation and preparedness efforts under a changing climate.

# Chapter 6

# Summary and Conclusions

In this study, we evaluated both the predictability and underlying physical drivers of three extreme precipitation events, the 2022 Pakistan floods and the 2017 and 2023 Peru extreme precipitation events. These cases were regionally anomalous and had severe societal impacts, underscoring the need to improve early warning systems. Our findings highlight that predictive skill is highly event- and region-specific, with no universal source of predictability.

For Pakistan, atmospheric dynamics, particularly anomalous easterly winds south of the Tibetan Plateau, played a central role in the July and August 2022 events, with oceanic variability also influencing conditions at times. This result contrasts with previous findings that emphasized northward-propagating monsoon pulses as a key driver. While earlier research has proposed a variety of potential drivers behind the summer 2022 events, our methodology allowed us to break down these drivers and assess their relative contributions leading to different results from Singh et al. (2024). Additionally, we provided new insights into forecast skill, using the NCAR CESM2 reforecast and reforecast experiments and ACC.

In contrast, Peru's extreme precipitation events were more consistently governed by oceanic processes, particularly Coastal El Niño conditions, with atmospheric contributions from the ITCZ in 2017 and Cyclone Yaku in 2023. Research up to date has largely characterized Coastal El Niño events through individual case studies, leading to a fragmented understanding. This study not only compares the two most recent extreme Coastal El Niño events but also begins to build a broader understanding of their variability, associated precipitation patterns, and connections with basin-scale ENSO phases. We further assessed the predictability of precipitation linked to these events, an aspect that has been underexplored. Although both events were driven by similar primary mechanisms, their precipitation responses differed, complicating assumptions about predictability and highlighting additional challenges for forecasting precipitation during Coastal El Niño events.

For both case studies, we applied CESM2 reforecast experiments to evaluate which earth system components contributed most to prediction skill. These experiments are novel in that they are the first to quantify the contributions of individual earth system components to predictability on the subseasonal timescale. By setting selected components to climatological initial conditions, we isolated the influence of their initial conditions on the forecast evolution. Our use of these experiments is also unique as this marks the first application to case study analysis, offering new insight into how initial conditions across different components affect the predictability of specific precipitation events in various geographic regions. These results highlight the value of tools like the NCAR CESM2 reforecast experiments, combined with region-specific diagnostics, in disentangling the complex interaction among ocean, atmosphere, and land processes on subseasonal timescales.

To provide structure and consistency in our analysis, we developed and applied a reusable framework. This framework is designed to analyze extreme weather events, such as heavy precipitation, drought, or extreme heat, by systematically addressing key scientific questions using advanced modeling tools. It begins with the identification of a past extreme event, followed by three central questions: (1) What are the key characteristics of the extreme event? (2) How far in advance could subseasonal forecasts have provided useful predictive information? (3) Which earth system components contributed most to the predictability and occurrence of the event? To address these questions, the framework leverages the CESM2 subseasonal reforecasts and targeted reforecast experiments, which allow for the evaluation of predictability sources by modifying initial conditions in specific earth system components. This structured approach and methodology offers a generalizable method for evaluating a variety of extreme events across diverse regions, as demonstrated in this study.

A limitation of this study is that the results, including sources of predictability and drivers, is not yet generalizable to other events within these regions as we applied and demonstrated its potential for individual case studies. However, continued application and further development of this framework to similar precipitation events will build a broader knowledge base, ultimately supporting the creation of a generalizable framework that can be applied to extreme events shortly after they occur or in real-time as they are predicted. To make this framework generalizable, it must be applied to a broader range of past events that vary not only by region but also by event type (e.g., drought, extreme heat). This would support the continued development of the framework and improve understanding of the consistent sources of predictability and key drivers behind different types of extreme events in specific regions. Additionally, this study's evaluation of the reforecast and reforecast experiments is limited to the ensemble mean, which does not capture extremes or outliers among individual ensemble members.

Improving the accuracy and lead times of subseasonal forecasts can provide risk-based guidance to support decision-making and potentially reduce both short- and long-term impacts. A critical step toward this goal is understanding how well past extreme events were predicted at these timescales. Importantly, this includes evaluating not just forecast accuracy, how close predictions were to observed outcomes, but also forecast skill. Forecast skill is often assessed using metrics like ACC or reflects how much better the forecast performs compared to a reference, such as climatology. The framework presented can be applied to help entities such as the GWSC and similar stakeholders to enhance confidence, trust, and understanding in subseasonal forecasts, providing actionable information for client briefings and public communication. More specifically, analyzing past events can help organizations determine whether and how subseasonal predictions might be effectively used in the future to support their missions. As the climate continues to change, integrating such frameworks and analysis will be essential to better preparing vulnerable communities for future extremes.

# Reference List


An, D., J. Eggeling, L. Zhang, H. He, A. Sapkota, Y.-C. Wang, and C. Gao, 2023: Extreme precipitation patterns in the asia–pacific region and its correlation with el niño-southern oscillation (enso). *Scientific Reports*, **13 (1)**, 11 068, https://doi.org/https://doi.org/10.1038/s41598-023-38317-0.

Annamalai, H., 2010: Moist dynamical linkage between the equatorial indian ocean and the south asian monsoon trough. *Journal of the Atmospheric Sciences*, **67 (3)**, 589–610, https://doi.org/https://doi.org/10.1175/2009JAS2991.1.

Annamalai, H., 2024: Unprecedented monsoon precipitation over southwest pakistan in 2022: Regional processes in moistening the climatological heat low. *Quarterly Journal of the Royal Meteorological Society*, **150 (764)**, 4391–4416, https://doi.org/https://doi.org/10.1002/qj.4821.

Assessment Capacity Project, 2024: Pakistan floods 2022 impact assessment. Tech. rep., Assessment Capacity Project. URL https://www.acaps.org/fileadmin/Data_Product/Main_media/20240319_ACAPS_briefing_note_Peru_-_Humanitarian_impact_of_heavy_rainfall_and_flooding.pdf.

Beames, P., and Coauthors, 2025: Pathways to instability: A synthetic framework to parse connections between water and conflict. *Environment and Security*, In press.

Benson, D. O., and P. A. Dirmeyer, 2021: Characterizing the relationship between temperature and soil moisture extremes and their role in the exacerbation of heat waves over the contiguous united states. *Journal of Climate*, **34 (6)**, 2175–2187, https://doi.org/https://doi.org/10.1175/JCLI-D-20-0440.1.

Berghuijs, W. R., E. E. Aalbers, J. R. Larsen, R. Trancoso, and R. A. Woods, 2017: Recent changes in extreme floods across multiple continents. *Environmental Research Letters*, **12 (11)**, 114 035, https://doi.org/https://doi.org/10.1088/1748-9326/aa8847.

Bhatti, A. S., G. Wang, W. Ullah, S. Ullah, D. F. T. Hagan, I. K. Nooni, D. Lou, and I. Ullah, 2020: Trend in extreme precipitation indices based on long term in situ precipitation records over pakistan. *Water*, **12 (3)**, 797, https://doi.org/https://doi.org/10.3390/w12030797.

Bhutto, F., 2022: The west is ignoring pakistan's super-floods. heed this warning: tomorrow it will be you. *The Guardian*, URL https://www.theguardian.com/commentisfree/2022/sep/08/pakistan-floods-climate-crisis, accessed: 2025-04-25.

Black, J., N. C. Johnson, S. Baxter, S. B. Feldstein, D. S. Harnos, and M. L. L'Heureux, 2017: The predictors and forecast skill of northern hemisphere teleconnection patterns for lead times of 3–4 weeks. *Monthly Weather Review*, **145 (7)**, 2855–2877, https://doi.org/https://doi.org/10.1175/MWR-D-16-0394.1.

Blöschl, G., and Coauthors, 2019: Changing climate both increases and decreases european river floods. *Nature*, **573 (7772)**, 108–111, https://doi.org/https://doi.org/10.1038/s41586-019-1495-6.

Brunet, G., and Coauthors, 2010: Collaboration of the weather and climate communities to advance subseasonal-to-seasonal prediction. *Bulletin of the American Meteorological Society*, **91 (10)**, 1397–1406, https://doi.org/https://doi.org/10.1175/2010BAMS3013.1.

Burke, M. B., E. Miguel, S. Satyanath, J. A. Dykema, and D. B. Lobell, 2009: Warming increases the risk of civil war in africa. *Proceedings of the national Academy of sciences*, **106 (49)**, 20 670–20 674, https://doi.org/https://doi.org/10.1073/pnas.0907998106.

Cai, W., and Coauthors, 2023: Anthropogenic impacts on twentieth-century enso variability changes. *Nature Reviews Earth & Environment*, **4 (6)**, 407–418, https://doi.org/https://doi.org/10.1038/s43017-023-00427-8.

Chakraborty, A., and P. Singhai, 2021: Asymmetric response of the indian summer monsoon to positive and negative phases of major tropical climate patterns. *Scientific reports*, **11 (1)**, 22 561, https://doi.org/https://doi.org/10.1038/s41598-021-01758-6.

Chen, G., J. Ling, Z. Lin, Z. Xiao, and C. Li, 2023: Role of tropical-extratropical interactions in the unprecedented 2022 extreme rainfall in pakistan: a historical perspective. *Atmospheric Research*, **291**, 106 817, https://doi.org/https://doi.org/10.1016/j.atmosres.2023.106817.

Choudhury, A. D., and R. Krishnan, 2011: Dynamical response of the south asian monsoon trough to latent heating from stratiform and convective precipitation. *Journal of the Atmospheric Sciences*, **68 (6)**, 1347–1363, https://doi.org/https://doi.org/10.1175/2011JAS3705.1.

Chughtai, A., 2022: Mapping the scale of damage by the catastrophic pakistan floods. *Aljazeera*, URL https://www.aljazeera.com/news/longform/2022/9/16/mapping-the-scale-of-destruction-of-the-pakistan-floods.

Coelho, C. A. d. S., C. B. Uvo, and T. Ambrizzi, 2002: Exploring the impacts of the tropical pacific sst on the precipitation patterns over south america during enso periods. *Theoretical and applied climatology*, **71**, 185–197, https://doi.org/https://doi.org/10.1007/s007040200004.

Collyns, D., 2017: How can peru prepare to withstand more devastating floods and landslides? *The Guardian*, URL https://www.theguardian.com/global-development-professionals-network/2017/apr/13/peru-prevent-floods-landslides-climate-change.

Croci-Maspoli, M., C. Schwierz, and H. C. Davies, 2007: Atmospheric blocking: Space-time links to the nao and pna. *Climate Dynamics*, **29**, 713–725, https://doi.org/https://doi.org/10.1007/s00382-007-0259-4.

De Andrade, F. M., C. A. Coelho, and I. F. Cavalcanti, 2019: Global precipitation hindcast quality assessment of the subseasonal to seasonal (s2s) prediction project models. *Climate Dynamics*, **52 (9)**, 5451–5475, https://doi.org/https://doi.org/10.1007/s00382-018-4457-z.

de los Milagros Skansi, M., and Coauthors, 2013: Warming and wetting signals emerging from analysis of changes in climate extreme indices over south america. *Global and planetary change*, **100**, 295–307, https://doi.org/https://doi.org/10.1016/j.gloplacha.2012.11.004.

DelSole, T., L. Trenary, M. K. Tippett, and K. Pegion, 2017: Predictability of week-3–4 average temperature and precipitation over the contiguous united states. *Journal of Climate*, **30 (10)**, 3499–3512, https://doi.org/https://doi.org/10.1175/JCLI-D-16-0567.1.

Dirmeyer, P. A., C. A. Schlosser, and K. L. Brubaker, 2009: Precipitation, recycling, and land memory: An integrated analysis. *Journal of Hydrometeorology*, **10 (1)**, 278–288, https://doi.org/https://doi.org/10.1175/2008JHM1016.1.

Diro, G., and H. Lin, 2020: Subseasonal forecast skill of snow water equivalent and its link with temperature in selected subx models. *Weather and Forecasting*, **35 (1)**, 273–284, https://doi.org/https://doi.org/10.1175/WAF-D-19-0074.1.

Echevin, V., F. Colas, D. Espinoza-Morriberon, L. Vasquez, T. Anculle, and D. Gutierrez, 2018: Forcings and evolution of the 2017 coastal el niño off northern peru and ecuador. *Frontiers in Marine Science*, **5**, 367, https://doi.org/https://doi.org/10.3389/fmars.2018.00367.

Endo, H., A. Kitoh, R. Mizuta, and M. Ishii, 2017: Future changes in precipitation extremes in east asia and their uncertainty based on large ensemble simulations with a high-resolution agcm. *Sola*, **13**, 7–12, https://doi.org/https://doi.org/10.2151/sola.2017-002.

Fadil, A., 2022: The west is ignoring pakistan's super-floods. heed this warning: tomorrow it will be you. *United Nations Children's Fund*, URL https://www.unicef.org/press-releases/devastating-floods-pakistan-claim-lives-more-500-children, accessed: 2025-04-25.

Ford, T. W., P. A. Dirmeyer, and D. O. Benson, 2018: Evaluation of heat wave forecasts seamlessly across subseasonal timescales. *NPJ Climate and Atmospheric Science*, **1 (1)**, 20, https://doi.org/https://doi.org/10.1038/s41612-018-0027-7.

Funk, C., and Coauthors, 2015: The climate hazards infrared precipitation with stations—a new environmental record for monitoring extremes. *Scientific Data*, **2**, 150 066, https://doi.org/https://doi.org/10.1038/sdata.2015.66.

Garreaud, R. D., 2018: A plausible atmospheric trigger for the 2017 coastal el niño. *International Journal of Climatology*, https://doi.org/https://doi.org/10.1002/joc.5426.

Goldberg, R. A., G. Tisnado M, and R. Scofield, 1987: Characteristics of extreme rainfall events in northwestern peru during the 1982–1983 el niño period. *Journal of Geophysical Research: Oceans*, **92 (C13)**, 14 225–14 241, https://doi.org/https://doi.org/10.1029/JC092iC13p14225.

Goswami, B. N., G. Wu, and T. Yasunari, 2006: The annual cycle, intraseasonal oscillations, and roadblock to seasonal predictability of the asian summer monsoon. *Journal of climate*, **19 (20)**, 5078–5099, https://doi.org/https://doi.org/10.1175/JCLI3901.1.

Government of Pakistan, 2022: Pakistan floods 2022 impact assessment. Tech. rep., Finance Division. URL https://www.finance.gov.pk/survey/chapters_23/Annex_III_Pakistan_Floods_2022.pdf.

Guo, J., G. Huang, X. Wang, Y. Li, and Q. Lin, 2018: Dynamically-downscaled projections of changes in temperature extremes over china. *Climate Dynamics*, **50**, 1045–1066, https://doi.org/https://doi.org/10.1007/s00382-017-3660-7.

Han, T., H. Chen, X. Hao, and H. Wang, 2018: Projected changes in temperature and precipitation extremes over the silk road economic belt regions by the coupled model intercomparison project phase 5 multi-model ensembles. *International Journal of Climatology*, **38 (11)**, 4077–4091, https://doi.org/https://doi.org/10.1002/joc.5553.

Hanif, M., A. H. Khan, and S. Adnan, 2013: Latitudinal precipitation characteristics and trends in pakistan. *Journal of Hydrology*, **492**, 266–272, https://doi.org/https://doi.org/10.1016/j.jhydrol.2013.03.040.

Hanjra, M. A., and M. E. Qureshi, 2010: Global water crisis and future food security in an era of climate change. *Food policy*, **35 (5)**, 365–377, https://doi.org/https://doi.org/10.1016/j.foodpol.2010.05.006.

Hartmann, H., and H. Buchanan, 2014: Trends in extreme precipitation events in the indus river basin and flooding in pakistan. *Atmosphere-Ocean*, **52 (1)**, 77–91, https://doi.org/https://doi.org/10.1080/07055900.2013.859124.

He, C., T. Zhou, L. Zhang, X. Chen, and W. Zhang, 2023: Extremely hot east asia and flooding western south asia in the summer of 2022 tied to reversed flow over tibetan plateau. *Climate Dynamics*, **61 (5)**, 2103–2119, https://doi.org/https://doi.org/10.1007/s00382-023-06669-y.

Hendrix, C. S., and S. M. Glaser, 2007: Trends and triggers: Climate, climate change and civil conflict in sub-saharan africa. *Political geography*, **26 (6)**, 695–715, https://doi.org/https://doi.org/10.1016/j.polgeo.2007.06.006.

Hersbach, H., and Coauthors, 2020: The era5 global reanalysis. *Quarterly Journal of the Royal Meteorological Society*, **146 (730)**, 1999–2049, https://doi.org/https://doi.org/10.1002/qj.3803.

Hong, C.-C., H.-H. Hsu, N.-H. Lin, and H. Chiu, 2011: Roles of european blocking and tropical-extratropical interaction in the 2010 pakistan flooding. *Geophysical Research Letters*, **38 (13)**, https://doi.org/https://doi.org/10.1029/2011GL047583.

Hsu, H.-H., C.-C. Hong, A.-Y. Huang, W.-L. Tseng, M.-M. Lu, and C.-C. Chang, 2022: Linkage between record floods in pakistan and a severe heatwave in china in the boreal summer of 2022. Tech. rep., ResearchSquare. https://doi.org/https://doi.org/10.21203/rs.3.rs-2353452/v1, in Review.

Hu, Z., Q. Li, X. Chen, Z. Teng, C. Chen, G. Yin, and Y. Zhang, 2016: Climate changes in temperature and precipitation extremes in an alpine grassland of central asia. *Theoretical and Applied Climatology*, **126**, 519–531, https://doi.org/https://doi.org/10.1007/s00704-015-1568-x.

Hu, Z.-Z., B. Huang, J. Zhu, A. Kumar, and M. J. McPhaden, 2019: On the variety of coastal el niño events. *Climate Dynamics*, **52**, 7537–7552, https://doi.org/https://doi.org/10.1007/s00382-018-4290-4.

Huang, K., J. H. Richter, and K. V. Pegion, 2023: Captured qbo-mjo connection in a subseasonal prediction system. *Geophysical Research Letters*, **50 (8)**, e2022GL102 648, https://doi.org/https://doi.org/10.1029/2022GL102648.

Hussain, M. S., and S. Lee, 2013: The regional and the seasonal variability of extreme precipitation trends in pakistan. *Asia-Pacific Journal Atmospheric Sciences*, **49 (4)**, 421–441, https://doi.org/https://doi.org/10.1007/s13143-013-0039-5.

Iqbal, M. F., and H. Athar, 2017: Variability, trends, and teleconnections of observed precipitation over pakistan. *Theoretical and Applied Climatology*, **134**, 613–632, https://doi.org/https://doi.org/10.1007/s00704-017-2296-1.

Kim, G., and Coauthors, 2018a: Future changes in extreme precipitation indices over korea. *International Journal of Climatology*, https://doi.org/https://doi.org/10.1002/joc.5414.

Kim, H., J. H. Richter, and Z. Martin, 2019: Insignificant qbo-mjo prediction skill relationship in the subx and s2s subseasonal reforecasts. *Journal of Geophysical Research: Atmospheres*, **124 (23)**, 12 655–12 666, https://doi.org/https://doi.org/10.1029/2019JD031416.

Kim, H., F. Vitart, and D. E. Waliser, 2018b: Prediction of the madden–julian oscillation: A review. *Journal of Climate*, **31 (23)**, 9425–9443, https://doi.org/https://doi.org/10.1175/JCLI-D-18-0210.1.

Kirtman, B. P., and Coauthors, 2014: The north american multimodel ensemble: phase-1 seasonal-to-interannual prediction; phase-2 toward developing intraseasonal prediction. *Bulletin of the American Meteorological Society*, **95 (4)**, 585–601, https://doi.org/https://doi.org/10.1175/BAMS-D-12-00050.1.

Lagos, P., and J. Buizer, 1992: El niño and peru: A nation's response to interannual climate variability. *El Niño and Perú: A nation's response to interannual climate variability*, 16–16, URL http://campus.bvs.hn/geeklog/docum/crid/CD_nino/pdf/eng/doc6133/doc6133-a.pdf.

Lau, W. K., and K.-M. Kim, 2012: The 2010 pakistan flood and russian heat wave: Teleconnection of hydrometeorological extremes. *Journal of Hydrometeorology*, **13 (1)**, 392–403, https://doi.org/https://doi.org/10.1175/JHM-D-11-016.1.

Lee, J.-Y., and Coauthors, 2021: *Climate Change 2021: The Physical Science Basis. Contribution of Working Group I to the Sixth Assessment Report of the Intergovernmental Panel on Climate Change*, chap. Future global climate: Scenario-based projections and near-term information, 553–672. Cambridge University Press, https://doi.org/https://doi.org/10.1017/9781009157896.006.

Lim, Y., S.-W. Son, and D. Kim, 2018: Mjo prediction skill of the subseasonal-to-seasonal prediction models. *Journal of Climate*, **31 (10)**, 4075–4094, https://doi.org/https://doi.org/10.1175/JCLI-D-17-0545.1.

Lim, Y., S.-W. Son, A. G. Marshall, H. H. Hendon, and K.-H. Seo, 2019: Influence of the qbo on mjo prediction skill in the subseasonal-to-seasonal prediction models. *Climate Dynamics*, **53**, 1681–1695, https://doi.org/https://doi.org/10.1007/s00382-019-04719-y.

Liu, F., and Coauthors, 2024: Opportunities and barriers for skillful subseasonal prediction of east asian summer precipitation. *Bulletin of the American Meteorological Society*, **105 (11)**, E2216–E2230, https://doi.org/https://doi.org/10.1175/BAMS-D-24-0055.1.

Lübbecke, J. F., D. Rudloff, and L. Stramma, 2019: Stand-alone eastern pacific coastal warming events. *Geophysical Research Letters*, **46 (21)**, 12 360–12 367, https://doi.org/https://doi.org/10.1029/2019GL084479.

L'Heureux, M. L., and Coauthors, 2017: Observing and predicting the 2015/16 el niño. *Bulletin of the American Meteorological Society*, **98 (7)**, 1363–1382, https://doi.org/https://doi.org/10.1175/BAMS-D-16-0009.1.

Ma, Y., X. Hu, Y. Chen, Z. Hu, T. Feng, and G. Feng, 2023: Different characteristics and drivers of the extraordinary pakistan rainfall in july and august 2022. *Remote Sensing*, **15 (9)**, 2311, https://doi.org/https://doi.org/10.3390/rs15092311.

Malik, I., and V. Mishra, 2025: Sub-seasonal prediction of compound hot and dry extremes in india. *Climate Dynamics*, **63 (4)**, 191, https://doi.org/https://doi.org/10.1007/s00382-025-07668-x.

Malik, N., B. Bookhagen, and P. J. Mucha, 2016: Spatiotemporal patterns and trends of indian monsoonal rainfall extremes. *Geophysical Research Letters*, **43 (4)**, 1710–1717, https://doi.org/https://doi.org/10.1002/2016GL067841.

Mariotti, A., P. M. Ruti, and M. Rixen, 2018: Progress in subseasonal to seasonal prediction through a joint weather and climate community effort. *Npj Climate and Atmospheric Science*, **1 (1)**, 4, https://doi.org/https://doi.org/10.1038/s41612-018-0014-z.

Mariotti, A., and Coauthors, 2020: Windows of opportunity for skillful forecasts subseasonal to seasonal and beyond. *Bulletin of the American Meteorological Society*, **101 (5)**, E608–E625, https://doi.org/https://doi.org/10.1175/BAMS-D-18-0326.1.

Mayta, V., Q.-J. Lin, A. F. Adames Corralize, and E. C. Mayta, 2024: Impact of tropical waves on extreme rainfall events during coastal el niño. *Environmental Research Letters*, **19**, 094 037, https://doi.org/https://doi.org/10.3389/fmars.2018.00367.

Meehl, G. A., and Coauthors, 2021: Initialized earth system prediction from subseasonal to decadal timescales. *Nature Reviews Earth & Environment*, **2 (5)**, 340–357, https://doi.org/https://doi.org/10.1038/s43017-021-00155-x.

Merryfield, W. J., and Coauthors, 2020: Current and emerging developments in subseasonal to decadal prediction. *Bulletin of the American Meteorological Society*, **101 (6)**, E869–E896, https://doi.org/https://doi.org/10.1175/BAMS-D-19-0037.1.

Millin, O. T., and J. C. Furtado, 2022: The role of wave breaking in the development and subseasonal forecasts of the february 2021 great plains cold air outbreak. *Geophysical Research Letters*, **49 (21)**, e2022GL100 835, https://doi.org/https://doi.org/10.1029/2022GL100835.

Miralles, D. G., A. J. Teuling, C. C. Van Heerwaarden, and J. Vilà-Guerau de Arellano, 2014: Mega-heatwave temperatures due to combined soil desiccation and atmospheric heat accumulation. *Nature geoscience*, **7 (5)**, 345–349, https://doi.org/https://doi.org/10.1038/ngeo2141.

Misra, A. K., 2014: Climate change and challenges of water and food security. *International Journal of Sustainable Built Environment*, **3 (1)**, 153–165, https://doi.org/https://doi.org/10.1016/j.ijsbe.2014.04.006.

Nanditha, J., and Coauthors, 2023: The pakistan flood of august 2022: causes and implications. *Earth's Future*, **11 (3)**, e2022EF003 230, https://doi.org/https://doi.org/10.1029/2022EF003230.

National Centers for Environmental Information, 2025: Equatorial pacific sea surface temperatures (sst). URL https://www.ncei.noaa.gov/access/monitoring/enso/sst, accessed: 2025-05-06.

Nayak, S., K. Dairaku, I. Takayabu, A. Suzuki-Parker, and N. N. Ishizaki, 2018: Extreme precipitation linked to temperature over japan: current evaluation and projected changes with multi-model ensemble downscaling. *Climate Dynamics*, **51 (11)**, 4385–4401, https://doi.org/https://doi.org/10.1007/s00382-017-3866-8.

Norwegian Refugee Council, 2024: Global report on displacement. Tech. rep., Internal Displacement Monitoring Centre. URL https://www.internal-displacement.org/global-report/grid2024/.

Ormaza-González, F., and J. Cedeño, 2017: Coastal el niño 2017 or simply: The carnival coastal warming event. *MOJ Ecology & Environmental Science*, **2 (8)**, https://doi.org/https://doi.org/10.15406/mojes.2017.02.00054.

Otto, F. E., and Coauthors, 2023: Climate change increased extreme monsoon rainfall, flooding highly vulnerable communities in pakistan. *Environmental Research: Climate*, **2 (2)**, 025 001, https://doi.org/https://doi.org/10.1088/2752-5295/acbfd5.

Pai, D., L. Sridhar, M. Badwaik, and M. Rajeevan, 2015: Analysis of the daily rainfall events over india using a new long period (1901–2010) high resolution (0.25× 0.25) gridded rainfall data set. *Climate dynamics*, **45**, 755–776, https://doi.org/https://doi.org/10.1007/s00382-014-2307-1.

Pan American Health Organization, 2023: Situation report n.1: Dengue epidemiological situation in the americas - 14 december 2023. Tech. rep., World Health Organization. URL https://www.paho.org/sites/default/files/2023-12/denguesitrep14dec2023finalv3.pdf.

Pegion, K., and Coauthors, 2019: The subseasonal experiment (subx): A multimodel subseasonal prediction experiment. *Bulletin of the American Meteorological Society*, **100 (10)**, 2043–2060, https://doi.org/https://doi.org/10.1175/BAMS-D-18-0270.1.

Peng, Q., S.-P. Xie, G. A. Passalacqua, A. Miyamoto, and C. Deser, 2024: The 2023 extreme coastal el niño: Atmospheric and air-sea coupling mechanisms. *Science Advances*, **10 (12)**, eadk8646, https://doi.org/https://doi.org/10.1126/sciadv.adk8646.

Peng, Q., S.-P. Xie, D. Wang, X.-T. Zheng, and H. Zhang, 2019: Coupled ocean-atmosphere dynamics of the 2017 extreme coastal el niño. *Nature communications*, **10 (1)**, 298, https://doi.org/https://doi.org/10.1038/s41467-018-08258-8.

Priya, P., R. Krishnan, M. Mujumdar, and R. A. Houze, 2017: Changing monsoon and midlatitude circulation interactions over the western himalayas and possible links to occurrences of extreme precipitation. *Climate Dynamics*, **49**, 2351–2364, https://doi.org/https://doi.org/10.1007/s00382-016-3458-z.

Pushpanjali, B., M. Subrahmanyam, and K. Murty, 2014: Sea surface temperature and find later jet variations over arabian sea during summer monsoon. *J. Climatol. Weather Forecast*, **2 (2)**, 1000 111, https://doi.org/https://doi.org/10.4172/2332-2594.1000111.

Qiao, S., and Coauthors, 2023: Unprecedented 2022 yangtze river valley heatwaves linked to the record-breaking pakistan flood and triple-dip la niña. Tech. rep., ResearchSquare. https://doi.org/https://doi.org/10.21203/rs.3.rs-2411329/v1, in Review.

Rasmussen, K., A. Hill, V. Toma, M. Zuluaga, P. Webster, and R. Houze Jr, 2015: Multiscale analysis of three consecutive years of anomalous flooding in pakistan. *Quarterly Journal of the Royal Meteorological Society*, **141 (689)**, 1259–1276, https://doi.org/https://doi.org/10.1002/qj.2433.

Rasmusson, E. M., and T. H. Carpenter, 1982: Variations in tropical sea surface temperature and surface wind fields associated with the southern oscillation/el niño. *Monthly Weather Review*, **110 (5)**, 354–384, https://doi.org/https://doi.org/10.1175/1520-0493(1982)110⟨0354:VITSST⟩2.0.CO;2.

Rau, P., L. Bourrel, D. Labat, P. Melo, B. Dewitte, F. Frappart, W. Lavado, and O. Felipe, 2017: Regionalization of rainfall over the peruvian pacific slope and coast. *International Journal of Climatology*, **37 (1)**, 143–158, https://doi.org/https://doi.org/10.1002/joc.4693.

Richter, J. H., and Coauthors, 2022: Subseasonal earth system prediction with cesm2. *Weather and Forecasting*, **37 (6)**, 797–815, https://doi.org/https://doi.org/10.1175/WAF-D-21-0163.1.

Richter, J. H., and Coauthors, 2024: Quantifying sources of subseasonal prediction skill in cesm2. *npj Climate and Atmospheric Science*, **7 (1)**, 59, https://doi.org/https://doi.org/10.1038/s41612-024-00595-4.

Robertson, A. W., A. Kumar, M. Peña, and F. Vitart, 2015: Improving and promoting subseasonal to seasonal prediction. *Bulletin of the American Meteorological Society*, **96 (3)**, ES49–ES53, https://doi.org/https://doi.org/10.1175/BAMS-D-14-00139.1.

Rodriguez-Morata, C., H. Díaz, J. A. Ballesteros-Canovas, M. Rohrer, and M. Stoffel, 2019: The anomalous 2017 coastal el niño event in peru. *Climate Dynamics*, **52**, 5605–5622, https://doi.org/https://doi.org/10.1007/s00382-018-4466-y.

Rollenbeck, R., J. Orellana-Alvear, J. Bendix, R. Rodriguez, F. Pucha-Cofrep, M. Guallpa, A. Fries, and R. Clleri, 2022: The coastal el niño event of 2017 in ecuador and peru: A weather radar analysis. *Remote Sensing*, **14 (4)**, 824, https://doi.org/https://doi.org/10.3390/rs14040824.

Roxy, M. K., S. Ghosh, A. Pathak, R. Athulya, M. Mujumdar, R. Murtugudde, P. Terray, and M. Rajeevan, 2017: A threefold rise in widespread extreme rain events over central india. *Nature communications*, **8 (1)**, 1–11, https://doi.org/https://doi.org/10.1038/s41467-017-00744-9.

Schroers, M. A., T. A. Dickinson, P. Ćwik, R. A. McPherson, and E. R. Martin, 2024: Listening to stakeholders iii: Potential users evaluate product content and design for subseasonal extreme precipitation forecasts. *Bulletin of the American Meteorological Society*, **105 (8)**, E1422–E1437, https://doi.org/https://doi.org/10.1175/BAMS-D-23-0233.1.

Seneviratne, S. I., and Coauthors, 2021: *Climate Change 2021: The Physical Science Basis. Contribution of Working Group I to the Sixth Assessment Report of the Intergovernmental Panel on Climate Change*, chap. Weather and climate extreme events in a changing climate, 1513–1766. Cambridge University Press, https://doi.org/https://doi.org/10.1017/9781009157896.013.

Singh, B., M. A. Ehsan, and A. W. Robertson, 2024: Calibrated probabilistic subseasonal forecasting for pakistan's monsoon rainfall in 2022. *Climate Dynamics*, **62 (5)**, 3375–3393, https://doi.org/https://doi.org/10.1007/s00382-023-07071-4.

Siswanto, G. J. Van Oldenborgh, G. Van Der Schrier, G. Lenderink, and B. Van Den Hurk, 2015: Trends in high-daily precipitation events in jakarta and the flooding of january 2014. *Bulletin of the American Meteorological Society*, **96 (12)**, S131–S135, https://doi.org/https://doi.org/10.1175/BAMS-D-15-00128.1.

Son, R., S.-Y. S. Wang, W.-L. Tseng, C. W. Barreto Schuler, E. Becker, and J.-H. Yoon, 2020: Climate diagnostics of the extreme floods in peru during early 2017. *Climate dynamics*, **54**, 935–945, https://doi.org/https://doi.org/10.1007/s00382-019-05038-y.

Stan, C., D. M. Straus, J. S. Frederiksen, H. Lin, E. D. Maloney, and C. Schumacher, 2017: Review of tropical-extratropical teleconnections on intraseasonal time scales. *Reviews of Geophysics*, **55 (4)**, 902–937, https://doi.org/https://doi.org/10.1002/2016RG000538.

Sui, Y., X. Lang, and D. Jiang, 2018: Projected signals in climate extremes over china associated with a 2 c global warming under two rcp scenarios. *International Journal of Climatology*, **38**, e678–e697, https://doi.org/https://doi.org/10.1002/joc.5399.

Sulca, J., K. Takahashi, J.-C. Espinoza, M. Vuille, and W. Lavado-Casimiro, 2018: Impacts of different enso flavors and tropical pacific convection variability (itcz, spcz) on austral summer rainfall in south america, with a focus on peru. *International Journal of Climatology*, **38 (1)**, 420–435, https://doi.org/https://doi.org/10.1002/joc.5185.

Sun, L., J. Perlwitz, J. H. Richter, M. P. Hoerling, and J. W. Hurrell, 2020: Attribution of nao predictive skill beyond 2 weeks in boreal winter. *Geophysical Research Letters*, **47 (22)**, e2020GL090 451, https://doi.org/https://doi.org/10.1029/2020GL090451.

Syed, F., F. Giorgi, J. S. Pal, and M. King, 2006: Effect of remote forcings on the winter precipitation of central southwest asia part 1: observations. *Theoretical and Applied Climatology*, **86**, 147–160, https://doi.org/https://doi.org/10.1007/s00704-005-0217-1.

Takahashi, H. G., 2024: Role of tropical disturbances along the south asian monsoon trough in the 2022 pakistan floods and the implications for interannual variability. *Journal of Climate*, **37 (21)**, 5609–5627, https://doi.org/https://doi.org/10.1175/JCLI-D-23-0186.1.

Takahashi, K., 2004: The atmospheric circulation associated with extreme rainfall events in piura, peru, during the 1997–1998 and 2002 el niño events. *Annales Geophysicae*, Copernicus GmbH, Vol. 22, 3917–3926, URL https://angeo.copernicus.org/articles/22/3917/2004/angeo-22-3917-2004.pdf.

Takahashi, K., and A. G. Martínez, 2019: The very strong coastal el niño in 1925 in the far-eastern pacific. *Climate Dynamics*, **52 (12)**, 7389–7415, https://doi.org/https://doi.org/10.1007/s00382-017-3702-1.

The White House, 2015: National security strategy. Tech. rep., Executive Office of the President. URL https://obamawhitehouse.archives.gov/sites/default/files/docs/2015_national_security_strategy_2.pdf.

Trenberth, K. E., 2018: Climate change caused by human activities is happening and it already has major consequences. *Journal of energy & natural resources law*, **36 (4)**, 463–481, https://doi.org/https://doi.org/10.1080/02646811.2018.1450895.

Trenberth, K. E., and J. T. Fasullo, 2012: Climate extremes and climate change: The russian heat wave and other climate extremes of 2010. *Journal of Geophysical Research: Atmospheres*, **117 (D17)**, https://doi.org/https://doi.org/10.1029/2012JD018020.

Tripathi, O. P., and Coauthors, 2015: The predictability of the extratropical stratosphere on monthly time-scales and its impact on the skill of tropospheric forecasts. *Quarterly Journal of the Royal Meteorological Society*, **141 (689)**, 987–1003, https://doi.org/https://doi.org/10.1002/qj.2432.

VanBuskirk, O., P. Ćwik, R. A. McPherson, H. Lazrus, E. Martin, C. Kuster, and E. Mullens, 2021: Listening to stakeholders: Initiating research on subseasonal-to-seasonal heavy precipitation events in the contiguous united states by first understanding what stakeholders need. *Bulletin of the American Meteorological Society*, **102 (10)**, E1972–E1986, https://doi.org/https://doi.org/10.1175/BAMS-D-20-0313.1.

VanBuskirk, O. G., T. A. Dickinson, M. A. Schroers, R. A. McPherson, and E. R. Martin, 2023a: Listening to stakeholders ii:adapting research products on subseasonal to seasonal heavy precipitation events by exploring options with users. *Bulletin of the American Meteorological Society*, https://doi.org/https://doi.org/10.1175/BAMS-D-22-0229.2.

VanBuskirk, O. G., R. A. McPherson, and L. E. Mullenbach, 2023b: What floodplain managers want: Using weather and climate information for decision-making. *Weather, Climate, and Society*, **15 (3)**, 759–772, https://doi.org/https://doi.org/10.1175/WCAS-D-22-0080.1.

Vigaud, N., A. W. Robertson, and M. Tippett, 2017: Multimodel ensembling of subseasonal precipitation forecasts over north america. *Monthly Weather Review*, **145 (10)**, 3913–3928, https://doi.org/https://doi.org/10.1175/MWR-D-17-0092.1.

Vitart, F., and A. W. Robertson, 2018: The sub-seasonal to seasonal prediction project (s2s) and the prediction of extreme events. *npj climate and atmospheric science*, **1 (1)**, 3, https://doi.org/https://doi.org/10.1038/s41612-018-0013-0.

Vitart, F., A. W. Robertson, and D. L. Anderson, 2012: Subseasonal to seasonal prediction project: Bridging the gap between weather and climate. *Bulletin of the World Meteorological Organization*, **61 (2)**, 23.

Vitart, F., and Coauthors, 2017: The subseasonal to seasonal (s2s) prediction project database. *Bulletin of the American Meteorological Society*, **98 (1)**, 163–173, https://doi.org/https://doi.org/10.1175/BAMS-D-16-0017.1.

Wang, Y., X. Yuan, Y. Ren, M. Bushuk, Q. Shu, C. Li, and X. Li, 2023: Subseasonal prediction of regional antarctic sea ice by a deep learning model. *Geophysical Research Letters*, **50 (17)**, e2023GL104 347, https://doi.org/https://doi.org/10.1029/2023GL104347.

Wayand, N., C. Bitz, and E. Blanchard-Wrigglesworth, 2019: A year-round subseasonal-to-seasonal sea ice prediction portal. *Geophysical Research Letters*, **46 (6)**, 3298–3307, https://doi.org/https://doi.org/10.1029/2018GL081565.

White, C. J., and Coauthors, 2017: Potential applications of subseasonal-to-seasonal (s2s) predictions. *Meteorological applications*, **24 (3)**, 315–325, https://doi.org/https://doi.org/10.1002/met.1654.

World Bank Group, 2025a: The world bank in pakistan. URL https://www.worldbank.org/en/country/pakistan/overview, accessed: 2025-04-25.

World Bank Group, 2025b: The world bank in peru. URL https://www.worldbank.org/en/country/peru/overview, accessed: 2025-04-25.

Wu, J., J. Li, Z. Zhu, and P.-C. Hsu, 2023: Factors determining the subseasonal prediction skill of summer extreme rainfall over southern china. *Climate Dynamics*, **60 (1)**, 443–460, https://doi.org/https://doi.org/10.1007/s00382-022-06326-w.

Xiang, B., Y. Q. Sun, J.-H. Chen, N. C. Johnson, and X. Jiang, 2020: Subseasonal prediction of land cold extremes in boreal wintertime. *Journal of Geophysical Research: Atmospheres*, **125 (13)**, e2020JD032 670, https://doi.org/https://doi.org/10.1029/2020JD032670.

Xu, Y., B.-T. Zhou, J. Wu, Z.-Y. Han, Y.-X. Zhang, and J. Wu, 2017: Asian climate change under 1.5–4 c warming targets. *Advances in Climate Change Research*, **8 (2)**, 99–107, https://doi.org/https://doi.org/10.1016/j.accre.2017.05.004.

Yamagami, A., and M. Matsueda, 2020: Subseasonal forecast skill for weekly mean atmospheric variability over the northern hemisphere in winter and its relationship to midlatitude teleconnections. *Geophysical Research Letters*, **47 (17)**, e2020GL088 508, https://doi.org/https://doi.org/10.1029/2020GL088508.

Yan, L., and G. Li, 2018: Double intertropical convergence zones over the eastern pacific ocean: Contrasting impacts of the eastern pacific-and central pacific-type el niños. *Atmospheric Science Letters*, **19 (10)**, e852, https://doi.org/https://doi.org/10.1002/asl.852.

Yao, J., Y. Chen, J. Chen, Y. Zhao, D. Tuoliewubieke, J. Li, L. Yang, and W. Mao, 2021: Intensification of extreme precipitation in arid central asia. *Journal of Hydrology*, **598**, 125 760, https://doi.org/https://doi.org/10.1016/j.jhydrol.2020.125760.

Yao, Y., D. Luo, A. Dai, and S. B. Feldstein, 2016: The positive north atlantic oscillation with downstream blocking and middle east snowstorms: Impacts of the north atlantic jet. *Journal of Climate*, **29 (5)**, 1853–1876, https://doi.org/https://doi.org/10.1175/JCLI-D-15-0350.1.

Yglesias-González, M., and Coauthors, 2023: Reflections on the impact and response to the peruvian 2017 coastal el niño event: Looking to the past to prepare for the future. *Plos one*, **18 (9)**, e0290 767, https://doi.org/https://doi.org/10.1371/journal.pone.0290767.

Zahid, M., and G. Rasul, 2012: Changing trends of thermal extremes in pakistan. *Climatic change*, **113 (3)**, 883–896, https://doi.org/https://doi.org/10.1007/s10584-011-0390-4.

Zampieri, L., H. F. Goessling, and T. Jung, 2018: Bright prospects for arctic sea ice prediction on subseasonal time scales. *Geophysical Research Letters*, **45 (18)**, 9731–9738, https://doi.org/https://doi.org/10.1029/2018GL079394.

Zhao, S., and C. Karamperidou, 2022: Competing effects of eastern and central-western pacific winds in the evolution of the 2017 extreme coastal el niño. *Geophysical Research Letters*, **49 (15)**, e2022GL098 859, https://doi.org/https://doi.org/10.1029/2022GL098859.

Zhu, H., H. Chen, Y. Zhou, and X. Dong, 2019: Evaluation of the subseasonal forecast skill of surface soil moisture in the s2s database. *Atmospheric and Oceanic Science Letters*, **12 (6)**, 467–474, https://doi.org/https://doi.org/10.1080/16742834.2019.1663123.